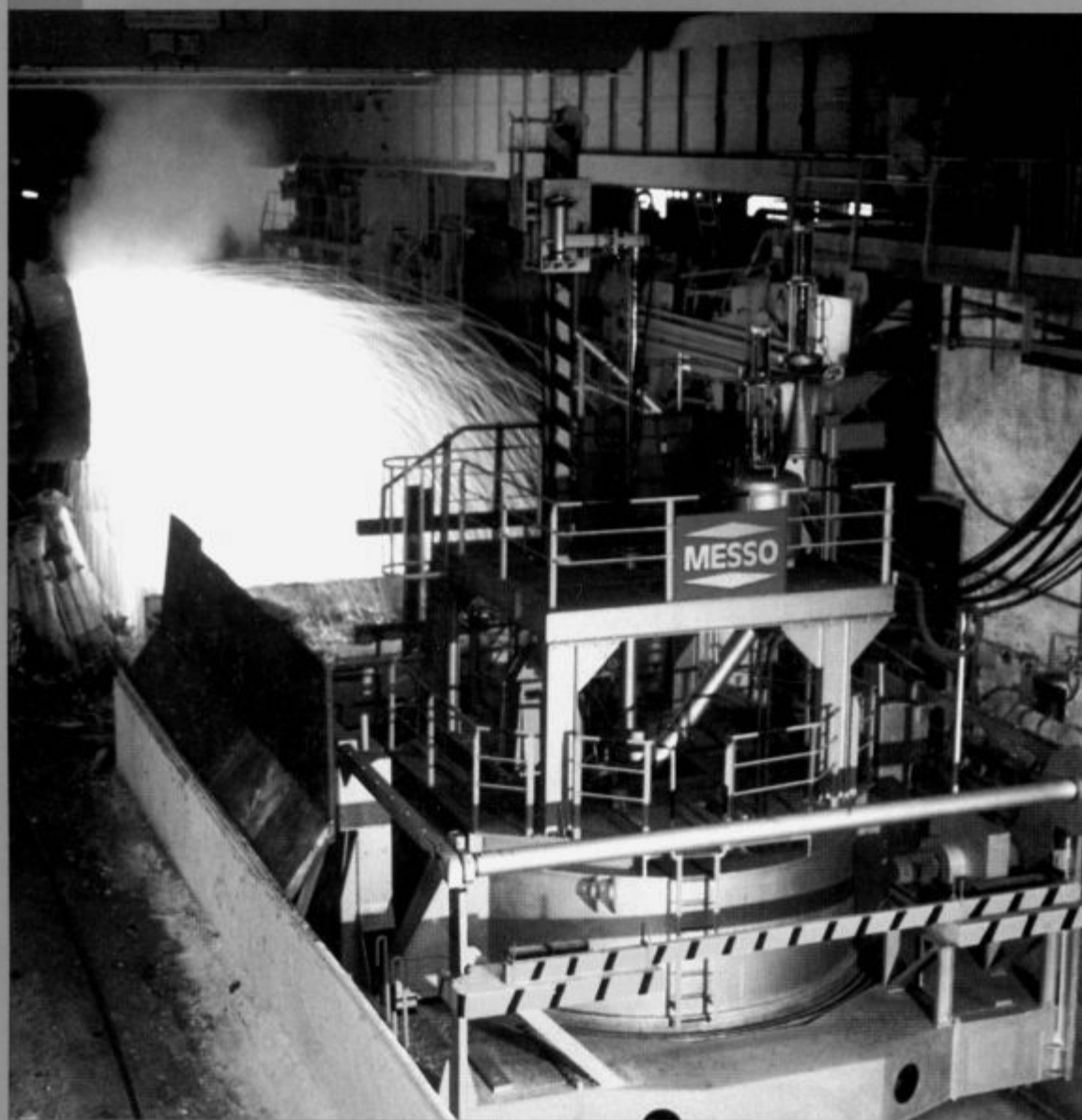


KOVINE ZLITINE TEHNOLOGIJE

METALS ALLOYS TECHNOLOGIES

LETO 27 št. 4. 1993



IZDAJAJO SŽ ACRONI JESENICE, METAL RAVNE, JEKLO ŠTORE IN
INŠTITUT ZA KOVINSKE MATERIALE IN TEHNOLOGIJE LJUBLJANA
REVIJA JE PREJ IZHAJALA POD NASLOVOM ŽELEZARSKI ZBORNIK

ISSN 1315-0010

Navodila avtorjem za pripravo člankov za objavo v reviji *Kovine, zlitine, tehnologije*

V letu 1992 uvajamo nov način tehničnega urejanja in priprave za tisk revije *Kovine, zlitine, tehnologije*. Da bi pocenili tiskarske stroške, skrajšali čas od prejema članka do njegove objave in prepustili avtorju končno odgovornost za morebitne neodkrita tipografske napake, smo se v uredništvu odločili, da izkoristimo možnosti, ki jih danes nudi namizno *založništvo*.

Avtor lahko pošlje članek napisan klasično – s pisalnim strojem. Zaželeno je, da avtor odda uredništvu članek oz. besedilo napisano na računalnik z urejevalniki besedil:

- WORDSTAR, verzija 4, 5, 6, 7 za DOS
- WORD za DOS ali WINDOWS
- WORDPERFECT.

Če je besedilo napisano z urejevalnikom besedil: CHI WRITER, naj ga avtor prekonvertira v WORDSTAR DOCUMENT.

Naprošamo avtorje, da pošljejo uredništvu disketo z oznako datoteke in računalniškimi izpisom te datoteke na papirju.

Formule naj bodo v datoteki samo naznačene, na papirju pa ročno izpisane.

Vsebina članka

Kako naj članek izgleda vsebinsko, naj si avtorji ogledajo v starih izdajah *Železarskega zbornika*. Vsak članek pa mora vsebovati:

- slovenski in angleški naslovi članka,
- imena ter naslove avtorjev,
- povzetka v angleščini in slovenščini,
- reference, ki naj bodo v besedilu članka označene z zaporednimi številkami, primer¹⁻⁵. Način citiranja članka: avtor, inicialkam naj sledi priimek, naslov članka, ime revije, letnik, strani, leto. Način citiranja knjige: avtor, naslov, založnik in kraj izdaje, leto, po potrebi poglavje ali strani.

Besedilo članka naj bo razdeljeno na razdelke (označene z zaporednimi številkami) in po potrebi še na podrazdelke (označene z decimalno številko, kjer celi del označuje razdelek).

Slike

Vse slike naj bodo na posebnih listih papirja, z jasno označeno številko slike. Slike naj bodo označene z zaporednimi številkami povsod v članku. Originali za vse vrste slik naj bodo ostri in brez šuma. *Risbe* naj bodo narisane s črnim na belem ozadju. Vse oznake in besedila na risbah naj bodo v istem jeziku kot besedilo članka in dovolj velike, da omogočajo pomanjšanje slike na 8 cm. Le izjemoma lahko slika sega čez obe koloni besedila (16,5 cm). *Fotografije* so lahko katerekoli običaj-

ne dimenzije, na svetlečem papirju in z dobrim kontrastom. Mikroskopska in makroskopska povečevanja označite v podpisu na sliki, še bolje pa z vrisanjem ustrezne skale na fotografiji.

Za vsako sliko naj avtor predvidi, kam naj se slika v besedilu članka uvrsti, kjer naj se nahaja ustrezen pod-napis z zaporedno številko slike (na primer: "Slika 3 prikazuje...", nikakor pa ne: "Na spodnji sliki vidimo...").

Tabele

Avtor naj se izogiba zapletenih tabel z mnogo podatki, ki bralca ne zanimajo, posebej še, če so isti podatki tudi grafično ponazorjeni. Nad vsako tabelo naj se nahaja zaporedna številka tabele s pojasnilom. Tabele naj bodo povsod v članku označene z zaporednimi številkami.

Pisanje besedil na računalniku

Avtorje naprošamo, da pri pisanju besedil na računalniku upoštevajo naslednja navodila, saj le-ta precej olajšajo naše nadaljnje delo pri pripravi za tisk:

- ne puščajte praznega prostora pred ločili (pikami, vejicami, dvopičji) in za predklepaji oziroma pred zaklepaji,
- puščajte prazen prostor za vsemi ločili (pikami, vejicami, dvopičji) – razen decimalno piko,
- pišite vse naslove in besede z majhnimi črkami (razen velikih začetnic in kratic),
- besedilo naj ne vsebuje deljenih besed na koncu vrstice.

Če avtor pripravlja ilustracije na računalniku, ga naprošamo, da priloži datoteke s slikami na disketo z besedilom članka, s pojasnilom, s katerim programom so narejene.

Krtačni odtis

Krtačni odtis – končna podoba članka – bo poslan avtorju v končno revizijo. Avtorja naprošamo, da čim hitreje opravi korekture in ga pošlje nazaj na uredništvo. Hkrati naprošamo avtorje, da popravljajo samo napake, ki so nastale med stavljenjem članka. Če avtor popravljenega članka ne vrne pravočasno, bo objavljen nepopravljen, kar bo tudi označeno.

Uredništvo

KOVINE ZLITINE TEHNOLOGIJE

METALS ALLOYS TECHNOLOGIES

|| 229280

KOVINE ZLITINE TEHNOLOGIJE

Izdajajo (Published by): SŽ ACRONI Jesenice, METAL Ravne, JEKLO Štore in Inštitut za kovinske materiale in tehnologije Ljubljana

Izdajanje KOVINE ZLITINE TEHNOLOGIJE delno sofinancira:
Ministrstvo za znanost in tehnologijo

UREDNIŠTVO (EDITORIAL STAFF)

Glavni in odgovorni urednik (Editor): Jožef Arh, dipl. ing.

Uredniški odbor (Associate Editors): dr. Aleksander Kveder, dipl. ing., dr. Jože Rodič, dipl. ing., prof. dr. Andrej Paulin, dipl. ing., dr. Monika Jenko, dipl. ing., dr. Ferdo Grešovnik, dipl. ing., Franc Mlakar, dipl. ing., dr. Karel Kuzman, dipl. ing., Jana Jamar

Tehnični urednik (Production editor): Jana Jamar

Lektorji (Lectors): Cvetka Martinčič, Jana Jamar

Prevodi (Translations): prof. dr. Andrej Paulin, dipl. ing., dr. Nijaz Smajić, dipl. ing. (angleški jezik), Jožef Arh, dipl. ing. (nemški jezik)

NASLOV UREDNIŠTVA (EDITORIAL ADDRESS): KOVINE ZLITINE TEHNOLOGIJE,

ACRONI Jesenice d.o.o., 64270 Jesenice, Slovenija

Telefon: (064) 861-441

Telex: 37219

Telefax: (064) 861-412

Žiro račun: 51530-601-25734

Stack: Majda Kuraš, **Tisk:** Gorenjski tisk, Kranj, **Oblikovanje ovitka:** Ignac Kofol,

Fotografija na naslovnici: Vakuumska naprava tipa VD/VOD, **Foto:** MESSOMETALLURGIE

IZDAJATELJSKI SVET (EDITORIAL ADVISORY BOARD):

Predsednik: prof. dr. Marin Gabrovšek, dipl. ing.; **člani:** dr. Božidar Brudar, dipl. ing., prof. dr. Vincenc Čížman, dipl. ing., prof. dr. D. Drobňjak, dipl. ing., prof. dr. Blaženko Koroušič, dipl. ing., prof. dr. Ladislav Kosec, dipl. ing., prof. dr. Josip Krajcar, dipl. ing., prof. dr. Alojz Križman, dipl. ing., prof. dr. Karel Kuzman, dipl. ing., dr. Aleksander Kveder, dipl. ing., prof. dr. Andrej Paulin, dipl. ing., prof. dr. Boris Sicherl, dipl. ing., dr. Nijaz Smajić, dipl. ing., prof. dr. J. Sušnik, dr. Leopold Vehovar, dipl. ing., prof. dr. Franc Vodopivec, dipl. ing.

Po mnenju Ministrstva za znanost in tehnologijo Republike Slovenije št. 23-335-92 z dne 09. 06. 1992 šteje KOVINE ZLITINE TEHNOLOGIJE med proizvode, za katere se plačuje 5-odstotni davek od prometa proizvodov.



Contents

Vsebina

<i>B. Ule, M. Lovrečič-Saražin, J. Vojvodič-Gvardjančič, A. Ažman, A. Lagoja:</i> Relationship between Fracture Toughness and Mechanical Properties of some Structural Steels at Low Temperatures Odvisnost med lomno žilavostjo in mehanskimi lastnostmi nekaterih konstrukcijskih jekel pri nizkih temperaturah	283
<i>M. Torkar, B. Šuštaršič, F. Vodopivec:</i> Recrystallization of Ni-based Superalloy after Cold Deformation Rekristalizacija Ni-superzlitine po hladni deformaciji	289
<i>G. G. Shlomchack, I. Mamuzič:</i> The Rheological Model of Deformation Nidus in the Process of Rolling Reološki model deformacijskega prostora v procesu valjanja	295
<i>A. Osojnik, T. Drglin:</i> Comparision of Graphite Furnace - and Hydride Generation AAS for Trace Analysis of Tin in Steels and Nickel Alloys Primerjava elektrotermične - in hidridne tehnike AAS za analizo sledov kositra v jeklih in nikljevih zlitinah	301
<i>M. Gojić, M. Balenocić, L. Kosec, L. Vehovar:</i> The Susceptibility to Hydrogen Embrittlement of Low Alloy Cr-Mo Steel Tubing Občutljivost cevi iz nizkolegiranega Cr-Mo jekla na vodikovo krhkost	307
<i>B. Koroušič:</i> Predicting Oxide Activities in CaO-Al ₂ O ₃ -SiO ₂ System by Computer Model Napovedovanje aktivnosti oksidov v sistemu CaO-Al ₂ O ₃ -SiO ₂ z računalniškim modelom.....	313
<i>B. Kosec, L. Kosec:</i> Composite Mechanism of Scale Adhesiveness Kompozitni mehanizem oprijemljivosti škaje	319
<i>L. Kosec, V. Gontarev, B. Kosec, M. Mlakar:</i> Embrittlement of Copper Wire Due to Oxygen Krhkost bakra zaradi kisika	323
Letno kazalo	329

INŠTITUT ZA KOVINSKE MATERIALE IN TEHNOLOGIJE, LJUBLJANA
KEMIJSKI INŠTITUT, LJUBLJANA
SLOVENSKO DRUŠTVO ZA MATERIALE
SLOVENSKO KEMIJSKO DRUŠTVO: SEKCIJI ZA POLIMERE IN KERAMIKO
DRUŠTVO ZA VAKUUMSKO TEHNIKO SLOVENIJE

organizirajo

45. POSVETOVANJE O METALURGIJI IN KOVINSKIH GRADIVIH

2. POSVETOVANJE O MATERIALIH

14. SLOVENSKO VAKUUMSKO POSVETOVANJE

5.–7. oktober 1994, Hoteli Bernardin, Portorož

in vabijo

Strokovnjake z industrije, inštitutov in univerz, ki delajo na teh področjih k aktivnemu sodelovanju
Posvetovanje je namenjeno predstavitvi temeljnih in aplikativnih raziskovalnih ter razvojnih dosežkov s
področja tehnologije in uporabe materialov.

Obravnavana bodo naslednja področja:

- sinteza sodobnih kovinskih, polimernih, keramičnih in kompozitnih materialov
- razvoj modernih tehnologij proizvodnje materialov
- kakovost
- matematično modeliranje in računalniška simulacija procesov in tehnologij
- korozija in propad gradiv
- sodobne termične obdelave
- karakterizacija materialov
- vakuumaska tehnika in tehnologije
- tanke plasti in površine
- tribologija
- varstvo okolja

V posebni sekciji bodo lahko razstavljalci predstavili najnovejše proizvode in opremo.

V okviru posvetovanja bomo organizirali razstavo, na kateri se bodo predstavila slovenska in tuja podjetja,
proizvajalci in uporabniki materialov, gradiv in opreme.

Delovna jezika na posvetovanju sta slovenski in angleški jezik.

Vabimo vas k aktivnemu sodelovanju na področjih znanstvenega programa SMMM-45, SM-2 in SVS-14.
Program, bo obsegal vabljen predavanja, govorne prispevke mladih raziskovalcev in postrske
prispevke.

Povzetek pošljite na naslov: Organizacijski odbor Portorož 94
Inštitut za kovinske materiale in tehnologije
pp 431
61001 Ljubljana

Zadnji rok za oddajo je 30. april 1994.

Dela, uvrščena v program posvetovanja, bodo natisnjena v prvi številki znanstvene revije:
KOVINE, ZLITINE, TEHNOLOGIJE v letu 1995.

Najbolje ocenjeni prispevki mladih raziskovalcev posameznih področjih (metalurgija in kovinski materiali,
kjeramika, polimeri in vakuumaska tehnika), bodo nagrajeni z denarno nagrado 300 DEM v tolaški
protivrednosti.

Prosimo vse mlade raziskovalce, da na poslanem povzetku označijo, da sodelujejo v sekciji **Mladi
raziskovalci**.

Dodatne informacije: tajništvo IMT Ljubljana – telefon (061) 125 11 61, fax: (061) 213 780

Beseda glavnega urednika



Težko je pisati uvodnike, ko se razmere v Slovenskih železarnah spreminjajo iz dneva v dan. Nihče v tej družbi ne ve povedati ali Slovenija železarne potrebuje, ali ne. S takšnim občutkom živijo ljudje v teh krajih. Lahko bi rekli, da se lastniki obnašajo do njih precej nestrokovno in neodgovorno. Pa vendar za Jesenice lahko trdimo, da izgledi za nadaljni obstoj in razvoj niso slabi. Pri visokolegiranih nerjavnih jeklih sploh ne. Enako velja tudi za elektropločevine, kjer smo na Jesenicah uspešni.

ACRONI Jesenice je majhno podjetje, izredno prilagodljivo v današnjih tržnih razmerah. Prav to majhnost moramo izkoristiti, da se uveljavimo na tistih trgih in s tistimi vrstami jekel, ki za druga velika podjetja niso zanimivi.

Zelo hitro se v svetu uveljavlja nova tehnologija vlivanja tankih slabov in direktnega valjanja v trakove in pločevino. Le-ta bo v naslednjem tisočletju morala najti pot tudi na Jesenice. 60 do 70 US \$ prihranka pri toni dajo misliti. Ali bodo naši bodoči lastniki dovolj modri in pogumni in ali bodo imeli dovolj znanja, da bodo uvideli potrebo po bolj sodobni tehnologiji?

Še pred leti je veljala trditev, da je mogoče dobro jeklo za globoko vlečenje izdelati le v LD konvertorjih. Danes v elektro pečeh po novi tehnologiji, tako pri firmi Arvedi, kot pri Nucor Steel, izdelujejo enako kakovostno jeklo za globoki vlek, potreben je le čisti vložek. Že sedaj moramo misliti na uporabo direktno reduciranih peletov (DRI) na Jesenicah.

Vsekakor se prav na področju proizvodnje jekel za globoki vlek za slovenske potrebe na Jesenicah obetajo velike možnosti povečati izkoriščenost jeklarne. Če bo le volja tam pri vrhu. Znanje imamo, le izkoriščati ga ne znamo.

45th SYMPOSIUM ON METALLURGY AND METALIC MATERIALS, SMMM-45

2nd SYMPOSIUM ON MATERIALS, SM-2

14th SLOVENIAN VACUUM SYMPOSIUM, SVS-14

October 5–7, 1994, BernardinHotels Ltd., Portorož

organized by

INSTITUTE OF METALS AND TECHNOLOGY, LJUBLJANA
NATIONAL INSTITUT OF CHEMISTRY, LJUBLJANA
SLOVENIAN SOCIETY OF MATERIALS
SLOVENIAN CHEMICAL SOCIETY: DIVISIONS OF POLYMERS AND CERAMICS
SLOVENIAN VACUUM SOCIETY

Material scientists from Industry, Universities and Institutes are cordially invited to attend the joint SMMM-45/SM-2/SVC-14 symposium and to contribute to its scientific programme.

The scientific programme covers

- Synthesis of advanced metallic, polymer, ceramic and composite materials
- Development of advanced manufacturing technology
- Quality
- Mathematical modelling and computer simulation of processes and technologies
- Corrosion and destruction of materials
- Advanced thermal treatment
- Characterization of materials
- Vacuum technique and technology
- Thin films and surfaces
- Tribology
- Environmental protection

Exhibitors will be able to present their latest products and equipment in a Technical Session.

During the Symposium a technical exhibition of materials, equipment and scientific literature will be held.

The Symposium languages will be Slovene and English.

You are invited to submit contributed papers in the fields of the scientific programmes of SMMM-45, SM-2 and SVS-14. There will be plenary sessions for invited lecturers, oral sessions for young scientists and poster sessions.

**Abstract are to be submitted to: Organizing Committee Portorož 94
Institute of Metals and Technology
Box 431
61001 Ljubljana, Slovenia**

Deadline for abstract submission is April 30, 1994

The Symposium Proceedings will be published as a special issue of the Slovenian scientific journal **Metals, Alloys, Technologies**.

The best young scientists' contributions will each be awarded 300 DEM equivalent in for topics (Metallurgy and Metallic Materials, Ceramics, Polymers and Vacuum Technique).

Young scientists are kindly requested to mark their manuscript clearly with the symbol MR.

Contact address: Dr. M. Jenko, Organizing Committee,
IMT Ljubljana, 61001 Ljubljana,
Box 431, Slovenia
Phone: 386 61 125 11 61, Fax: 386 61 213 780
e-mail: monika.jenko@quest.arnes.si

Relationship between Fracture Toughness and mechanical Properties of some Structural Steels at Low Temperatures

Odvisnost med lomno žilavostjo in mehanskimi lastnostmi nekaterih konstrukcijskih jekel pri nizkih temperaturah

B. Ule, M. Lovrečič-Saražin, Inštitut za kovinske materiale in tehnologije, Ljubljana
J. Vojvodič-Gvardjančič, Inštitut za metalne konstrukcije, Ljubljana
A. Ažman, A. Lagoja, Acroni Jesenice

The effect of strain-aging on the impact toughness characteristic of Charpy specimens (CVN) and on quasi-static fracture toughness values K_{IC} of some structural steels was investigated in the temperature range of nil-ductility temperatures. Strain-aging provokes shifts of Charpy curves to higher temperatures, but it decreases the nil-ductility temperatures regarding to as purchased steels. The correlation between K_{IC} and conventional mechanical properties valid for low temperatures confirms that K_{IC} and probably also K_{arrest} of as strain-aged steels are higher than that of as purchased steels with the same Charpy energy.

Key words: fine-grain low-alloy steels, fracture mechanics, fracture toughness, drop-weight test, nil ductility temperature.

Raziskali smo vpliv deformacijskega staranja nekaterih konstrukcijskih jekel na njihovo udarno Charpyjevo žilavost (CVN) ter kvazi-statično lomno žilavost K_{IC} v temperaturnem območju ničelne duktilnosti. Deformacijsko staranje pomakne Charpyjeve krivulje k višjim temperaturam, vendar pa zniža temperature ničelne duktilnosti glede na jekla v dobavnem stanju. Korelacija med K_{IC} in konvencionalnimi mehanskimi lastnostmi, veljavna pri nizkih temperaturah, kaže, da je K_{IC} in verjetno tudi K_{arrest} vrednost staranih jekel višja kot pri jeklih v dobavnem stanju z enako Charpyjevo energijo.

Ključne besede: drobnozrnata malolegirana jekla, mehanika loma, lomna žilavost, test s padajočim bremenom, temperatura ničelne duktilnosti.

1. Introduction

The relationship of microstructure to mechanical properties in low-alloy structural steels has been the subject of considerable research. Such steels with increased yield stress are sometimes alloyed with small additions of various elements so that the characteristics and the properties of such steels are substantially affected presumably due to the reduction of the austenite and ferrite grain size and because their yield stress, strength and toughness increase while the ductile/brittle transition temperature decreases which is perhaps one of the most important aspects of microalloying. In most of the previous investigations, fracture behaviour of steels has been evaluated mainly by means of the Charpy impact test because of its convenience and familiarity. Although the material requirements for a lot of practical applications are based on concepts of fracture mechanics, they are specified in terms of Charpy V-notch impact test results (CVN). Toughness requirements for thick-walled nuclear pressure-vessel steels are based on minimum dynamic toughness values, K_{Id} . However, the actual material-toughness requirements for steels used in these pressure vessels are specified using NDT (nil-ductility transition) values and CVN impact values using lateral expansion measurements. Empirical correlations, engineering judgment and experience are thus used to translate the fracture-mechanics guidelines or controls into actual material-toughness

specifications¹⁾. A comprehensive concept for a practical estimation of the dynamic fracture toughness from the CVN impact energy vs. temperature curve was proposed by the MPC/PVRC Working Group on Reference Toughness²⁾. It was proved that lower bound curves can be derived from the CVN vs. T-curve for the quasi-static and low rate dynamic fracture toughness (K_{IC}), dynamic and high-rate dynamic fracture toughness (K_{Id}) and crack arrest toughness (K_{Ia})³⁾. Besides this, some other correlations between conventional mechanical properties and K_{IC} values for ductile/brittle transition range or for lower Charpy shelves are also well-known^{4,5)}. However, it is well-known too that strain-aging of several low-alloy structural steels causes some shifts along the temperature axis which is not the same for both the CVN data and the K_{Id} data. The purpose of the present paper is therefore to determine the more relevant correlation between the conventional mechanical properties and the K_{IC} values for some structural steels in the nil-ductility temperature range.

2. Experimental procedure

Nine non-, micro- and low-alloy structural steels in the form of hot-rolled and heat-treated flats were used in this investigation. The chemical composition, the designation of the steels and the thickness of the flats are given in **Table 1**. These

steels with 0.05 to 0.21 wt.% carbon were either non-alloyed or alloyed with chromium, nickel, molybdenum, niobium and vanadium in different combinations. The microstructure of the investigated steels which was hot-rolled and subsequently cooled at different cooling rates was mainly ferritic with different shares of perlite (Nioval 47, Č.0562 and Č.1204) or bainite (Niomol 490 K). Only two types of low-alloyed steels (Nionical 70 and Nionical 90) have a microstructure of tempered martensite. The yield stress of the investigated steels varied from 265 MPa for plain carbon steel to 1003 MPa for Nionical 96 i.e. for submarine steel alloyed with chromium, nickel and molybdenum. All the investigated steels were tested as purchased i.e. hot-rolled and cooled at different cooling rates but they were tested also after strain-aging, i.e. after cold-rolling with a reduction in thickness of 10% and additionally heating for 30 minutes at 250°C.

Table 1: Chemical composition of the investigated steels (weight %)

No.	Grade (thickness)	C	Si	Mn	P	S	Cr	Ni	Mo	Nb	V
1	Nioval 47 (20 mm)	0.19	0.42	1.49	0.013	0.005	0.13	0.10	0.04	0.05	0.07
2	Nioval 47 (65 mm)	0.14	0.33	1.53	0.014	0.005	0.16	0.15	0.01	0.04	0.07
3	Nionical 70 (20 mm)	0.11	0.28	0.27	0.009	0.007	1.07	2.80	0.26		0.06
4	Nionical 70 (50 mm)	0.11	0.37	0.34	0.009	0.003	1.03	2.63	0.27		0.08
5	Nionical 96 (50 mm)	0.14	0.29	0.51	0.017	0.009	1.64	2.76	0.42		
6	Niomol 490 K (60 mm)	0.05	0.35	0.42	0.011	0.004	0.75	0.29	0.33	0.06	
7	Č.0562 (25 mm)	0.17	0.32	1.28	0.020	0.009	0.21	0.23	0.05		
8	Č.0562 (80 mm)	0.18	0.46	1.29	0.036	0.004	0.30	0.15	0.03		
9	Č.1204 (30 mm)	0.21	0.25	0.51	0.011	0.025	0.02	0.04	0.01		

Test specimens were cut from the plates in transverse orientation and machined to the required dimensions. Besides the standard Charpy V-notch- and Drop-weight test specimens of P3 type (15.9 x 51 x 127 mm), a large number of round-notched and pre-fatigue cracked tensile specimens for the low-temperature measurements of quasi-static fracture toughness K_{Ic} was made. The drop-weight test specimens were prepared

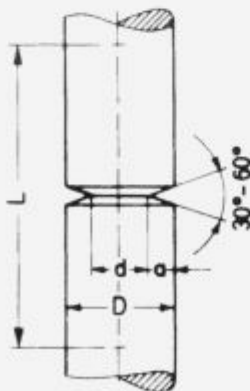


Figure 1: Geometry of a round-notched and precracked tensile specimen

Slika 1: Geometrija nateznega preiskusańca z zarezo in razpoko po obodu

in accordance with the ASTM E208-84a where the crack starter bead application is performed by the one bead technique to avoid the undesirable variation of NDT⁶. The geometry of the round-notched precracked tensile specimens, prepared according Dieter's recommendation⁷ is shown in **Figure 1**.

At the experiments, it is essential that the fatigue annulus be of a uniform width and concentric with the outer diameter of the specimen in order to obtain a state of plain strain at fracture. The fatigue crack grew to a depth of about 0.2 mm, leaving an unfractured ligament approximately 6.5 mm in diameter.

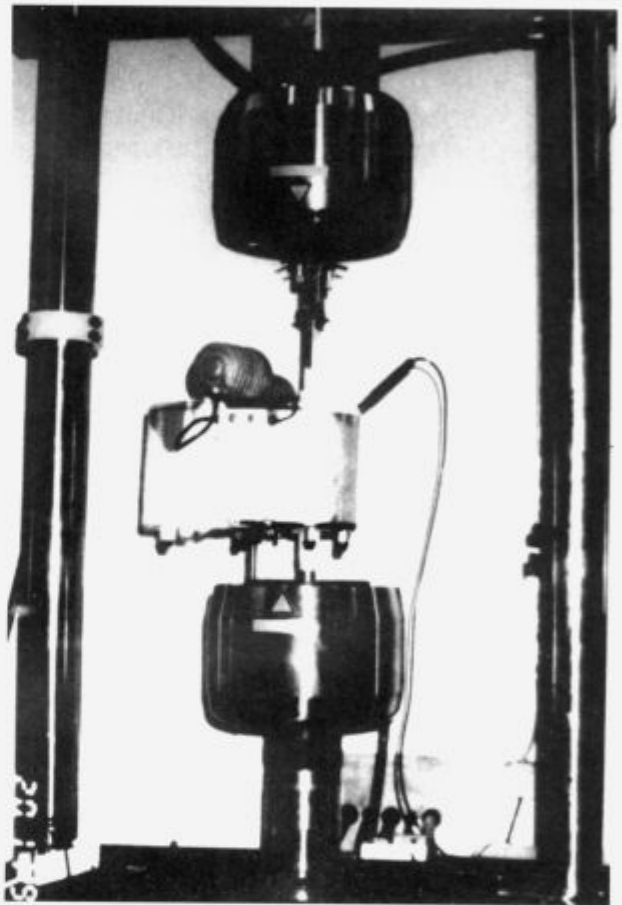


Figure 2: Experimental set-up with cryostat chamber
Slika 2: Eksperimentalna ureditev s kriostatsko komoro

A cryostat chamber filled with liquid nitrogen and petroleum ether was used during the test to control the specimen temperature range from -140°C to room temperature and the fracture in the quasi-static test at crosshead speed of 1 mm/min was reached by using a universal testing machine (**Figure 2**). For a round-notched precracked specimen, the stress intensity factor is given by Dieter⁷ as

$$K_I = \frac{P}{D^{3/2}} (-1.27 + 1.72 D/d) \quad (1)$$

where d is the radius of the uncracked ligament after fatiguing, P is the applied fracture load, and D is the outer diameter of the cylindrical specimen. In order to apply linear-elastic fracture mechanics (LEFM) concepts, the size of the plastic zone at the crack tip must be small compared with the nominal dimensions of the specimen. The size requirement for a valid K_{Ic} test is given by Shen Wei et. al.⁸ as

$$D \geq 1.5 (K_{IC} / \sigma_{ys}) \quad (2)$$

where σ_{ys} is the initial yield stress of the material obtained at a strain rate comparable to that attained near the root of the notch in the fracture test. If the specimens did not comply with requirement (2) for valid fracture toughness (K_{IC}) measurements, K_{Iq} values were obtained instead of K_{IC} , according to E399. However, the concept of the equivalent energy adopted by Wang Chang⁹⁾ enabled us to determine the virtual fracture load P^* instead of load P in equation (1) after the transformations of the surface under the parabolic load-displacement curve into the quantitatively equal surface of the triangle as shown on Figure 3.

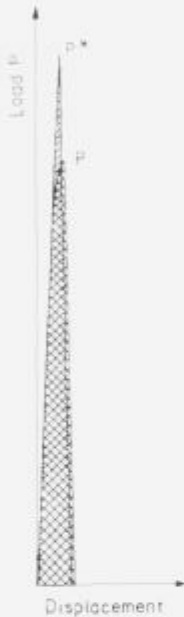


Figure 3: To the explanation of the concept of equivalent energy
Slika 3: K razlagi koncepta ekvivalentne energije

Therefore, the weak elasto-plastic fracture behaviour of the investigated steels even in the vicinity of the nil-ductility

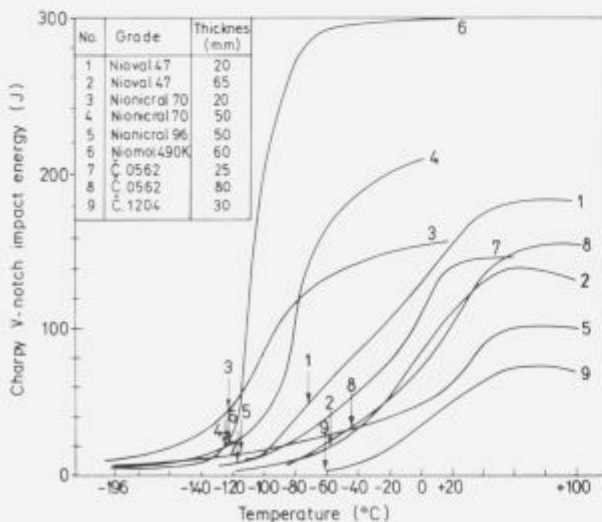


Figure 4: Charpy V-notch impact energy versus temperature behaviour of as-purchased steels. Arrows indicate the NDT temperatures
Slika 4: Charpyjeve energije v odvisnosti od temperature preiskovanja jekel v dobavnem stanju. S puščicami so označene temperature ničelne duktilnosti

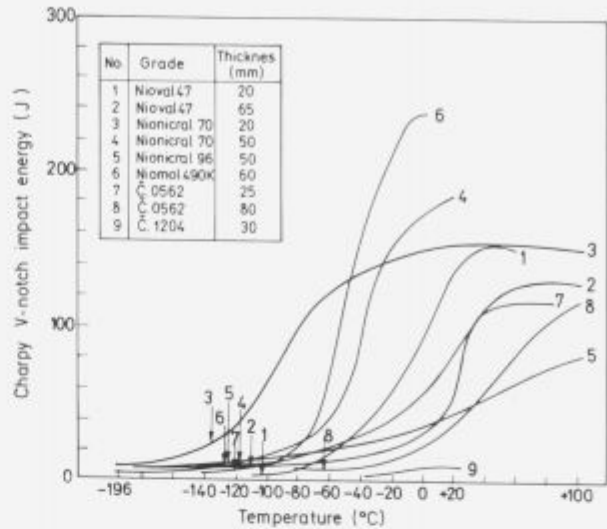


Figure 5: Charpy V-notch impact energy versus temperature behaviour of as-strain-aged steels. Arrows indicate the NDT temperatures
Slika 5: Charpyjeve energije v odvisnosti od temperature preiskovanja jekel v staranem stanju. S puščicami so označene temperature ničelne duktilnosti

transition temperatures was approximated with linear elastic fracture behaviour.

3. Results

Figure 4 shows the Charpy impact energy of as-purchased steels as a function of the testing temperature whereas Figure 5 shows the same relationship for investigated steels as strain-aged. The nil-ductility transition temperatures (NDT) measured at drop-weight test are also indicated in both diagrams. As may be seen, the ductile/brittle transition temperatures of the investigated steels are shifted against higher values due to strain-aging. However, the shift of nil-ductility transition temperatures nearly in all the cases shows a slightly opposite trend which is somewhat surprising.

The CVN impact energy, the yield stress σ_{ys} and the fracture toughness K_{IC} of the investigated steels measured at nil-ductility temperatures are given in Table 2 for both as-purchased and as strain-aged condition. However, because of

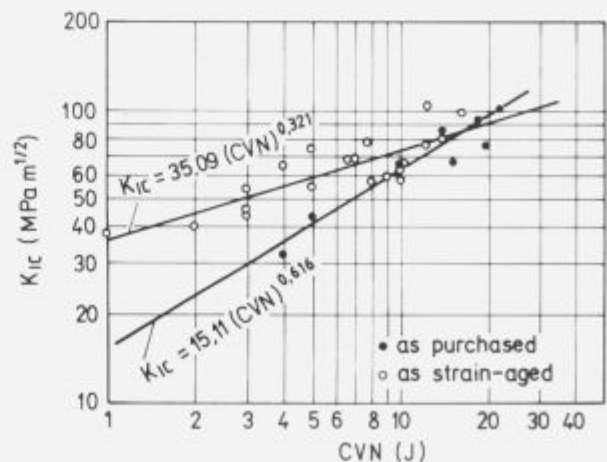


Figure 6: Relation between K_{IC} and CVN values in the nil-ductility temperature range
Slika 6: Odvisnost med K_{IC} in Charpyjevo udarno žilavostjo z V zarezo v območju temperatur ničelne duktilnosti

the lack of diameter of the round-notched specimens for K_{IC} measurements, only the limited number of the entire data are taken into account, namely only data complying with the requirement (2).

Table 2: Mechanical properties of the investigated steels at nil-ductility temperatures (28 valid measurements)

No.	σ_{ys} (MPa)	CVN (J)	K_{IC} (MPa m ^{1/2})	
			measured	calculated Eq.(5)
As purchased				
1	908	13	68.5	75.2
2	900	19	76	80.4
3	524	5	43.5	45.1
4	354	4	31.5	34.2
5	717	10	65	62.1
6	1071	12	85	81.8
7	1056	17	91.5	86.7
8	1054	21	100.5	90.1
As strain-aged				
9	681	7	68.5	56.3
10	780	3	53	52.0
11	780	4	63	54.9
12	745	5	73	55.7
13	803	8	56.5	63.7
14	791	10	58.2	65.9
15	781	10	65.5	65.9
16	1074	11	106	80.6
17	790	9	59	64.5
18	791	3	45	51.2
19	675	5	53	52.5
20	665	10	62.3	59.4
21	658	1	38.5	38.1
22	595	2	40	40.9
23	564	3	44.5	42.8
24	933	6.5	68.5	67.0
25	855	7.5	76.5	65.4
26	1343	11	75.5	92.2
27	1308	12	80	92.2
28	1293	14	99	94.3

The relationship between the CVN impact energy and the fracture toughness K_{IC} of the investigated steels is shown in the diagram of **Figure 6**. From the data point distribution it can be concluded that two different correlations between K_{IC} and CVN could be deduced, one for steels as purchased and another one for steels as strain-aged. Mathematical approximation with power function shows that the correlation for steels as purchased can be expressed as:

$$K_{IC} = 15.11 (CVN)^{0.616} \quad (3)$$

with a regression coefficient of 0.945, whereas the correlation for steels as strain-aged can be represented as:

$$K_{IC} = 35.09 (CVN)^{0.321} \quad (4)$$

with a regression coefficient of 0.819. As strain-aging provokes a considerable increasing of the yield stress of all the investigated steels, we tried to establish a unique correlation between K_{IC} on one side and both the properties CVN and σ_{ys} on the other side. The following correlation

$$K_{IC} = 0.776 \sigma_{ys}^{0.030} (CVN)^{0.19} \quad (5)$$

with a regression coefficient of 0.921 was deduced from the whole set of experimental data given in **Table 2**.

4. Discussion

Charpy V-notch impact toughness measurements and quasi-static fracture toughness measurements on some none- and low-alloyed structural steels in as purchased and as strain-

aged condition respectively were performed over the temperature range of nil-ductility transition temperatures i.e. over the temperature range of -140°C to -40°C. The decrease of the NDT temperatures of steels as strain-aged regarding to the as purchased steels suggests that NDT temperature of steels as strain-aged is a good enough index temperature to represent the quasi-static fracture toughness transition behaviour of such steels, but it is maybe not an enough conservative estimation for the determination of the FTE temperature (NDT + 40°C). A similar ascertainment, but for dynamic fracture toughness transition behaviour of some stress-relief heat-treated steels for nuclear reactor pressure vessels, has been previously published by Tanaka and coworkers⁸. Nevertheless, it seems that the NDT temperatures, measured either in steels as purchased or after strain-aging, correspond to the adequate K_{arrest} value. Because the drop-weight test employs a sharp crack, moving rapidly from the notched brittle weld bead into the test plate, it does not come as a surprise either to find that the NDT temperature defined by this test correlates well with the beginning of an increase in fracture toughness with temperature measured in quantitative, sharp-crack tests¹³.

Two different correlations between fracture toughness K_{IC} and CVN values for both groups of steels in the temperature range investigated show that steels after strain-aging have a noticeable higher fracture toughness K_{IC} than as purchased steels with the same Charpy energy. However, a very good correlation between K_{IC} and both properties, CVN and σ_{ys} was also deduced from all the data. The regression coefficient of Equation (5) is relatively high so that this approach seems to be relevant. Rolfe and Barsom¹¹ ascertained that the effects of both the notch acuity and the loading rate should be considered to establish correlations between K_{IC} and CVN test results in the transition-temperature region. They found out that K_{IC} values and CVN values in the transition-temperature region can be correlated (a) when the test results for slow-bend K_{IC} specimens are related to the test results for slow-bend fatigue-cracked CVN specimens and (b) when the test results for dynamic K_{IC} specimens are related to the test results for dynamic-cracked CVN impact specimens. The correspondence between K_{IC} and the CVN energy-absorption values obtained at a particular test temperature and the same strain-rate for both K_{IC} and CVN can be approximated by^{1,10}

$$K_{IC} = A E (CVN)^{0.5} \quad (6)$$

where A = constant of proportionality, E = Young's modulus, and K_{IC} and CVN are tested at the same temperature and strain rate.

The constant of proportionality, A, incorporates - in accordance with Rolfe and Barsom¹¹ - the effects of specimen size as well as notch acuity. By changing the value of A in Equation (6) it is then possible to correlate the K_{IC} data and the CVN energy-absorption values obtained by testing V-notched specimens. This equation suggests that the relationship between slow-bend K_{IC} and slow-bend CVN test results is the same as the relationship between the impact K_{IC} (i.e. K_{ICd}) and the impact CVN results. This observation is not unexpected because it was shown¹¹ that a particular change in loading rate causes an equal shift along the temperature axis for both the CVN data and the K_{IC} data. Both authors also concluded that an engineering estimation of K_{IC} at any strain-rate can be predicted by using impact CVN data in conjunction with Equation (6) and then shifting the curve to lower temperatures. This approach has been used in investigating the effects of irradiation for steels used in nuclear reactors¹¹. The magnitude of the temperature shift between dynamic and slow-bend curves was given by

$$T_{shift}(^{\circ}C) = 118.4 - 0.12 \sigma_{ys} \quad (7)$$

and valid for steels with the yield stress σ_{ys} up to a value of 1000 MPa approximately, whereas it is diminished at steels with higher yield stresses. The general procedure to estimate K_{IC} values in the transition-temperature region from CVN impact results comprises the calculation of K_{Id} values at each test temperature using Equation (6) with followed shift of K_{Id} values at each temperature by the temperature shift calculated with Equation (7) to obtain static K_{IC} values as a function of temperature. This procedure was adopted from more recent recommendations of Rolfe and Barsom¹⁾ and it represents a conceptual advantage compared to the previously published methods^{4,5)}. By comparing our Equation (3) for as purchased steels with the Rolfe-Barsom Equation (6) one can see that the exponents in both equations are relatively close. If the exponent of 0.5 is adopted also in our case owing to simplicity and considering some unaccuracy in our calculations (small number of data for relevant statistical analyse), then Equation (3) can be transformed into

$$K_{IC} = 20 (CVN)^{0.5} \quad (8)$$

where the calculated constant of 19.97 was rounded up to a value of 20.

It could be assumed that Equation (8) represents the lower envelope of all the measured values i.e. it represents the realistic conservative estimation of the fracture toughness of the investigated steels in the temperature range of nil-ductility transition temperatures irrespective by their microstructure or prehistory. Nevertheless, at very low CVN absorbed energies our equation gives higher K_{IC} values compared with the values obtained from the previously established Barsom-Rolfe equation for the transition temperature range⁴⁾. Namely, the mentioned authors⁴⁾ found that the plane strain fracture toughness K_{IC} in the transition region is related to the Charpy energy CVN by

$$K_{IC}^2 = 0.22 E (CVN)^{3/2} \quad (9)$$

where the Young modulus E is expressed in GPa, K_{IC} is expressed in $\text{MPa m}^{1/2}$, and CVN in Joules. The 54 J Charpy energy commonly used to determine the transition temperature of similar steels¹²⁾ corresponds roughly to 150 $\text{MPa m}^{1/2}$ when the relationship (9) is used. Quite a similar value is obtained also with Equation (8), which means that both equations could be applied in the transition temperature range. It is not surprising because the loading rate and the notch acuity do not have a great influence on the fracture-toughness behaviour at slightly higher toughness values.

Besides the above mentioned equations of Barsom and Rolfe^{4,10)} (6),(8) there are also some other successful attempts. Namely, Begley and Logsdon⁵⁾ suggested that for low temperatures where the behaviour is predominantly brittle, the fracture toughness (in $\text{MPa m}^{1/2}$) may be related empirically to the yield stress σ_{ys} (in MPa) alone:

$$K_{IC} = 0.0717 \sigma_{ys} \quad (10)$$

Although Equation (10) essentially differs either from the equations of Barsom and Rolfe^{4,10)} or from our equations (3) and (4), it is not in larger disagreement with our observations since for lower Charpy shelves both approaches give a considerably higher fracture toughness for as strain-aged steels with higher yield stress. The empirical correlation (10) is also in good agreement with K_{Id} data¹⁴⁾ so our linking the Eq. (10) with the equation of the type $K_{IC} = A (CVN)^b$ into a single form (5) was relevant. The relatively high regression coefficient for this new correlation (5) i.e. a correlation which is compatible with the Barsom and Rolfe^{4,10)} approach as well as with the approach of Begley and Logsdon⁵⁾ confirm that Eq. (5) enables the best empirical estimation of the low-temperature fracture toughness K_{IC} calculated on the basis of

conventional mechanical properties measured in the temperature range investigated as it is also shown in Table 2.

5. Conclusions

1. The fracture toughness was measured in the temperature range of nil-ductility temperatures of nine non- and low-alloy structural steels either in as purchased or as strain-aged condition and it was correlated with the Charpy V-notch impact energies. Although the strain-aging reduces the Charpy energies i.e. provokes some shifts of Charpy values to higher temperatures, it also decreases the nil-ductility temperatures of such steels.

2. The fracture toughness K_{IC} of the investigated steels in the temperature range of nil-ductility temperatures can be successfully predicted either by the Equation (3) for as purchased steels or by the Equation (4) for steel as strain-aged. The estimation of K_{IC} , which would be conservative enough for both states of steels can be given by the Equation (8) which has also a simple form.

3. In general, the most suitable and still plain procedure for obtaining the actual fracture toughness K_{IC} of structural steels in the temperature range of nil-ductility temperatures, being also compatible with various other concepts^{1,4,5,10)}, would comprise tensile and Charpy testing at lower temperatures and further application of the generalized correlation (5).

The correlation (5) suggests that K_{IC} and probably also K_{arrest} of as strain-aged steels would be higher than that of as purchased steels with the same Charpy energy because of the increasing yield stress at strain-aging. Consequently, strain-aged steels have lower NDT temperatures than those of as purchased steels.

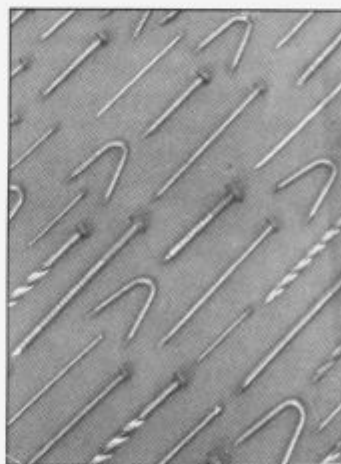
REFERENCES

- Rolfe, S.T.; Barsom, J.M.: *Fracture and Fatigue Control in Structures, Applications of Fracture Mechanics*. Englewood Cliffs, New Jersey, Prentice-Hall 1977.
- Bamford, W.; Oldfield, W.; Marston, T.: *An Improved Reference Fracture Toughness Procedure for Pressure Vessel Steels*, 5th ICPVT, San Francisco, 9./14.9.1984, p. 932/65.
- Kussmaul, K.; Demler, T.: *Steel Research* 63 (1992) No. 12, p. 545/53.
- Barsom, J.M.; Rolfe, S.T.: *Correlations Between K_{IC} and Charpy V-Notch Test Results in the Transition-Temperature Range*, Impact Testing of Metals, ASTM STP 466, American Society for Testing and Materials, Philadelphia, 1970, p. 281/302.
- Begley, J.A.; Logsdon, W.A.: *Correlation of Fracture Toughness and Charpy Properties for Rotor Steels*, Scientific Paper 71-1E7-MSLRP-P1, Westinghouse Research Laboratories, Pittsburg, July, 1971.
- Tanaka, Y.; Iwade, T.; Suzuki, K.: *Int. J. Pres. Ves. & Piping* 31 (1988), p. 221/236.
- Dieter, G.E.: *Mechanical Metallurgy*, McGraw-Hill, 1986, p. 358.
- Shen Wei et al.: *Engng. Fracture Mech.* 16 (1982), p. 69/82.
- Wang Chang: *Engng. Fracture Mech.* 28 (1987), p. 241/250.
- Barsom, J.M.: *Engng. Fracture Mech.* 7 (1975), p. 605/18.
- Hawthorne, J.R.; Mager, T.R.: *Relationship Between Charpy V and Fracture Mechanics K_{IC} Assessments of A533-B Class 2 Pressure Vessel Steel*, ASTM STP 514, American Society for Testing and Materials, Philadelphia, 1972.
- Faucher, B.; Dogan, B.: *Metallurgical Transactions A*, 19A (1988), 505/16.
- Langford, W.J.: *Canadian Metallurgical Quarterly* 19 (1980), p. 13/22.
- Scarlin, R.B.; Shakeshaft, M.: *Metals Technology*, January 1981, p. 1/9.

IZDELUJE



- žice
- paličasta jekla in vlečene žice
- dodatne materiale za varjenje
- žeblje



Recrystallization of Ni-based Superalloy after Cold Deformation

Rekristalizacija Ni-superzlitine po hladni deformaciji

M. Torkar, B. Šuštaršič and F. Vodopivec, Inštitut za kovinske materiale in tehnologije, Ljubljana

The strain hardening and isothermal recrystallization after cold deformation of Ni-based superalloy was investigated. Cold deformation below 10% and annealing temperature above 1050°C promote the growth of recrystallized grains. A cold deformation, not lower than 10% and annealing between 1000°C and 1050°C for 30 minutes, produce fine recrystallized grains.

Key words: Ni-based superalloy, cold deformation, strain hardening exponent, static recrystallization

Izvršena je bila raziskava utrjevanja pri hladni deformaciji in poteka izotermne rekristalizacije po hladni deformaciji Ni-superzlitine. Rezultati kažejo, da končna hladna deformacija pod 10% in temperatura žarenja nad 1050°C pospešujeta nastanek velikih rekristaliziranih zrn. Hladna deformacija nad 10% in 30 minutno rekristalizacijsko žarjenje med 1000°C in 1050°C zagotavljata drobno zrnato rekristalizirano mikrostrukturo.

Ključne besede: Ni-superzlitina, hladna deformacija, eksponent napetostnega utrjevanja, statična rekristalizacija.

1. Introduction

Ni-based superalloys are used in manufacturing of turbine-type machinery, for rotors, vanes and combustion chambers, for exhaust valves in automotive industry, in the tool industry for hot work dies, further in nuclear power plants and for petrochemical equipment as well as in many other places, where a combination of good mechanical properties and corrosion resistance are demanded. Despite of the material development, oriented to Fe-, Ni-, Ti-aluminides and other intermetallics, the Ni-based superalloys remain the base material for use for the critical components (ref. 1).

Ni-based superalloys with chromium and other alloying elements are strengthened by precipitation hardening. The matrix is strengthened by precipitation of (Ni₃AlTi) particles and the grain boundaries by carbide particles, which prevent the grain growth (ref. 2).

As cast Ni-based superalloys have a limited hot workability. The hot working is easier in a narrow temperature range above the creep range and below the solidus line, where virtually no precipitates are found in the microstructures. For most of the alloys with limited hot workability the use of hot extrusion is more suitable especially if it is performed at lower deformation rate (ref. 3).

Electric slag remelting also improves the hot workability of the alloy (ref. 4,5).

The mastering of the hot working in order to obtain the optimal properties, demands a strict control of the grain size and therefore it is important to control the process of grain growth and the grain size from the solidification to the final cold working. During the hot deformation dynamic recovery and recrystallization occur and cause a much lower rate of strain hardening than is found at room temperature (ref. 6). After cold deforma-

tion only static recrystallization occurs during the annealing. The aim of the research was to determine the strain hardening at cold deformation as well as to establish the influence of deformation grade and annealing temperature on the start of recrystallization and grain growth.

2. Experimental

The alloy with the following composition: 21% Cr, 1.7% Co, 2.5% Ti, 1.7% Al, 0.62% Mn, 0.72% Si, 0.74% Fe, 0.05% C, bal. Ni, all in wt. %, was melted in induction furnace. The ingots of 60 x 60 mm cross section were cast, electric slag remelted (ESR) into ingot of 100 mm diameter and forged to the bar of 15 mm diameter.

Cylindrical specimens with 13 mm of diameter and length of 10 mm were machined from the forged bar, solution annealed at 1150°C and water quenched. Some samples were continuously compressed with a maximal logarithmic deformation up to 0.9. The exponent of strain hardening (n) was calculated by the method described in ref. 7.

Other samples were subjected to 3, 5, 10, 20, 30 and 50% of cold deformation with compression. In both cases a teflon foil was used as lubricant to diminish the friction, between the tooling and the specimen.

After the cold deformation the specimens were isothermal annealed 30 minutes at 900, 1000, 1050, 1100 and 1150°C, water quenched and submitted to the examination in optical microscope.

3. Results

The microstructure of solution annealed and water quenched specimen is shown on Figure 1.

The strain hardening at cold deformation is shown on **Figure 2**. Factor k_f represents the true yield stress, i.e. the true stress in the sample in the moment of the load action. It was established (ref. 7) that the curve of flow stress at compression test in the interval from $\gamma = 0.2$ to $\gamma = 1.0$ can be approximated with the following parabolic function:

$$k_f = k_{f,0} \gamma^n$$

The exponent of strain hardening (n) can be estimated from the equation:

$$n = \frac{\ln k_{f,0.2} - \ln k_{f,1.0}}{\ln 0.2}$$

using the values for $k_{f,0.2}$ and $k_{f,1.0}$ from **figure 2**. The calculated exponent of strain hardening was $n = 0.44$. The value for k_f (N/mm^2) can be calculated by using the following equation:

$$k_f = 1770 \times \gamma^{0.44}$$

The logarithmical deformation ϕ is calculated by the following equation:

$$\gamma = \frac{h_0}{h}$$

where h_0 - represents the initial height of the sample and h - the true height of the loaded sample at each step of deformation.

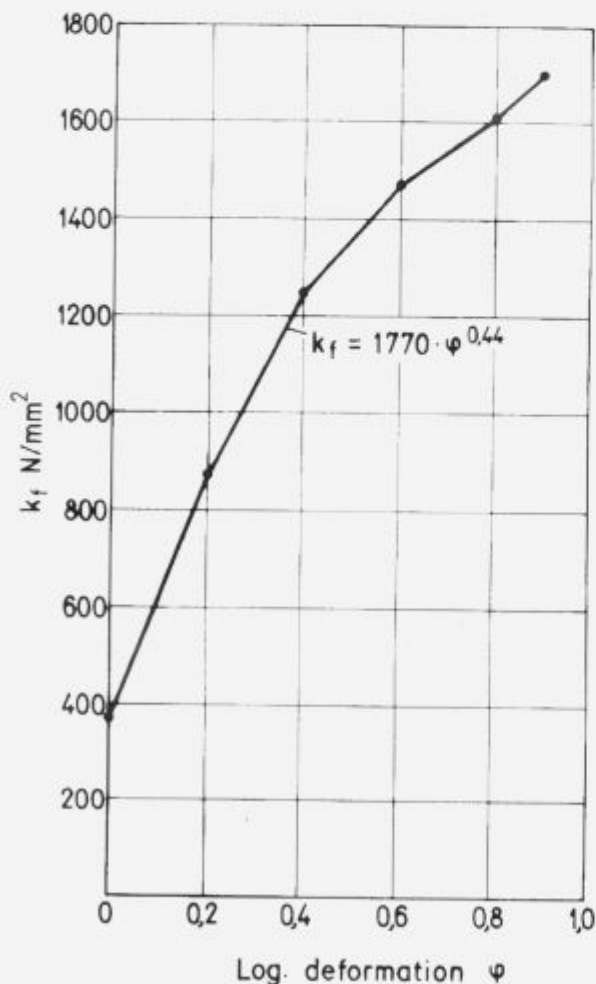


Figure 2: The strain-stress relationship
Slika 2: Odvisnost med deformacijo in silo

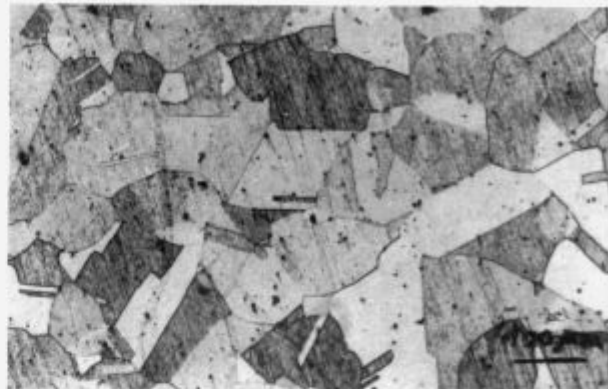


Figure 1: Microstructure after solution annealing
Slika 1: Mikrostruktura po toplinem žarjenju

The microstructure of the alloy after cold deformation and annealing in temperatures range 900 to 1050°C for 30 minutes are shown in **Figure 3, 4 and 5**.

Elongated grains on **Figure 3** show the alloy remain unrecrystallized after annealing at 900°C. At 1000°C the recrystallization occurs by at least 10% of cold deformation.

The lowest temperature at which recrystallization occurs at all grades of deformation is about 1050° C.

At the same annealing temperature the grain size of recrystallized grains decreases with the increasing deformation. At higher temperature the recrystallized grain starts to grow. **Figure 6** shows the connections between the grade of cold deformation and the temperature on the start and advance of recrystallization.

Both, higher annealing temperature and higher cold deformation promotes the start of recrystallization.

The grain size was measured from the micrographs, and represented as ASTM number in **Figure 7**, as relationship between the size of recrystallized grains, the grade of cold deformation and the annealing temperature.

A fine grained recrystallized microstructure can be obtained by at least 10% grade of cold deformation at temperature between 1000 and 1050°C and after 30 minutes of annealing. Higher annealing temperature promotes the grain growth of recrystallized grains.

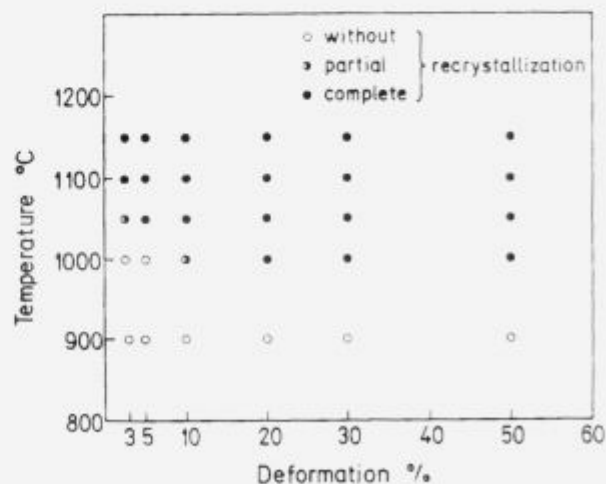


Figure 6: Relationship between the grade of cold deformation, the temperature of annealing and the start of recrystallization.

Slika 6: Povezava med stopnjo hladne deformacije, temperaturo žarjenja in pričetkom rekristalizacije.

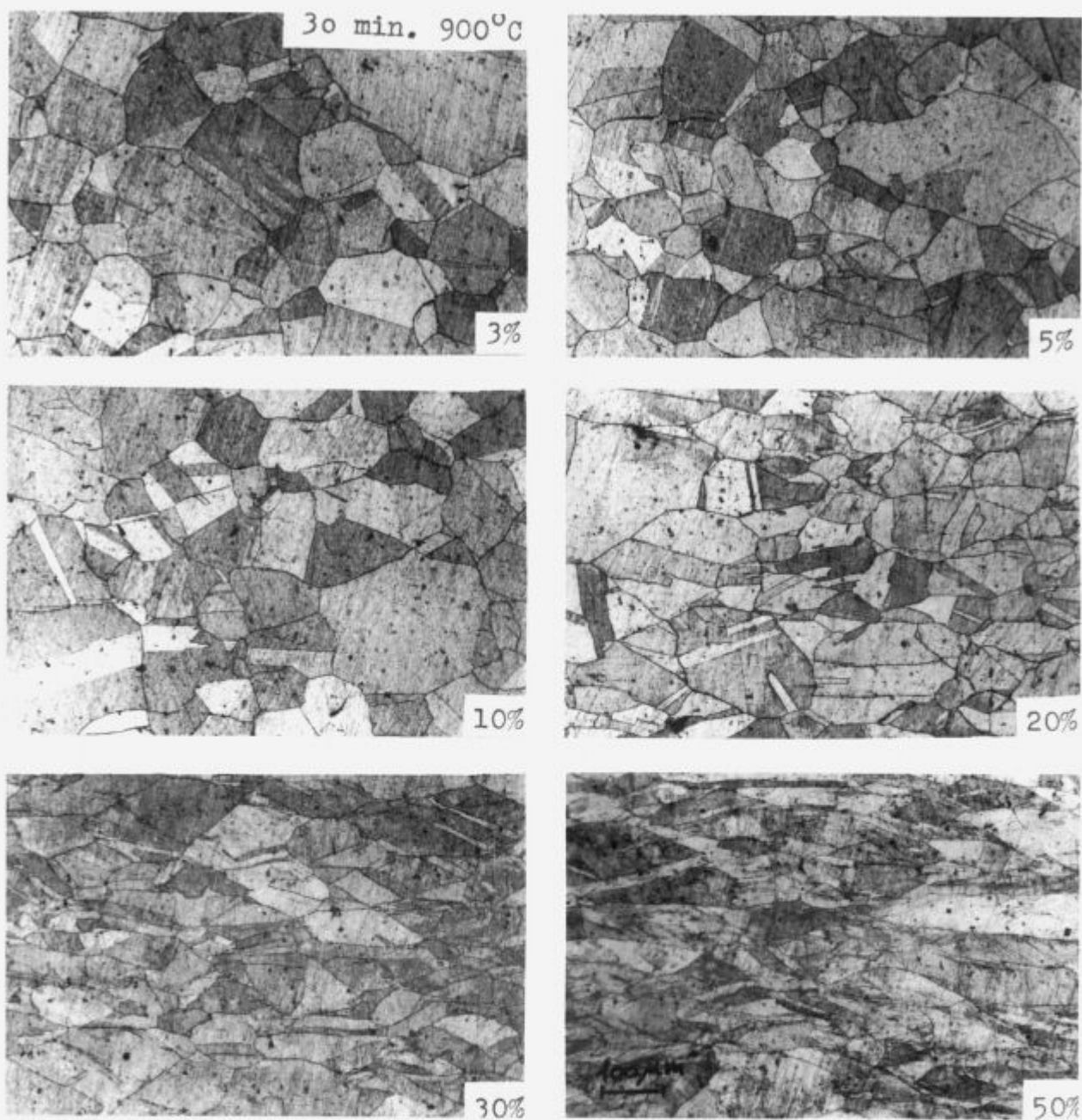


Figure 3: Microstructure of the alloy after cold deformation 3 to 50% and annealing 30 minutes at 900°C.
Slika 3: Mikrostruktura hladno deformirane (stopnja deformacije 3 do 50%) zlitine po 30 minutnem žarjenju na 900°C.

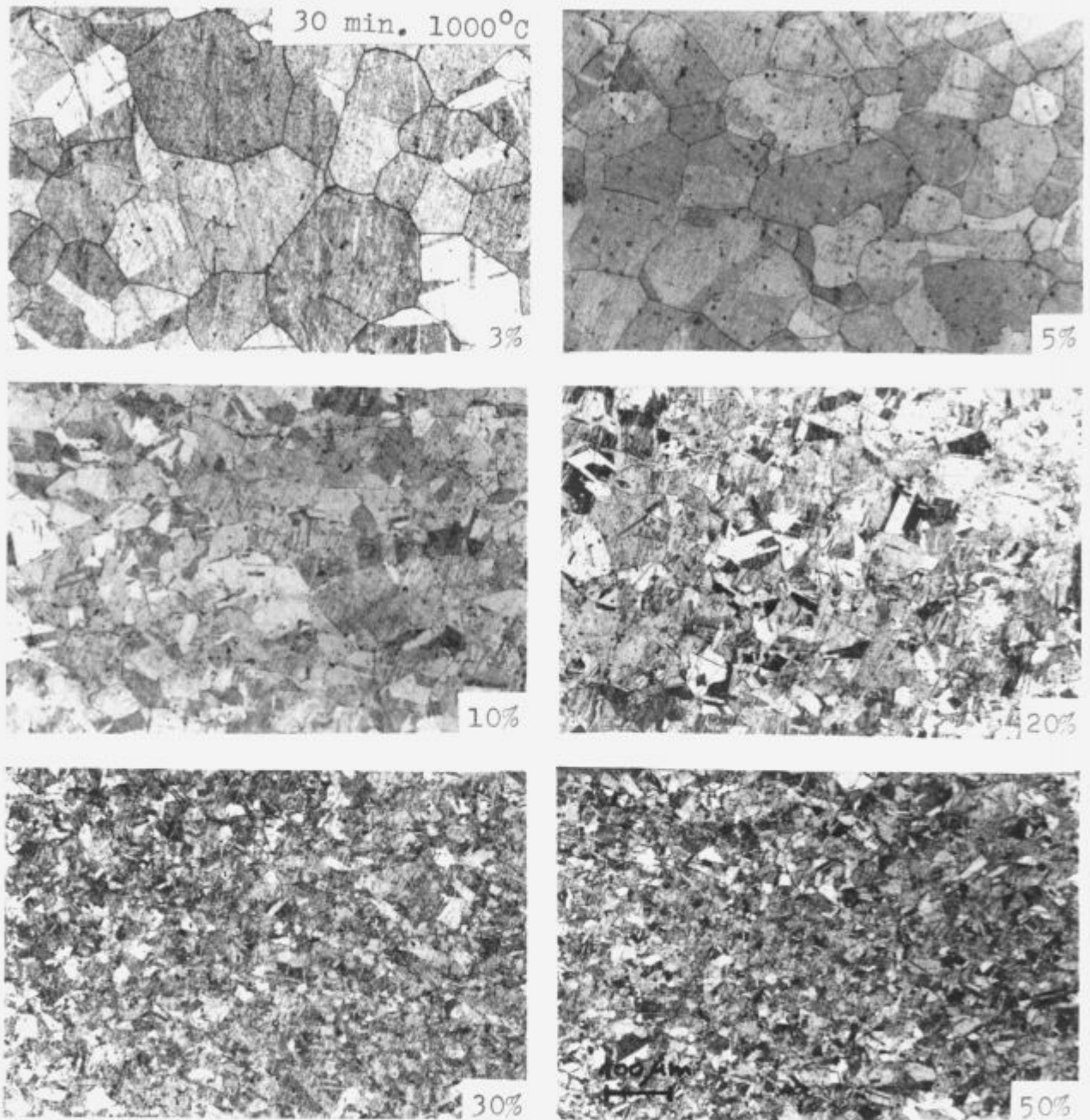


Figure 4: Microstructure of the alloy after cold deformation 3 to 50% and annealing 30 minutes at 1000°C.
Slika 4: Mikrostruktura hladno deformirane (stopnja deformacije 3 do 50%) zlitine po 30 minutnem žarjenju na 1000°C.

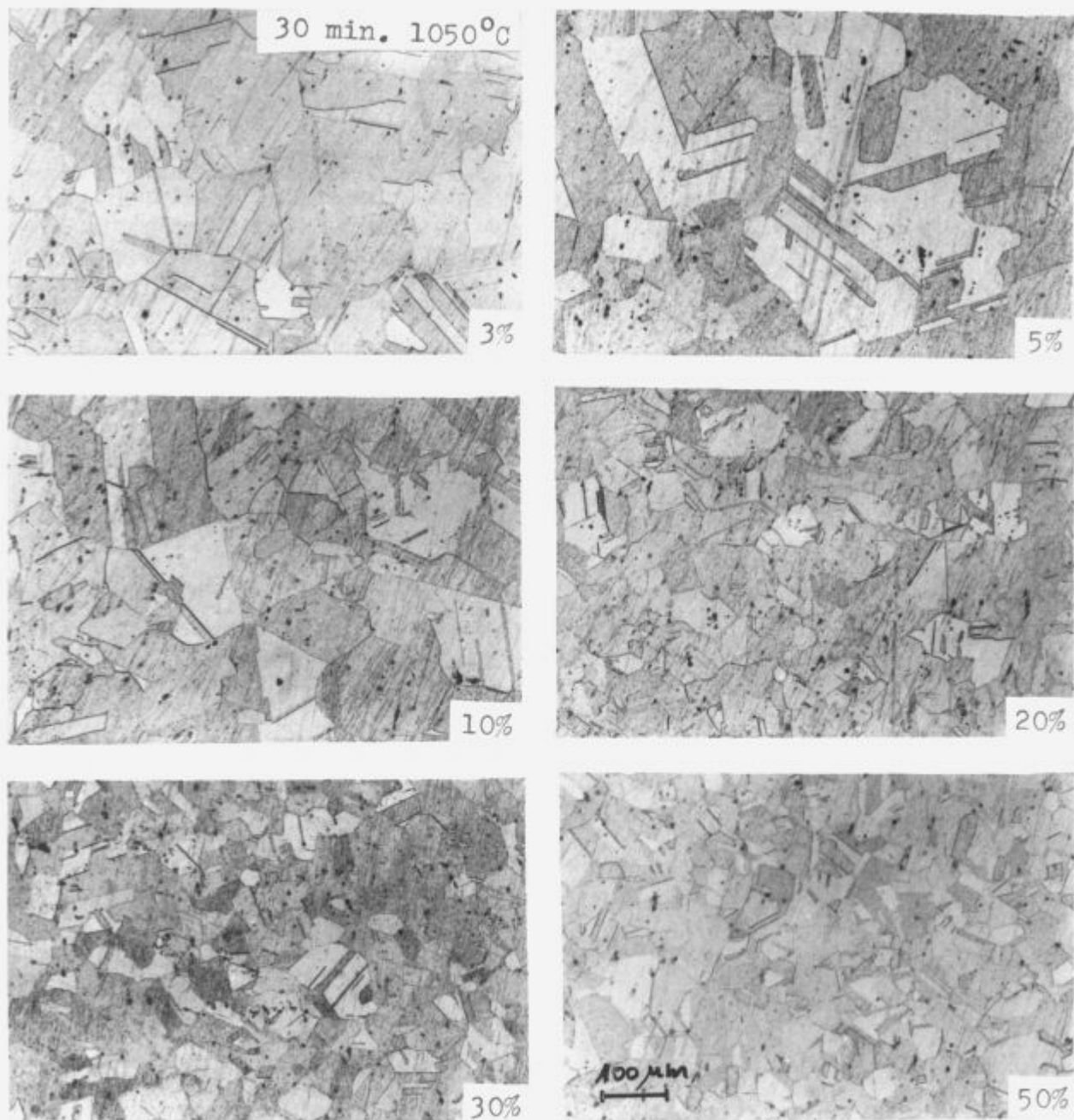


Figure 5: Microstructure of the alloy after cold deformation 3 to 50% and annealing 30 minutes at 1050°C.
Slika 5: Mikrostruktura hladno deformirane (stopnja deformacije 3 do 50%) zlitine po 30 minutnem žarjenju na 1050°C.

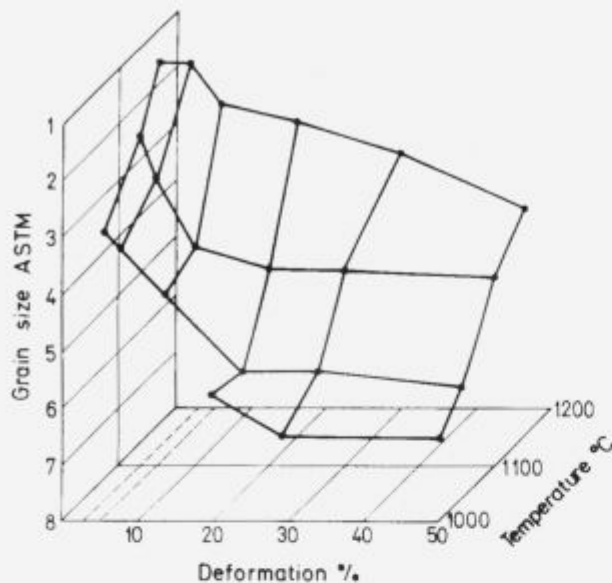


Figure 7: Effect of cold deformation and annealing temperature on recrystallized grain size after 30 minutes of annealing.

Slika 7: Vpliv stopnje hladne deformacije in temperature žarjenja na velikost rekristaliziranih zrn po 30 minutnem žarjenju.

4. Conclusions

Ni-based superalloy was cold deformed by compression test and a hardening exponent $n = 0.44$ was obtained. The strain hardening can be calculated by the following equation:

$$k_r = 1770 \times \gamma^{0.44}$$

The investigation of the isothermal recrystallization of the superalloy showed that a small grade of deformation (below

10%) and a higher temperature (above 1050°C) of annealing promotes the recrystallized grain growth.

The occurrence of partial recrystallization is limited to a relatively narrow temperature range near 1050°C at deformation below 10% and near 1000°C at deformation over 10%.

Finer recrystallized grains of Ni-based superalloy are obtained after a cold deformation not lower than 10% and 30 minutes of annealing between 1000°C and 1050°C.

At annealing above the 1050°C the recrystallized grains start to growth.

5. Acknowledgements

The authors wish to express their gratitude to the Ministry of Science and Technology of Slovenia for the financial assistance of this research.

6. References

- ¹ G.Sauthoff: Z. Metallkde., Bd.81 (1990), H.12, 855-861
- ² N.L.Loh, K.Y.Sia: Journal of Materials Processing Technology, 30, (1992), 45-65
- ³ G.N.Maniar, D.A.Nail, H.D.Solomon: Optimization of Processing, Properties and Service Performance through Microstructural Control, ASTM Special Technical Publication 672, Philadelphia 1979
- ⁴ M.Torkar, A.Kveder, F.Vodopivec, A.Rodič, I.Kos: Poročilo MIL, Nr. 86-029, 1986, Ljubljana
- ⁵ A.Choudhury: ISIJ International, Vol.32 (1992), No. 5, 563-574
- ⁶ H.J.McQueen, G.Gurewitz, S.Fulop: High Temperature Technology, February 1983, 131-138
- ⁷ B.Ule: Poročilo MIL, Nr.85-033, 1985, Ljubljana.

The Rheological Model of Deformation Nidus in the Process of Rolling

Reološki model deformacijskega prostora v procesu valjanja

G. G. Shlomchack, Dnepropetrovsk Metallurgical Institute, Ukraine

I. Mamuzić, Metalurški fakultet, Sisak, Hrvatska

F. Vodopivec, Inštitut za kovinske materiale in tehnologije, Ljubljana

On the basis of contemporary ideas on the metal pressure shaping theory and investigation results of the metal stress-strained state during rolling and using variation principles of mechanics, the plastometric classification of metals and alloys, a new rheological model of the high deformation nidus is proposed in this work. The model explains the regularities in the distribution of plastic deformation intensity in the non-contact zones as well as the formation of the feed front end deformation in dependence of the plastometric properties of metals. Experimental data confirming the validity of the model are given also.

Key words: rolling, plastometry, rheology, deformation, straining, deformation nidus.

Na osnovi sodobnih pogledov o teoriji oblikovanja kovin, raziskav napetostnega stanja v kovini med valjanjem, z uporabo variacijskih načel mehanike in plastometrične razvrstitve kovin in zlitin, se predlaga nov reološki model visoko deformiranega prostora. Ta model razlaga regularnosti v porazdelitvi intenzitete plastične deformacije v coni brez kontakta in nastanek čela deformacijskega prehitevanja v odvisnosti od plastometričnih lastnosti kovin. V članku so priloženi eksperimentalni podatki, ki potrjujejo veljavnost modela.

Ključne besede: valjanje, plastometrija, reologija, deformacijska utrditev, deformacijski prostor.

1. Introduction

In spite of the intensive development of mathematical modelling and experimental methods of mechanics, the theory of rolling at present doesn't dispose of reliable informations on the mechanism of building-up of the deformation nidus. Especially little is known on the regularities of metal flow at unstable stages of the process. This may result in the slow development of blooming rolling technology, a low rolling yield and sometimes also in an unsuitable quality of semifabricate.

The plastometrical (rheological) properties of metals play a very important role in the formation of the deformation nidus. The influence of rheology on the development of regularities of deformation at rolling of rheologically complex materials is especially important by extremes on $\sigma - \epsilon$ curves. In references 1 and 2 the higher order deformation anomalies during the testing of rheologically complex materials by means of plastic tensional are described. The necking of the sample with the decrease of resistance to deformation ($d\sigma/d\epsilon < 0$) on the $\sigma - \epsilon$ curve represents the secondary deformation heterogeneity. With increased resistance to deformation, according to the $\sigma - \epsilon$ curve, a second secondary deformation homogeneity appears in form of uniform elongation of the neck. Thus, changes on the $d\sigma/d\epsilon$ curve are alternated by anomalies in deformation gradient and intensity. This is the base for the proposed rheological classification of materials shown in fig. 1 and established on the basis of experimental data: I class- simple unstrengthenable materials; II class-simple strengthenable materials; III-V classes - complex strengthenable materials.

The experimental investigation of the deformation nidus stress strained state was realised considering the requirements of

the similarity theory (3) and using a laboratory device (4). It was necessary to reveal the mechanism of the formation of the knurl on the ends of rollings-a wide-spread defect on blooming rolling (fig. 2).

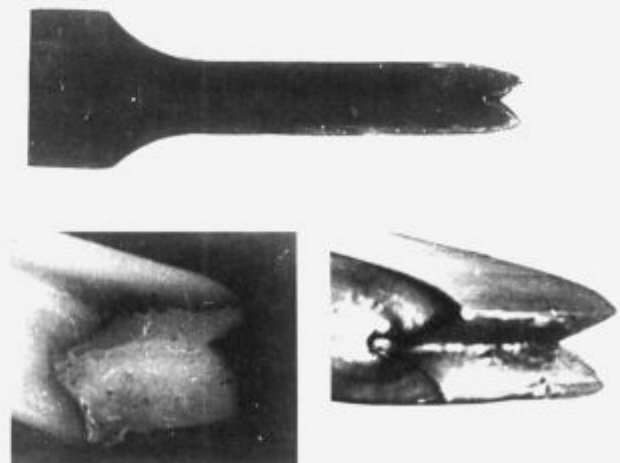


Figure 2: Widely spread defect: knurl on the front end of the rolling: a-general view; b-during rolling on the blooming "1300" at 1150°-1200°C; e-laboratory model of knurling.

Slika 2: Zelo razširjena napaka: odprta ustnica in čelo valjanca: a-splošen pogled; b-po valjanju na blumingu "1300" pri 1150°C-1200°C; e-laboratorijski model ustničenja

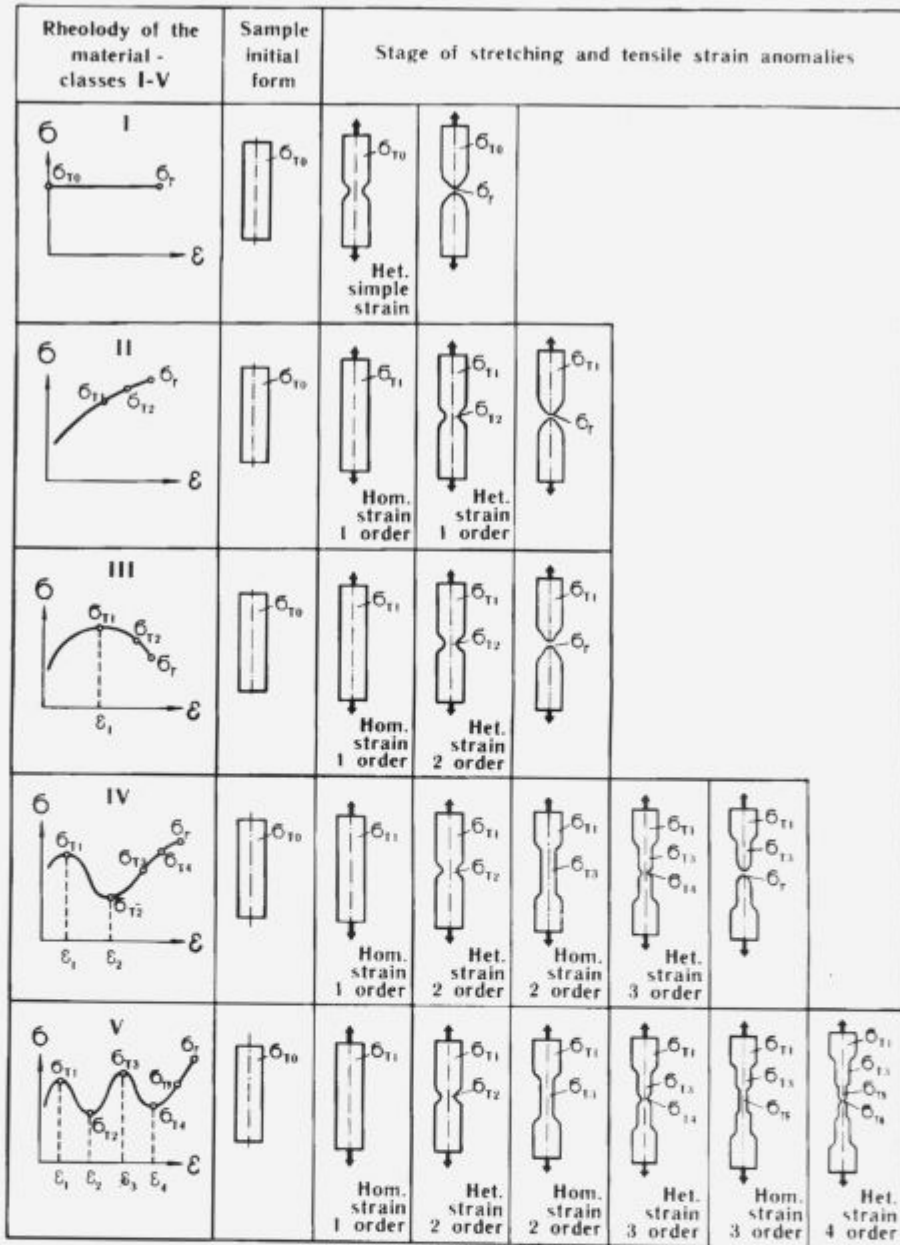


Figure 1: Rheological classes of materials

Slika 1: Reološki razredi kovin in zlitin

2. Experimental work and analysis of the results

Laboratory device for modelling

The investigated unstable process is a complex physical phenomenon in which all parameters: geometrical, rheological, evolution of deformation, stressed-deformed state and others change in time. A special automated laboratory equipment with modern measuring instruments was built for the modelling of this process considering the similarity criteria. The base of this device is a new rolling mill without spindles (fig. 3) - a model of blooming (5), with roll diameter of 80...200 mm and length of 120 mm, and a rolling force of 0.3 MN. The main drive is a direct-current motor of 1.5 kW. The circumferential speed of rolls varies within the ranges of 0-100 mmph and of 2-50 mmphs. On the device it is possible to obtain an unfinished rolling (an instantaneous deformation nidus) by means of "shooting off" the upper roll at a determined moment and use modern investigation

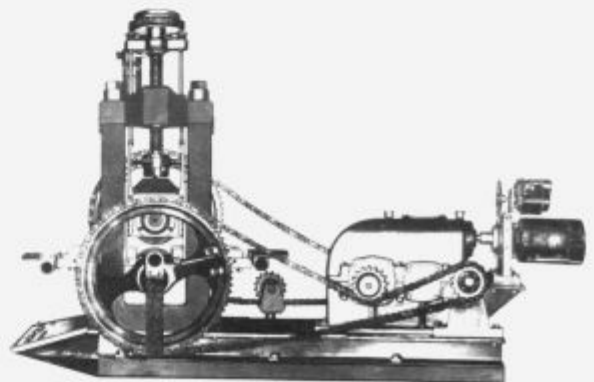


Figure 3: General view of the new laboratory rolling mill

Slika 3: Splošen pogled na novo laboratorijsko valjarno

methods such as moire, photoelasticity, filming and strain measurement to measure the integral characteristics of the process (efforts, moments, displacements and others).

The laboratory equipment includes also auxiliary devices for the preparation and realization of the trial: presses, stamps, tensometric and optical instruments, etc. All parts of the device are unified in an integrated system with an automatic programmed control which ensures the precision and quality of the tests.

The rheological model

Lead-a natural model of hot steels and alloys, has the remarkable property of recrystallization at room temperature. It deforms at low efforts, it is brazed reliably after grating using the moire method and has a perfect plasticity.

A careful study of its rheology shows one more lead property (fig. 4). At various strain rates shows plastometric curves of different rheological classes, from simple unstrengthenable I class (at $\epsilon < 0,01 \text{ s}^{-1}$) and strengthenable II class (at $\epsilon = 1 \dots 13,5 \text{ s}^{-1}$) to complex strengthenable III class (at $\epsilon = 13,5 \dots 60 \text{ s}^{-1}$) and IV class ($\epsilon = 0,01 \text{ s}^{-1}$).

This behavior makes it possible to use lead and its alloys as rheological models for different steels and alloys. Earlier investigations (6) showed that its use makes it possible to respect strictly the similarity criteria in the modeling of rolling processes on rolls of optical and organic glass by means of photoelastic observations. Technically pure lead (99,98% Pb) was used in this work.

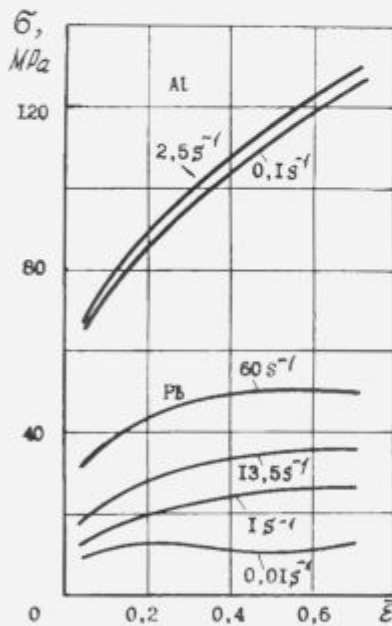


Figure 4: Plastometric curves Pb (99,98%) and Al (99,7%) at 20°C
Slika 4: Plastometrične krivulje za 99,98% Pb in za 99,7% Al pri 20°C

Nuclea of maximum strain rates during the rolling

Experimental investigations of the mechanism of the formation of the deformation nidus were performed after a theoretical and experimental analysis of the metal stress-strained state. Fig. 5a shows the intensity field of strain rates $H(x,y)$ obtained by solution of the variation problem using the methods proposed in ref. 7. Fig. 5b shows the experimental data for a stable process of rolling obtained by the moire method. Fig. 5c shows the field of strain rates $\epsilon(x,y)$ at the initial stage of cogging of the slab edges by edging rolls obtained by mathematical simulation using the method of finite elements (8).

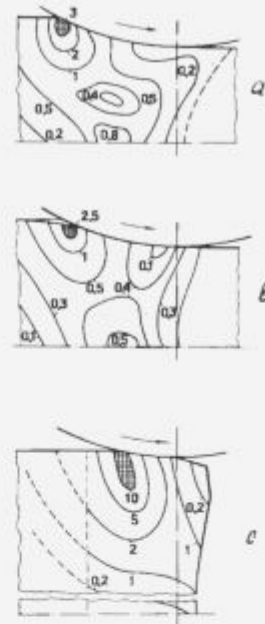


Figure 5: The field of strain rates in s^{-1} obtained by the methods of: a-finite differences (7); b-moire patterns and c-finite elements (8)
Slika 5: Polje deformacijskih hitrosti v s^{-1} izračunano po metodah: a-končne razlike (7); b-moire figure in c-končni elementi (8)

Though the methods were different, their results agree well and show several common features of the deformed state in the deformation nidus: 1-high heterogeneity of the deformation; 2-extension of plastic regions far beyond the geometrical limits of the deformation nidus, and the presence of the nuclea with maximum intensity of strain rates H_{\max} (hatched regions). The H_{\max} nuclea on fig.5a ($H_{\max} = 3 \text{ s}^{-1}$) and fig. 5b ($H_{\max} = 2,5 \text{ s}^{-1}$) are located in the initial contact regions at the very beginning of the deformation nidus.

An important conclusion can be derived from these results, the location of H_{\max} nuclea does not depend on the degree of metal fullness of the deformation nidus (see fig. 5c).

Mechanism of the formation of the knurl

The unstrengthenable metal through the regions of strain rates maximum intensity (H_{\max} nuclea) strives the flow towards the nearest free surface-towards the front end of the rolled piece. From the H_{\max} nucleus, as the source, it strives forward in direction of the rolling, overtaking the roll surface and the central part of the metal. This is how the knurl is formed (fig. 6a).

In case of rolling of strengthenable metal the size of the knurl depends on the strain hardening degree. This hardening grows adjacent, to contact layers and reaches in the nucleus a H_{\max} sufficient to deplace the stretching to deeper layers of the metal down to the center. Central layers rush forward and flatten the front edge of the rolled piece up to the complete elimination of the knurl (6b,c). Thus, the extension of strain in the front end of the rolled piece is determined by the rheological properties of the metal. During the hot rolling alternated by softening and recrystallization phenomena the rolling speed plays and important role. At low speed the H_{\max} strengthened nucleus has the time to soften. This explains the formation of the knurl while at high rolling speed and the virtual absence of softening the knurl is not formed.

Pictures of the samples in fig. 6a were obtained at different stages of the formation of the strain nidus and before the stabilization of the rolling process. The rolling was performed in the high-speed regime of the third rheological class, when the additional softening, which causes a strain heterogeneity of the sec-

ond order, occurs in the H_{max} nucleus. The layers adjacent to the contact surface do not soften not only because of shortage of time, but also because of the $d\sigma/d\epsilon < 0$ rheological anomaly. Sliding on the roll the metal in these layers is literally extruded from the strain nidus twisting towards the centre of the sample, and the formation of the knurl is intensified to the maximum.

During the rolling of lead in the regime of the second rheological class ($\epsilon = 1 \dots 1.5 s^{-1}$) the adjacent to contact layer of the metal has no time to soften and that prevents the formation of the knurl (fig. 6b).

Several experiments under the same conditions, but with different rolling speeds were performed additionally on aluminium with the aim to check the reliability of the explained mechanism. The plastometric characteristic of aluminium shows that it is a material of the second rheological class with strictly increasing function $\sigma - \epsilon$ (see fig. 4). In the deformation nidus it practically does not soften at room temperature. Thus the metal adjacent to the contact surface, strengthened by the passage of H_{max} nuclea (see fig. 5), is not elongated in the direction of the exit from the rolls and deeper layers of the metal are deformed. If at the first moment the adjacent to the contact layer of aluminium, which had no time to strengthen, outpaces the central area then, because of the strengthening, their deformation is delayed, while the central area is rushed forward outpacing the adjacent to the contact layers and prevents the formation of the knurl (see fig. 6c).

Thus, the mechanism of the formation of the strain nidus during the rolling is determined by the degree of metal rheological complexity.

The plants producing rolled carbon steels lose a considerable quantity of metal because of the cuttings. During the blooming rolling the shrinkage cavity is elongated simultaneously with the formation of the knurl and the quantity of rejects is increased. For

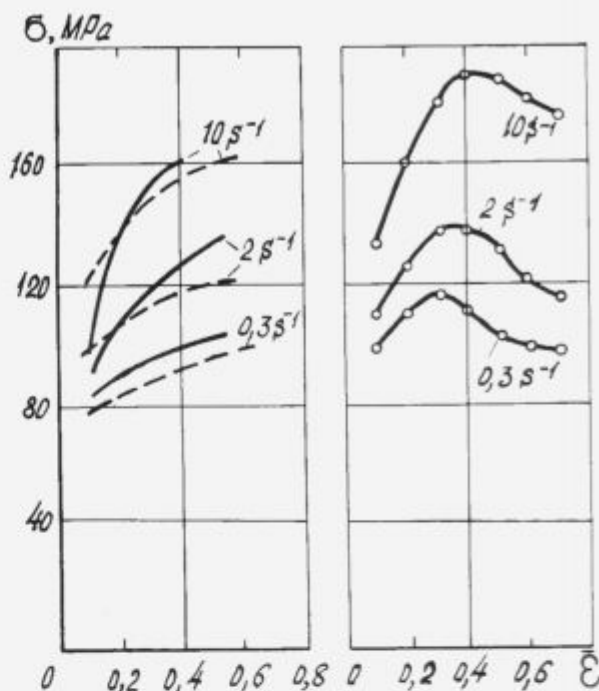


Figure 7: Plastometric curves of carbon steel (0.43% C; 0.26% Si; 0.74% Mn; 0.022% P; 0.016% S) at 900°C: a-from ref. (9), (10) (dotted line); and b-from ref. (11)

Slika 7: Plastometrične krivulje za ogljikovo jeklo (0,43% C; 0,26% Si; 0,74% Mn; 0,022% P; 0,016% S) pri 900°C: a-iz ref. (9), (10) (pikčasta črta); in b-iz ref. (11)

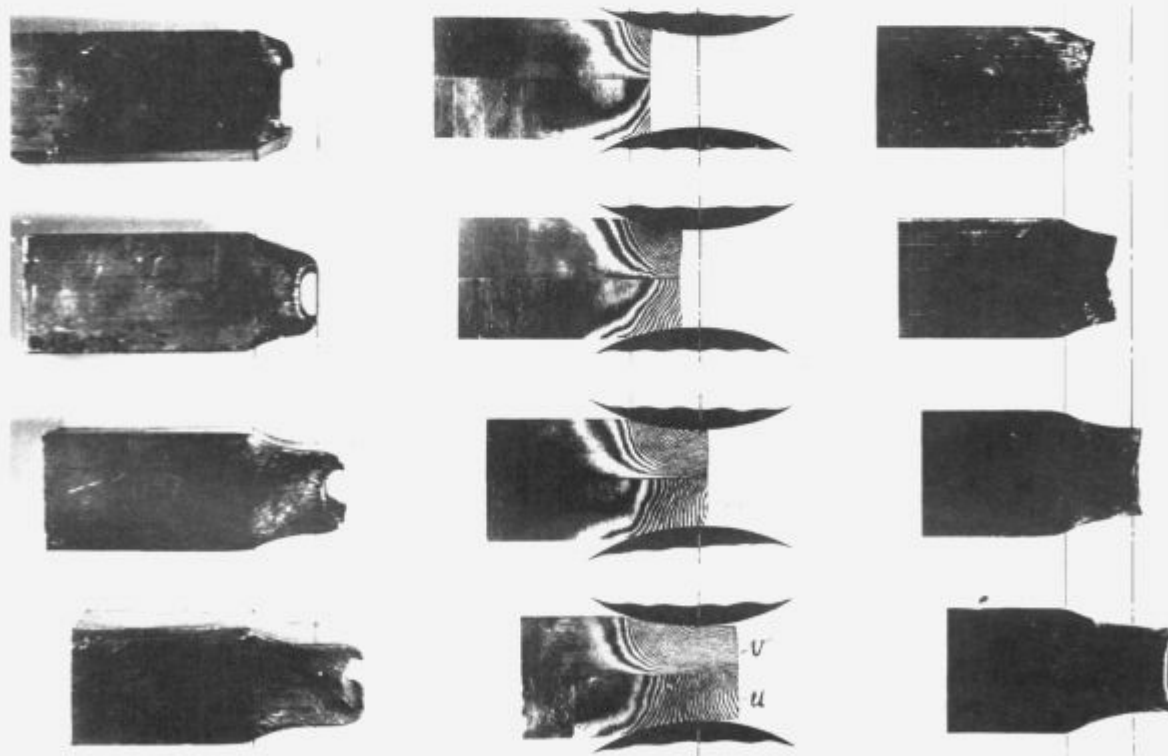


Figure 6: The modification of the front end of the rolled piece during the rolling at 20°C: a-lead in the high-speed regime of the third rheological class at $d\sigma/d\epsilon < 0$; b-lead in the regime of the second rheological class at $d\sigma/d\epsilon > 0$ (moiré stripes; u and v - vertical and horizontal displacements); c-aluminum (99.7%) at all speeds

Slika 6: Sprememba čela valjanca med valjanjem pri 20°C: a-svinec pri velikohitrostnem režimu tretjega reološkega področja z $d\sigma/d\epsilon < 0$; b-svinec v režimu drugega reološkega področja $d\sigma/d\epsilon > 0$ (moiré pasovi, u in v - navpični in vodoravni premiki); c-99,7% Al pri vseh hitrostih

that reason the elimination of the knurl with increased speed of gripping during blooming rolling of carbon steel ingots (0.43% C; 0.26% Si; 0.74% Mn; 0.22% P; 0.016% S) was checked. It failed because of the rheological properties of the steel (fig. 7). The plastometric curves from ref. [9] and [10] were used under assumption that the steel was rheologically simple and of the second class (see fig. 7a). In reality, according to the investigations of Suzuki, it is complex (fig. 7b) and of the third rheological class [11]. The reason for the knurling were the deformation anomalies of the second order at $d/d_0 < 0$. A diminution of the knurling could be obtained only by means of decrease of the deformation degree (in H_{max} nucleus).

The analysis of the rheology of carbon steels (0.2 - 1.0% C) according to Suzuki showed that these steels were rheologically complex of the third class with the maxima on $\sigma - \epsilon$ curves at all strain rates and temperatures. That means that the propensity to deformation anomalies is inherent to these steels. The formation of the knurl is inevitable and the only way to diminish it remains the change of the rolling regimes or of the form of the ingots.

Formation of the prenidus plastic zone

Fig. 8 shows the results of several experiments performed with the aim to explore the development of deformation in the prenidus zone by modelling on the laboratory rolling mill. Samples-ingots 40x40x200 mm prepared with high accuracy from preliminarily pressed and with stabilized properties (annealing one hour at 100°C and ageing at 25°C during 60 days) lead (99.98% Pb) were rolled with 80 mm rolls with a deformation $\epsilon = 25\%$.

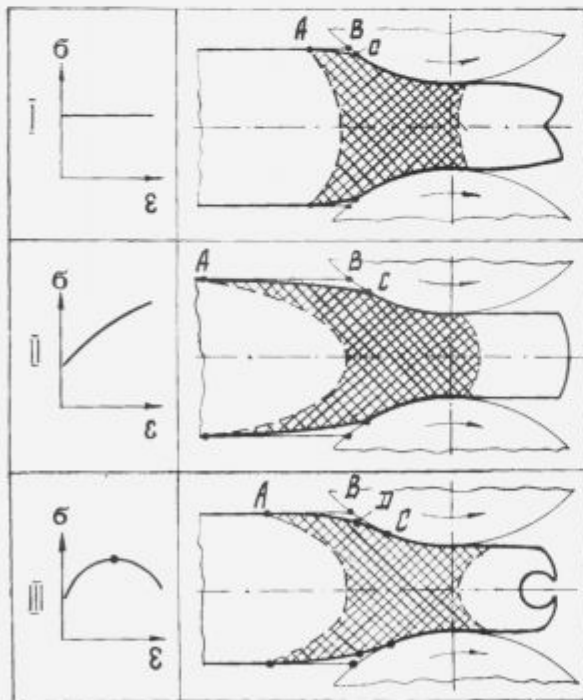


Figure 8: The shape of the deformation nidus during the rolling of metals with different rheology

Slika 8: Oblika deformacijskega prostora med valjenjem jekel z različno reologijo

The extension of the prenidus plastic region was determined by means of moire stripes and indicator devices operating with the error of ± 0.01 mm. Differences in rheology of the deformed material were achieved by change of strain rates in the range of $\dot{\epsilon} = 0.0005, 0.01$ and 1.5 s^{-1} .

During the rolling in regime of simple unstrengthenable first class the prenidus deformation was maximal (see fig. 8, I, AB). During rolling in the regime of the second rheological class (with maximum strengthening) the extension of the prenidus plastic zone was maximal. Strain homogeneity of the first order promotes the inclusion of layers of metal more distant from the rolls into the deformation. These materials are optimal from the rolling technology stand point.

The processes of the development of the second order strain heterogeneity were observed during the rolling of the material of the third rheological class with a maximum on the $\sigma - \epsilon$ curve (see fig. 8, III, AC). The extension of the zone of non-contact deformation in front of the rolls was smaller than in the previous case and the displacement of "C" point-the beginning of contact of the metal with the rolls, towards the line of roll centres was observed constantly. This could produce a strain heterogeneity of the second order with elongation of the surface layers joining points "D" and "C" in an avalanche and could lead to the destruction of metal, especially when concentrators of stresses in form of defects are present.

3. Conclusions

A new model for the formation of the plastic deformation nidus during the rolling was developed using a rheological classification of metals based on experimental data:

1. It is shown, that the strained state of metal in the nidus of deformation is characterized by the presence of regions with maximum strain rates - H_{max} nuclei and depends substantially on the rheology of the metal.
2. The mechanism of formation of the widely spread defect-knurl on the ends of the rolled pieces is explained. It was ascertained that the formation of the knurl depends on the rheology of the metal and the rolling speed.
3. Regularities of the formation of the non-contact prenidus zone of plastic deformation were ascertained.
4. Rheological $\sigma - \epsilon$ data available in scientific literature should be used carefully because in many cases methods of mathematical "smoothing" were used for processing the results of plastometric investigations and rheological anomalies fell-out of the researcher's field of vision.

5. References

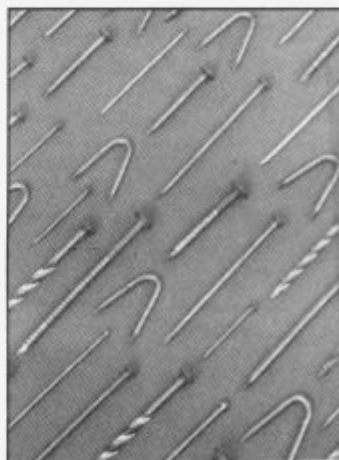
- 1 G.G. Shlomchack: Deformation features of the rheologically complex materials. Deposited in UkrNIINTI 13.08.91., No. 1167-Uk91, Kiev, 1991, 11 pp.
- 2 G.G. Shlomchack: Detection of regularities of deformation heterogeneities and anomalies of plasticity of rheologically complex and supercomplex materials. Deposited in UkrNIINTI 12.12.91., No. 1589-Uk91, Kiev, 1991, 21 pp.
- 3 G.G. Shlomchack, G.A. Fen, V.G. Kutsay: Izv. Vuzov, ChM, No. 3, M, 1980, pp 79-82.
- 4 G.G. Shlomchack, G.A. Fen, V.G. Kutsay: "Pressure shaping of metals", M. "Metallurgia", Dmetl, Research No. 60, pp. 121-122.
- 5 G.G. Shlomchack: Laboratory rolling mill, Russian patent 29.08.91. on the claim No. 4930929/27/035063.
- 6 G.G. Shlomchack: Izv. Ac. Sc. USSR, Metals No. 6, 1978, pp. 102-106.
- 7 G.A. Fen, G.G. Shlomchack and coll.: Metallurgia and coke chemistry, issue 46, Technicka, 1975, pp. 109-113.
- 8 H. Nicaido, T. Naoy, K. Sibata: Transl. from Jap. KI-73789, COONTI, Sosei to kako, v. 24, No. 268, 1983, pp. 486-492.
- 9 I.Y. Tarnovsky and coll.: Mechanical properties of steel at hot pressure shaping. Metallurgizdat, Sverdlovsk, 1960, p. 264.
- 10 V.I. Zyzin, M.Y. Brovman, A.F. Melnikov: M., Metallurgia, 1964, p. 270; 1964, p. 270.
- 11 H. Suzuki: Report of the Inst. of Industrial Science, the University of Tokyo, 1968, v. 18, No. 3, pp. 139-240.

slovenske železarne 
 ZELEZARNA JESENICE
FI PROM

**OUR PRODUCTION
PROGRAM INCLUDES:**



- MILD AND CARBON STEEL WIRES
- STEEL BARS AND WIRES
- WELDING CONSUMABLES
- NAILS



Slovenske železarne Železarna Jesenice FI PROM d.o.o. Cesta železarjev 8, 64270 Jesenice,
tel. centrala: +38 64 861-441, fax: uprava: 861-392, telex: 37219 ZELJSN SI

Comparison of Graphite Furnace - and Hydride Generation AAS for Trace Analysis of Tin in Steels and Nickel Alloys

Primerjava elektrotermične - in hidridne tehnike AAS za analizo sledov kositra v jeklih in nikeljevih zlitinah

A. Osojnik, T. Drglin, Inštitut za kovinske materiale in tehnologije, Ljubljana

The determination of tin in various types of steel and nickel superalloys at low concentration level using graphite furnace atomic absorption spectrometry (GF AAS) and batch system hydride generation atomic absorption spectrometry (HG AAS) is described. The analytical and instrumental parameters for both methods were optimized. The interferences of matrix elements and some metalloids were investigated. Certified standard reference materials of steels and nickel alloys were used to test the methods. Some performances and characteristic data (detection limit, characteristic mass, accurate and relative standard deviation) of the two methods are established and compared. The critical estimate of the both methods is performed. Key words: graphite furnace AAS, hydride generation AAS, interferences, steel, nickel alloys, tin determination.

Opisana je metoda ter optimizirani instrumentalni in analizni parametri za določanje sledov kositra v jeklih in nikeljevih zlitinah z metodo elektrotermične atomizacije (GF AAS) in hidridne tehnike-AAS (HG AAS). Študirali smo interference elementov osnove in nekaterih metaloidov. Rezultati so bili preverjeni s certificiranimi referenčnimi materiali jekel in nikeljevih zlitin. Podani so nekateri karakteristični podatki (meja zaznavnosti, karakteristična masa, točnost, relativni standardni odmik) ter primerjava in kritična ocena obeh uporabljenih metod. Ključne besede: elektrotermična AAS, hidridna tehnika AAS, interference, jeklo, nikeljeve zlitine, določanje kositra.

Introduction

Mechanical, physical and technological properties of various types of steel, and especially vacuum cast nickel superalloys for high temperature application strongly depend on trace elements contents such as Bi, Sb, Sn, As, Se, Te, and others. Because of their harmful effect already at the $\mu\text{g g}^{-1}$ levels and lower, the permissible concentrations of these elements are strongly limited, depends upon the element, the alloy type and application purpose. The traces of surface active elements such as Sb, Sn, Se, Te, and others influence the magnetic properties of nonoriented steel sheets. The knowledge of their contents is one of the useful factors for study of segregation phenomena.

Therefore the determination of these elements is extremely important and the development of a suitable, sensitive analytical method is necessary. Graphite furnace - and hydride generation atomic absorption spectrometry seems to be the appropriate techniques for this purpose, because of their sensitivity and relative simplicity.

The main problems in the determination of tin by GF AAS are the formation of volatile Sn compounds, interactions of tin with graphite during the atomization step (1, 2, 3, 4, 5) and matrix interferences (9, 13).

In order to overcome these problems, different chemical modifiers (5, 6, 7, 8), the oxidation of solution with nitric acid (1, 5, 7, 9) and pretreatment of the graphite tubes with refracto-

ry metals (1, 4, 6, 10, 11) and aluminium solution (9) have been suggested. In this way the losses of tin are diminished and efficiency of tin atomization is improved. The use of coated graphite tubes for tin determination has been proposed by many authors (1, 4, 6, 9, 10, 11). This treatment results in the enhancement of sensitivity (1, 4, 6, 7, 9, 10) and reproducibility of signal (9, 10), a reduction of interferences (6, 10), and in the increased life time of the graphite tubes (10). The knowledge and explanation of chemical reactions which occur in graphite furnace during tin determination (1, 2, 12) contribute to better understanding of the actions and the role of metal coatings, matrix modifiers and interfering elements.

Determination of tin by HG AAS has been described by a number of authors (14-20), although many problems exist for this element. It is well known that sensitivity of Sn signal depends strongly on the pH of the sample solution (14, 15, 19). Therefore for tin determination saturated solution of boric acid with addition of low concentrations of nitric (15) or hydrochloric acid (19, 20) for standards, sample and carrier solutions is recommended. Different reagents (acid, sodium tetrahydroborate reductant solution, sodium hydroxide) and their concentrations significantly influence not only sensitivity and peak shapes but also interferences in tin determination by HG AAS. Among the difficulties described in the literature are also high blank values (18, 20, 21), memory effects (20, 21), and interferences from transition metals ions such as Fe, Ni, Co, Cu which cause very

serious reduction of the tin signal (17, 22). The interferences caused by those elements can be partly or completely eliminated. The most common way to eliminate the interferences is masking of interfering ions by different masking agents (17, 22, 23), although the changes of acid and reductant solution concentrations are also useful for this purpose (15, 20). An additional problem in tin determination by HG AAS reported by B. Welz et al. (20) is the appearance of pre-peaks originated from the silica of quartz tube atomizer which can be volatilized and atomized in the presence of hydrogen, most probably via hydrogen radicals. These prepeaks are difficult to separate from the analytical signal and may cause errors in signal evaluation.

The present work involved an extensive study of optimal analytical and instrumental parameters for low level tin determination in steels and nickel alloys using GF AAS and HG AAS. The determination has been discussed regarding:

GF AAS

- influence of graphite tube coatings and modifier used on sensitivity and reproducibility of signal
- interferences of matrix elements
- selection of optimal pyrolysis and atomization temperature with regard to volatilization of analyte, background, interferences, sensitivity of signal and life time of graphite tube
- evaluation of results

HG AAS

- influence of acid concentration on analyte signal
- interferences of matrix elements and some metalloids
- evaluation of results

Experimental

Aparatus

The GBC 902 atomic absorption spectrometer, equipped with deuterium-arc background correction system, automated graphite furnace GF 2000, programmable auto-sampler PAL 2000 and CL 2000 controller was used for the measurements of analyte absorbances using GF AAS. The instrumental parameters and operating conditions are given in **Table 1**. The furnace program is shown in **Table 2**.

A Perkin-Elmer 2380 atomic absorption spectrometer, equipped with hydride generator MHS-10 and printer PRS-10 was used for hydride generation and absorbances measurements using HG AAS. The instrumental parameters and operating conditions are listed in **Table 3**.

Table 1: Instrumental parameters and operating conditions for GF-AAS

Spectrometer	GBC, double beam, 902
Wavelength	286.3 nm
Slit	1.0 nm
Light source	HCL, 10 mA
Measurement mode	peak height
Furnace	
Graphite tube	coated with Na ₂ WO ₄
Char temperature	800°C
Atomization temp.	2600°C
Sampler	
Sample volume	20 µl
Standard preparation	
Stock solution	1000 µg/ml Sn in 1 M HCl
Standard solutions	serial dilutions with 0.3 M HNO ₃
Sample preparation	
Dissolved in	20 ml aqua regia
Mass/volume	0.5 g/50 - 1 to 10/100 ml (diluted with 0.3 M HNO ₃)

Table 2: Graphite furnace temperature program for the determination of tin in steels and nickel alloys

Step number	Temp. (°C)	Ramp time (s)	Hold time (s)	Ar flow (l min ⁻¹)
1	90	1	9	1.3
2	120	10	10	1.3
3	80	10	10	1.3
4	800	1	1	-
5	2600	1	3	-
6	2650	1	6	1.3
7	20	1	5	1.3

Table 3: Instrumental parameters and operating conditions for HG-AAS

Spectrometer	Perkin-Elmer, 2380
Wavelength	286.3 nm
Slit	0.7 nm
Light source	EDL, 6 W
Hydride system	Perkin-Elmer, MHS-10
Stock solution	1000 µg/ml Sn (in 1 M HCl)
Standard solutions	serial dilutions with 0.1 M HCl
Carrier solution	H ₃ BO ₃ , sat./0.1 M HNO ₃
Calibration volume	25 ml
Reductant	3 g NaBH ₄ + 0.5 g NaOH/100 ml
Flame	air/acetylene: blue
Sample	
Dissolved in	20 ml aqua regia
Mass/volume	0.5 g/50 ml
Measuring volume	0.1-1.0 ml
Elimination of interferences	3 g sodium oxalate/100 ml

Reagents

All reagents were of highest available purity (p.a. or puriss. p.a.) obtained from Merck or Fluka. The solutions prepared were:

GF AAS

- aqua regia
- nitric acid, 0.3 M
- Pd/Mg nitrate modifier: 300 mg Pd (dissolved in nitric acid) + 200 mg Mg(NO₃)₂ · 6H₂O in 100 ml of water
- sodium tungstate dihydrate, 5 g in 100 ml of water

HG AAS

- aqua regia
- carrier solution: saturated boric acid containing 0.1 M nitric acid
- reduction solution: 3 g of sodium tetrahydroborate (Fluka) in 100 ml of water stabilised with 0.5 g of sodium hydroxide
- sodium oxalate, 3 g in 100 ml of water

Standard solutions

Stock solution of 1000 µg ml⁻¹ Sn was prepared by dissolving of 1.000 g of tin metal in 100 ml hydrochloric acid (1.16) and diluting to 1 l with deionized water. The other standard solutions were prepared from stock solution by serial dilution with 0.3 M nitric acid for GF AAS or with 0.1 M hydrochloric acid for HG AAS. Standard Sn solutions containing the interfering ions were prepared by adding the appropriate amounts of interfering ions to the standard solutions.

Sample preparation

0.5 g of sample was carefully dissolved in 20 ml of aqua regia (2 hours at 90°C). After cooling the digest was diluted to 50 ml with deionized water. Further dilution of sample solution (10-100 times) with 0.3 M nitric acid was used for GF AAS measurements.

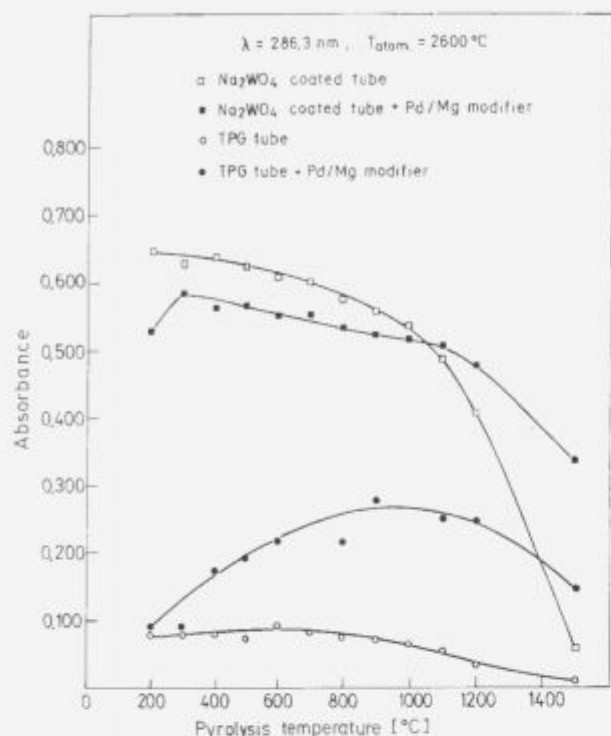


Figure 1: Effect of graphite tube coating and matrix modifier on signal for 2 ng Sn at different pyrolysis temperatures

Slika 1: Vpliv prevleke grafitnih cevki in modifikatorja na signal za 2 ng Sn pri različnih razkrojnih temperaturah

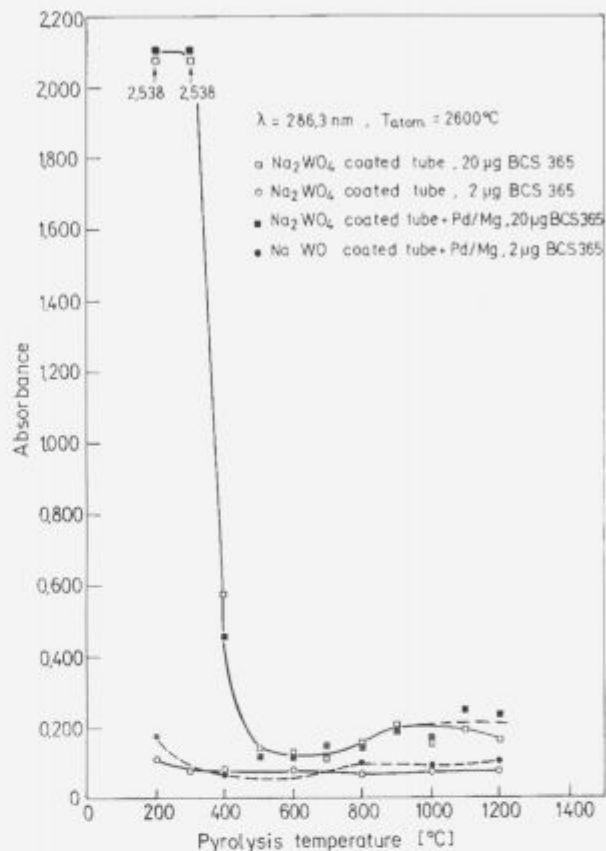


Figure 3: Determination of background for Sn in steel vs. pyrolysis temperature

Slika 3: Določanje ozadja za Sn v jeklih v odvisnosti od razkrojne temperature

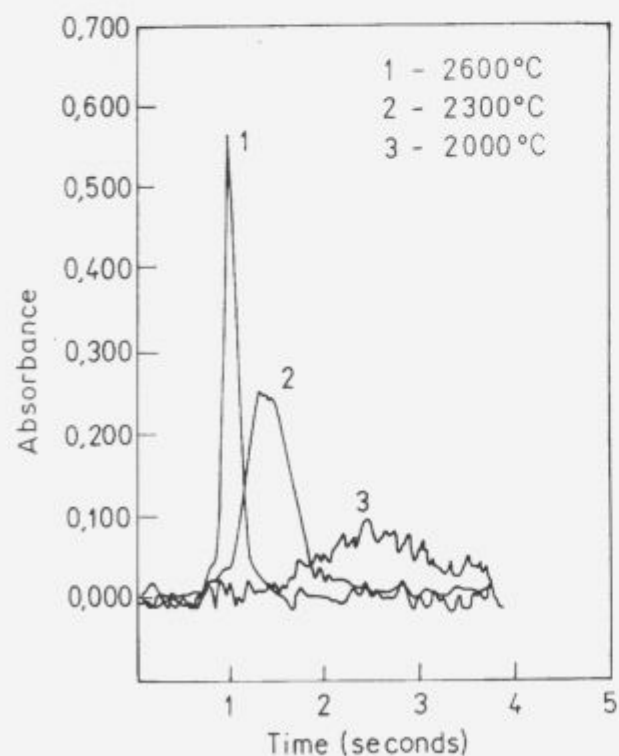


Figure 2: Effect of atomization temperature on signal for 2 ng Sn

Slika 2: Vpliv temperature atomizacije na signal za 2 ng Sn

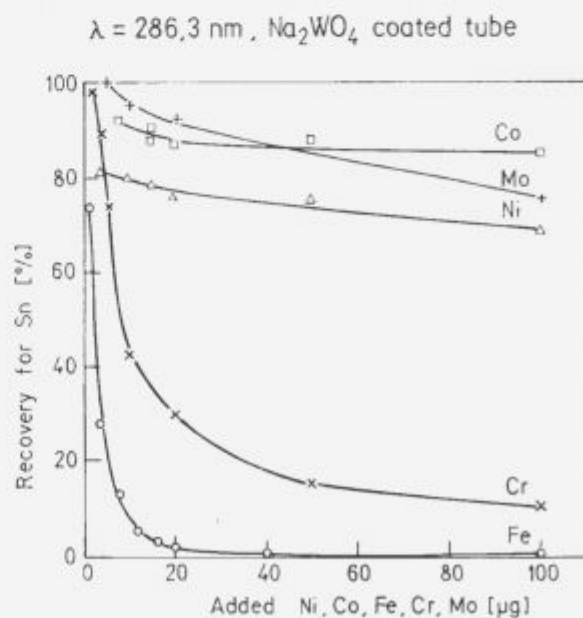


Figure 4: Influence of interferent elements on the signal for 2 ng Sn: GF AAS

Slika 4: Vpliv motečih elementov na signal za 2 ng Sn: GF AAS

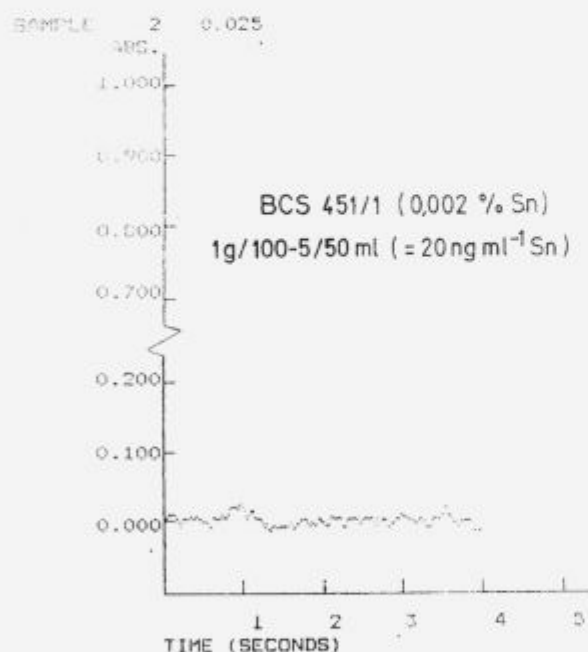
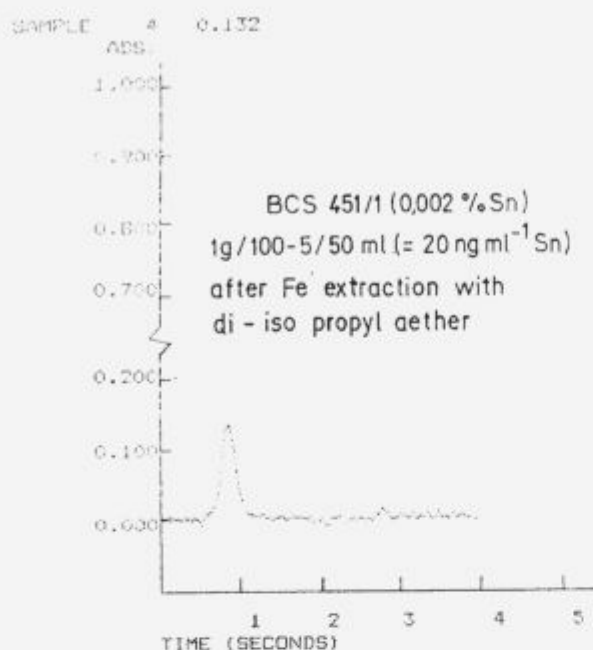


Figure 5: Effect of Fe extraction from steel on Sn-signal by GF AAS
Slika 5: Vpliv ekstrakcije železa iz jekla na Sn signal z metodo GF AAS

Pretreatment of graphite tube ⁽²⁴⁾

The graphite tube was soaked with sodium tungstate solution for 8 hours, than the tube was dried at 120°C and heated in the furnace tube under the conditions shown in Table 4. The whole procedure was repeated once more.

Table 4: Furnace conditions for W carbide coating

Step number	Temp. (°C)	Ramp time (s)	Hold time (s)	Ar flow (l min ⁻¹)
1	120	10	60	1.3
2	2600	90	10	—
3	2900	10	10	1.3

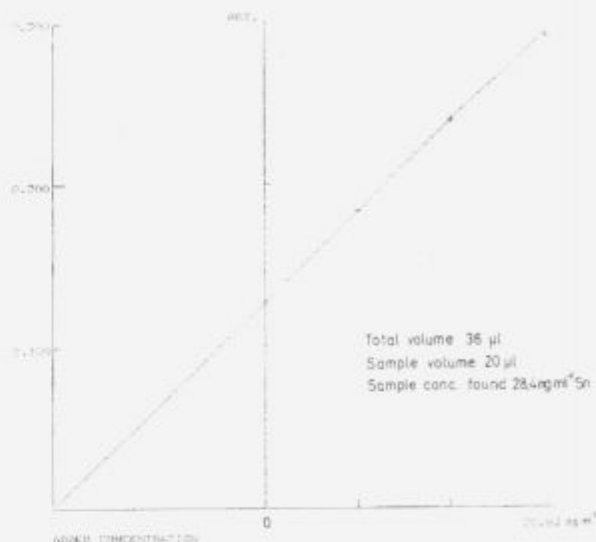


Figure 6: Standard addition method for the determination of Sn in steel by GF AAS

Slika 6: Metoda standardnega dodatka za določanje Sn v jeklih z metodo GF AAS

Calibration

The calibration curve made by standard addition method was applied using GF AAS.

For HG AAS calibration was carried out with standard solutions in the range from 10 to 100 ng Sn, matched with corresponding amounts of matrix elements.

Results and Discussion

The results of the work carried out with the intention of optimizing instrumental and analytical parameters for tin determination in steels and nickel alloys using GF AAS and HG AAS are shown in following figures.

Effect of graphite tube coating and matrix modifier on sensitivity of Sn signal at different pyrolysis temperatures is demonstrated in figure 1. The W-coated graphite tube shows the largest increase in sensitivity among the coatings used (W-, Ta-, Zr-coatings). It is evident that pyrolysis can be done at temperatures up to 1000°C without greater loss of Sn. The matrix modifier proposed by Schlemmer and Welz⁵ (Pd/Mg nitrate modifier) has essentially no influence on the absorbance signal of tin at this tem-

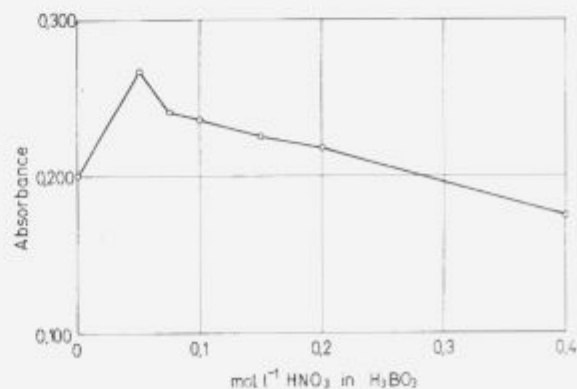


Figure 7: Influence of nitric acid concentration on Sn signal using HG AAS

Slika 7: Vpliv koncentracije dušikove (V) kisline na Sn signal z metodo HG AAS

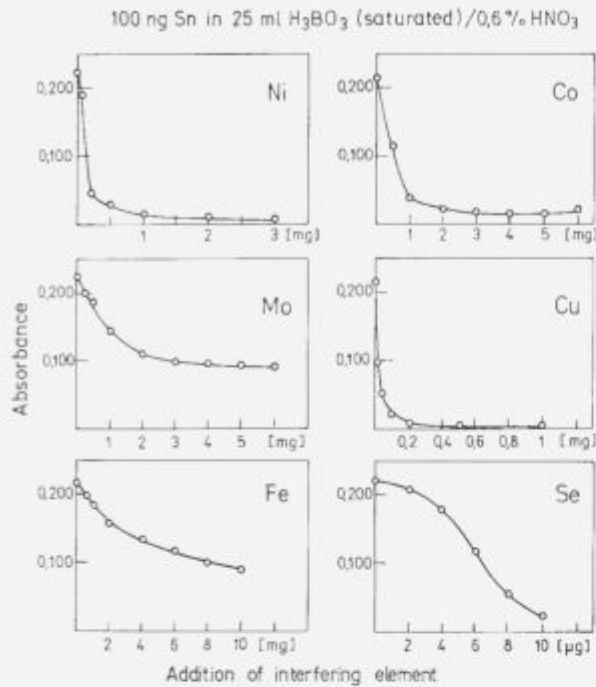


Figure 8: Influence of the interfering elements on signal for Sn by HG AAS

Slika 8: Vpliv motečih elementov na Sn signal z metodo HG AAS

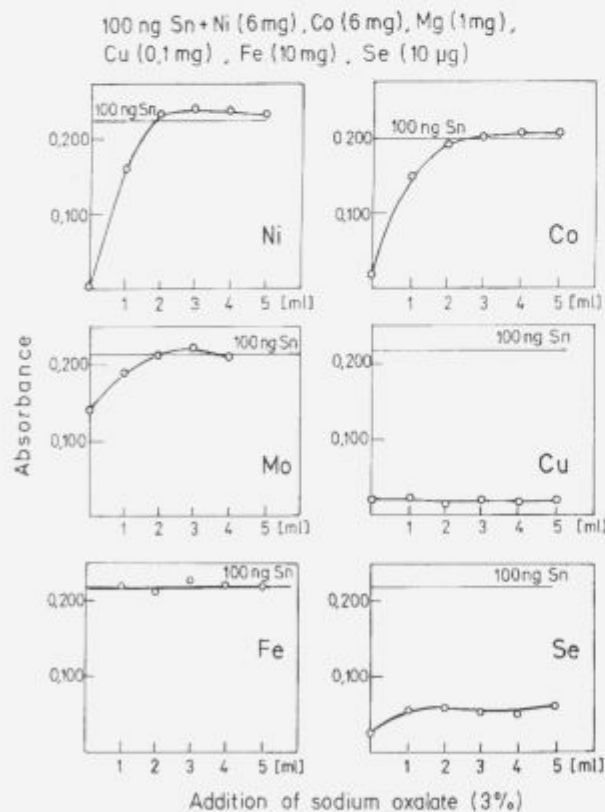


Figure 9: Elimination of interferences for Sn with the addition of sodium oxalate (HG AAS)

Slika 9: Eliminiranje motenj za Sn z dodatkom natrijevega oksalata (HG AAS)

perature. The sensitivity increase due to matrix modifier action is observed only at pyrolysis temperatures above 1200°C.

Effect of atomization temperature on Sn signal is shown in figure 2. The efficiency of tin atomization is improved at atomization temperature 2600°C.

The absorbance signal of background in dependence of pyrolysis temperature for Sn determination in steel samples is presented in figure 3. For sample amount of 20 μg the background is reduced on acceptable value at pyrolysis temperature above 500°C.

The interfering effect of matrix elements on signal of Sn is shown on figure 4. As indicated the presence of Fe and Cr depress the Sn signal strongly. Since it was confirmed (13, 15) that the extent of the interferences by the transition metal ions does not depend on the analyte - interferent ratio, but on the interferent concentration in the sample solution, larger matrix dilution for high Sn contents can be used to reduce these interferences.

In the case that Sn concentration in the sample is very low a prior separation (MIBK extraction) of interfering iron must be done. The depressing effect of iron on Sn signal can be seen from figure 5, where the comparison of peaks resulting from tin determination with and without the iron separation is shown. For tin determination in steels the dilution of sample is recommended. The absorbance signal for diluted steel sample is namely greater as for undiluted sample, although the tin amount for diluted sample is absolutely smaller. Therefore the evaluation of results has to be performed by the calibration curve made by the standard addition method which is demonstrated in figure 6.

The following figures present the results of our experiments made with intention of optimizing the analytical parameters for tin determination using HG AAS. The influence of nitric acid concentration in the carrier solution on sensitivity for tin is confirmed (figure 7). As reported (15, 19) the addition of low concentration of nitric acid to the saturated boric acid improves the sensitivity and reproducibility of Sn signal.

The influence of interfering elements on Sn signal by HG AAS is shown in figure 8. The presence of Ni, Fe, Co, Cu, Mo and Se depress the signal for Sn strongly.

The interfering effect of Ni, Fe, Co and Mo is eliminated by addition of sodium oxalate (figure 9), although a number of masking agents were examined. The interference of Se is stated only in concentrations much higher than in samples investigated.

Certified reference standard materials of steels and nickel alloys were used to test the methods. Certified values for Sn concentrations in standards used are collected in table 5. The comparison results of Sn determination in steel and nickel alloys are given in table 6. The results indicated a good agreement with certified values for both methods within the reported standard deviation, although the reproducibility of results is better by GF AAS.

Table 5: Certified reference standard materials used for Sn determination

Sign	Material	Atest μg g ⁻¹ Sn
BCS 239/3	0.3 % carbon steel	300
BCS 433	plain carbon steel	100
BCS-CRM 451/1	carbon steel	20
EURO-CRM 281-1	highly alloyed steel	90
EURONORM ZRM 285-1	highly alloyed steel	30
BCS-CRM 345	IN 100 alloy	6
BCS-SRM 346	IN 100 alloy	91
MBH 11982 B	nickel alloy IN 100	88
MBH 11980 F	nickel alloy IN 100	18

Table 6: Comparison of GF-AAS and HG-AAS results ($\mu\text{g g}^{-1}\text{Sn}$) with certified values

Certified references samples	Certified value	GF-AAS		HG-AAS	
		found	\pm RSD	found	\pm RSD
BCS 345	6 \pm 1.6	4.9	\pm 15.2 %	4.9	\pm 18.0%
BCS 345+10 $\mu\text{g g}^{-1}\text{Sn}$	16	15.8			
BCS 346	91 \pm 7	94.2	\pm 7.3	96.0	\pm 7.5%
MBH 11980	18	15.1 \pm	15.1 %	19.0	\pm 11.0%
MBH 11982	88	76.3	\pm 8.7 %	81.2	\pm 8.2 %
BCS 239/3	300(280-330)	320	\pm 1.7 %	309	\pm 5.0 %
BCS 433	100(80-110)	93	\pm 3.5 %	93	\pm 8.3%
BCS 451/1	20(13-23)	18	\pm 5.9 %	15	\pm 9.2 %
EURO-CRM 281-1	90 \pm 10	102	\pm 3.3 %	97	\pm 4.1%
EURO-ZRM 285-1	30 \pm 8	33	\pm 6.8 %	26	\pm 8.4 %

Some characteristic data of both methods used are collected in **table 7**. The calculated values are nearly in a good agreement with available reported data. The sensitivity (characteristic mass) of GF AAS method is better as for HG AAS, which is compensated with greater measuring volume by HG AAS. Interesting is the difference in the characteristic mass calculated from analysis results of diluted and undiluted samples which is the consequence of depressing effect of interfering elements.

Table 7: Characteristic data for method evaluation (detection limit, characteristic mass)

Method	Sample	Dilution	Measuring volume	DL ng ml ⁻¹	$\mu\text{g g}^{-1}$	m_0 pg
GF-AAS	standard solution		20 μl	1.2		17.1
GF-AAS	BCS 345	1g/100 ml	20 μl	5.4	0.54	79.1
GF-AAS	BCS 346	1g/100-10/50 ml	20 μl	3.7	1.84	27.0
GF-AAS	BCS 239/3	0.5g/50-10/100 ml	20 μl	7.2	7.2	106
GF-AAS	BCS 239/3	0.5g/50-1/50 ml	20 μl	1.3	1.7	17.9
GF-AAS	BCS 281/1	0.5g/50-10/100 ml	20 μl	2.5	2.5	36
GF-AAS	BCS 281-1	0.5g/50-1/100 ml	20 μl	0.7	7.3	10.7
HG-AAS	standard solution		1 ml	2.7		1982
HG-AAS	BCS 345	1g/100 ml	1 ml	3.3	0.33	2440
HG-AAS	BCS 346	1g/100-10/100 ml	1 ml	2.7	2.7	2010
HG-AAS	BCS 239/3	0.5g/50 ml	0.05 ml	2.1	4.2	1941
HG-AAS	BCS 451/1	1g/100 ml	0.1 ml	2.7	2.7	2514
HG-AAS	BCS 451/1	1g/100 ml	0.5 ml	3.2	0.64	2933

Conclusions

The W-coated graphite tubes was chosen to improve the sensitivity and reproducibility of Sn signal by GF AAS. The strongly interfering effect of iron and chromium was stated at analyses conditions used. Dilution of samples for high Sn contents or prior iron separation for steel samples in low concentration levels ($<20 \mu\text{g g}^{-1}$) is the only way to overcome this problem. The evaluation of results has to be performed by the calibration curve made by standard addition method.

The interferences of Ni, Fe, Co, Cu and Mo, due to preferential reduction of interfering elements to elementary state and kinetic changes of hydride forming reactions were established

using HG AAS. The interferences of hydride forming elements (Se) were stated only in concentrations much higher than in samples investigated. The interfering effect of Ni, Fe, Co and Mo is eliminated by addition of sodium oxalate.

Certified reference standards of steels containing 20-300 $\mu\text{g g}^{-1}$ Sn and nickel alloys containing 6-91 $\mu\text{g g}^{-1}$ Sn were used to test the methods. Characteristic mass is lower by GF AAS. This can be compensated with greater measuring volume by HG AAS. Reproducibility of results is in the range of ± 2 to $\pm 15\%$ for GF AAS and ± 4 to $\pm 18\%$ for HG AAS. The accuracy of results are in agreement with certified values within the reported standard deviation for the both methods.

References

- W. Wendl, G. Muller-Vogt and A. Bienhaus, Fortschritte in der atomspektrometrischen Spurenanalytik, B. Welz (ed.), WCH Verlagsgesellschaft, Weinheim, 1986, 125
- W. Wendl and G. Muller-Vogt, Spectrochim. Acta, 1984, 38, 237
- E. Iwamoto, N. Miyazaki, N. Ohkubo and T.J. Kumamaru, Anal. At. Spectrom., 1989, 4, 433
- E. Iwamoto, H. Shimazu, K. Yokota and T. Kumamaru, J. Anal. At. Spectrom., 1992, 7, 421
- P. Bermejo-Barrera, R.M. Soto-Ferreiro and A. Bermejo-Barrera, Fresenius J. Anal. Chem., 1993, 345, 60
- P. Hocquelllet and N. Labeirie, At. Absorpt. Newsl., 1977, 16, 124
- E. Pruszkovska, D.C. Manning, G.R. Carnick and W. Slavin, At. Spectrosc., 1983, 4, 87
- G. Schlemmer and B. Welz, Spectrochim. Acta, 1986, 4B, 1157
- K. Gruner, Neue Hutte, 1991, 36, 33
- H. Fritzsche, W. Wegscheider und G. Knapp, Talanta, 1979, 26, 219
- P. Hocquelllet, At. Spectrosc., 1985, 6, 69
- W. Wendl, G. Muller-Vogt and L. Hahn, Fresenius J. Anal. Chem., 1989, 333, 763
- Zhang Li, S. Mc Intosh, G.R. Carnick and W. Slavin, Spectrochim. Acta, 1992, 47B, 701
- F. J. Fernandez, At. Absorpt. Newsl., 1973, 12, 93
- B. Welz and M. Melcher, Spectrochim. Acta, 1981, 36B 439
- K. Petrick and W. Krivan, Fresenius Z. Anal. Chem., 1987, 327, 338
- J.O. Brindle and Xiao-chun Le, Analyst, 1988, 113, 1377
- J.R. Castillo, C. Martinez, R. Tomas and J.M. Mir, J. Anal. At. Spectrom., 1988, 3, 595
- B. Welz and M. Schubert-Jacobs, At. Spectrosc., 1991, 12, 91
- B. Welz, M. Schubert-Jacobs and T. Guo, Talanta, 1992, 39, 1097
- K. de Donker, R. Dumarey, R. Dams and J. Hoste, Anal. Chim. Acta, 1986, 187, 163
- M. Thompson and B. Pahlavanpour, Anal. Chim. Acta, 1979, 109, 251
- R. Bye, Fresenius Z. Anal. Chem., 1984, 317, 27
- H.M. Ortner and E. Kantuscher, Talanta, 1975, 22, 581.

The Susceptibility to Hydrogen Embrittlement of Low Alloy Cr-Mo Steel Tubing

Občutljivost cevi iz nizkolegiranega Cr-Mo jekla na vodikovo krhkost

M. Gojić, M. Balenović, Željezara Sisak, Hrvatska
L. Kosec, Fakulteta za naravoslovje in tehnologijo, Ljubljana
L. Vehovar, Inštitut za kovinske materiale in tehnologije, Ljubljana

In the paper the results of research in the susceptibility of as-rolled and heat treated low alloy Cr-Mo (microalloy by Nb) tubing to hydrogen embrittlement by method of cathodic polarization are shown. The results show that quenching at 870°C (both in water and oil) and tempering at high temperature (720°C) attain excellent resistance to hydrogen embrittlement which is indicated by a small embrittlement index (11.1–23.6%) by tough small-dimple fractures and relatively small content of absorbed hydrogen (3.2–3.4 ppm) at the cathodic polarization.

Key words: low alloy steel, tubing, hydrogen embrittlement, heat treatment, cathodic polarization

Raziskovali smo občutljivost valjanih in toplotno obdelanih cevi iz malolegiranega Cr-Mo jekla (mikrolegiranega z niobom) na vodikovo krhkost. Uporabili smo metodo katodne polarizacije. Rezultati kažejo, da s kaljenjem s temperature 870°C (v vodi ali olju) in z visokotemperaturnim popuščanjem (720°C), dosežemo odlično odpornost proti vodikovi krhkosti. Potrjuje jo majhen indeks krhkosti (11.1–23.2%), žilav, jamičasti izgled prelomne površine in relativno majhna vsebnost absorbiranega vodika (3.2–3.4 ppm) pri katodni polarizaciji.

Ključne besede: malolegirana jekla, cevi, vodikova krhkost, toplotna obdelava, katodna polarizacija.

1. Introduction

Corrosion costs of oil country tubular goods (OCTG) in oil industry are estimated to be some hundred millions dollars every year. At the begin of the fifties a lot of oil tubes in Canada, USA and France failed when API (American Petroleum Institute) pipes grade N-80 and P-110 were used in sour wells, with minimum yield strength of 552 MPa and 758MP, respectively. Nowadays great efforts are being made to decrease or reduce the process of corrosion to minimum, especially the sulfide stress corrosion cracking (SSCC) i.e. hydrogen embrittlement (HE). Most producers of oil country tubular goods adapt themselves to difficult conditions of oil and natural gas exploitation by developing and producing pipes from low alloy to high alloy steels and special alloys. Low alloyed steels mostly used for OCTG are made from medium carbon Mn, Mn-Mo and Cr-Mo type steels, microalloyed with vanadium, niobium, titan and bor¹. The sulfide stress corrosion cracking or hydrogen embrittlement of steels is quite a complex phenomenon not being yet completely unambiguous determined neither regarding the mechanism² nor the dominant influence of individual factors (mechanical properties, microstructure etc.). However it is often used to characterize the influences of hydrogen in steel at room temperatures. These influences are mostly manifested through the loss of ductility (decrease of reduction area and elongation). Therefore, in this paper is presented the analyse of low alloy Cr-Mo steel (microalloyed with niobium) susceptibility to hydrogen embrittlement from the point of view of mechanical properties, heat treat-

ment and microstructure. At the same time, the content of absorbed hydrogen was determined and fractographic analysis of fractured surfaces' specimens after cathodic polarization was carried out.

2. Experimental

Material

By procedure of laboratory electro slag remelting there were received low alloy Cr-Mo steel (microalloyed with niobium) ingots, ϕ 169 x 380 mm, which were after forged into billets \square 135 x 420 mm. The **table 1** shows chemical composition of the investigated steel.

On the **table 1** we can see that the investigated steel appropriate to the first type API grade C-90 by addition of niobium as a micro alloy element³. Alloying with higher content of molybdenum and microalloying with niobium AISI 4130 steel proved to be useful for increasing of resistance to hydrogen cracking because of the refined austenite grain and the size of

Steel	C	Mn	P	S	Si	V	Mo	Al	Cr	Nb
Cr-Mo	0.30	0.72	0.022	0.007	0.37	0.01	0.63	0.07	1.12	0.035

Table 1: The chemical composition of steel investigated, %

Tabela 1: Kemijska sestava jekla, %

carbide particles. In Iron Steel Works Sisak, billets \square 135 x 420 mm were hot rolled into seamless tubing ϕ 60.3 x 4.83 mm for oil industry.

Heat treatment

The temperatures of phase transformations needed for heat treatment were tested by dilatometer Lk.02 "Adamel Lhomargy". The specimens ϕ 2 x 12 mm were heated and cooled by heating and cooling rate of 0.05°C/s. On registered diagram dilatation/temperature, the temperature values of particular phase transformation were read off. On the basis of these results, the heat treatment of pipes which is consisting of normalization and tempering as well as quenching (with cooling in water and oil) and tempering were carried out in the laboratory electric resistance chamber furnace. Before and after heat treatment mechanical properties of ASTM standardized specimens were tested. The hardness test was performed by Brinell's method. In a view of obtaining phase composition a phase analysis by X-ray diffraction device and Philips numerical coating technique by use $\text{CoK}\alpha$ radiation.

Corrosion tests

Since the hydrogen embrittlement of the material presents in fact the loss of its ductility (due to absorbed hydrogen) a decrease of ductility parameters is obvious, i.e. the reduction area and elongation of specimens are always reduced^{2,4,6}. Among many electrochemical methods the cathodic polarization is one of the most appropriate methods for the determination of relative material susceptibility to hydrogen embrittlement. The specimens ϕ 3.5 x 110 mm made from steel investigated in as-rolled and heat treated state were put into electrochemical cell (fullfilled with 0.5 M H_2SO_4 + 10 mg As_2O_3 /l solution) which was put in Zwick 50 kN tensile machine and subjected to static load of 60 and 80% its of yield strength⁷. The cathodic polarization was carried out by Wenging's potentiostat at current density of 1.6; 4.0; 8.0 and 12.0 mA/cm². After cathodic polarization (duration of two hours) of stressed specimens testing to the fracture with deformation rate of 2.4×10^{-4} s⁻¹ was immediately carried out. On the base of change of specimens' reduction area embrittlement index was calculated according to the following equation:

$$F = \frac{RA_{\text{air}} - RA_{\text{H}}}{RA_{\text{air}}} \times 100 \quad (1)$$

Table 2: The mechanical properties of tubings Cr-Mo steel in as-rolled and heat treated state

Tabela 2: Mehanske lastnosti cevi iz Cr-Mo jekla v valjanem in toplotno obdelanem stanju

Specimen	Heat treatment	Yield strength MPa	Tensile strength MPa	Elongation %	Hardness HB	Energy impact at +20°C	Fracture toughness MPa $\sqrt{\text{m}}$
3	–	972	1145	8.9	400	4	50
30	Normalized 900°C/min, air + Tempered 700°C/60 min, air	605	725	25.5	230	18	84
36	Quenched 870°C/30 min, water + Tempered 720°C/60 min, water	721	765	25.5	252	19	94
39	Quenched 870°C/30 min, oil + Tempered 720°C/60 min, air	703	759	22.1	250	22	100

where are:

RA_{air} - reduction area prior cathodic to polarization (uncharged by hydrogen)

RA_{H} - reduction area after cathodic polarization (charged by hydrogen)

After corrosion tests the content of absorbed hydrogen in cathodic polarized specimens is determined on the exalograph EA-1 by the method of hot extraction.

Metallographic and fractographic testing

Microstructure of polished and etched (in nital) specimens before and after heat treatment were carried out by the scanning electronic microscope (SEM) type JOEL JXA-50 A, voltage to 50 kV. For determination series and manner fracture the analysis fractured surfaces of specimens were carried out.

3. Results of investigation

Investigation of mechanical properties were carried out by Instron 1196 tensile machine on two samples in as-rolled and heat treated state. Energy impact testing was carried out by Charpy clapper on three ISO specimens with V-notch at temperature 20°C. Average testing values of mechanical properties are showed in **table 2**.

On **table 2** can be seen that the tubing without heat treatment according to mechanical properties correspond to P-110 API grade which does not belong to the corrosion resistant oil country tubular goods. By normalizing at 900°C and tempering at 700°C was obtained corrosion resistance L-80 API grade. By the tubing heat treatment consisting of quenching at 870°C and tempering at high temperature of 720°C (specimens 36 and 39) there were obtained OCTG with mechanical properties C-90 grade. The index embrittlement as per equation (1) taking into account the specimens reduction area prior and after cathodic polarization. The average values of embrittlement index for as-rolled and heat treated tubes are shown in **table 3**.

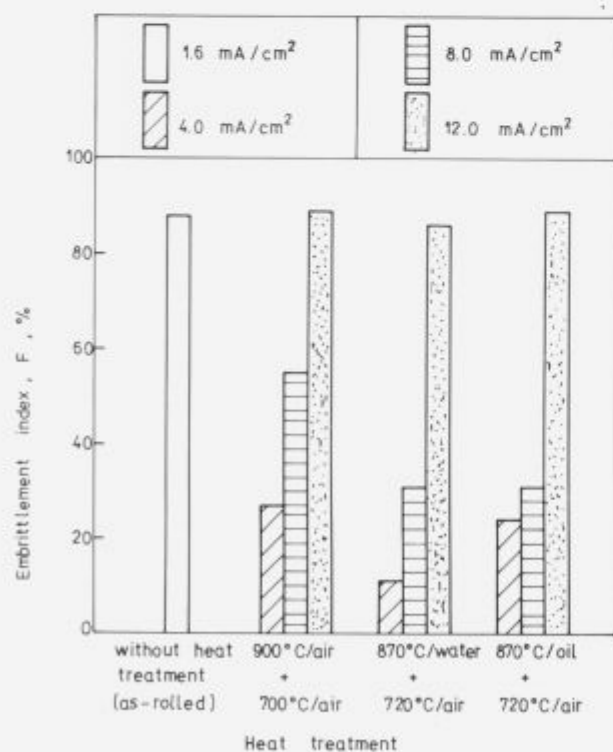
4. Discussion of results

The mechanical properties of Cr-Mo steel tubing in as-rolled state are high (API grade P-105, **table 2**) due to the chemical composition (modification with molybdenum and microalloying with niobium) and the presence of bainite microstructure (**figure**

Table 3: The values of embrittlement index and content absorbed hydrogen Cr-Mo steel by cathodic polarization**Tabela 3:** Vrednost indeksa krhkosti in vsebina absorbiranega vodika Cr-Mo jekla pri katodni polarizaciji

Specimen	Heat treatment	Yield strength MPa	Index embrittlement F (%)	Current density mA/cm ²	Content hydrogen ppm
3-6	-	972	87.6	1.6	2.7
30-4	Normalized 900°C/30 min, air	605	27.2	4.0	-
30-7	+		55.2	8.0	
30-6	Tempered 700°C/60 min, air		88.5	12.8	
36-3	Quenched 870°C/30 min, water	721	11.1	4.0	3.2
36-5	+		30.7	8.0	4.0
36-4	Tempered 720°C/60 min, air		86.2	12.0	4.8
39-3	Quenched 870°C/30 min, oil	703	23.6	4.0	3.4
39-5	+		31.1	8.0	4.4
39-4	Tempered 720°C/60 min, air		88.6	12.0	7.0

3a) appearing at usual air cooling of tubes with finish rolling temperature. The hardness is homogenous through the whole cross section and amounts to 400 HB and 230-250 HB for the pipes in as-rolled and heat treated state as well. As OCTG are also used in arctic fields they are supposed to be as tough as possible, especially at low temperatures. Energy impact of heat treated pipes is high and amounts to 18-22 J at 20°C retaining to same values also at -40°C. The fracture toughness (K_{IC} -value) is known to be an important characteristic of material, however, because of wall-thinnes (4,83 mm) K_{IC} was not defined by the way of Charpy's energy at 20°C as per Rolf-Novak's equation⁸.

**Figure 1:** The influence heat treatment on embrittlement index of low alloy Cr-Mo steel**Slika 1:** Vpliv toplotne obdelave na indeks krhkosti malolegiranege Cr-Mo jekla

$$\text{where are: } K_{IC} = R_{\text{eff}}(0,646 \text{ CVN}/R_{\text{eff}} - 0,00635)^{12} \quad (2)$$

R_{eff} - Upper yield strength (MPa)

CVN - Charpy energy impact (J)

On the base of calculated K_{IC} - values (table 2) it is clear that the fracture toughness of quenched and tempered pipes has high values which may be up to 100 MPam^{1/2}. The figure 1, in the manner of histogram, shows the change of embrittlement index at the cathodic polarization both for different states of material and different current densities and it can be seen that pipes resistance to hydrogen embrittlement increases through appliance of the heat treatment, specially quenching and tempering.

Although pipe specimens in as-rolled state were at test stressed on the level of 60% yield strength and polarized at current density of 1,6 mA/cm² a small resistance to hydrogen embrittlement with embrittlement index of 87,6% was obtained. The microfractography (figure 2a) of a fractured specimen made after cathodic polarization shows the presence of mixed fracture in which predominant brittle cleavage type of fracture. The reason for such a small resistance to hydrogen embrittlement is in the presence of untempered bainite microstructure (figure 3) which is by many investigators^{9,10} considered, after martensite structure, to be the most unfavourable microstructure with regard to the resistance in corrosion environments, especially in sulfide environments.

By normalization and tempering at 700°C the resistance to hydrogen embrittlement was increased can be seen from the index value of embrittlement 27,2% and from the ductile fracture with a small energy fracture (figure 2a). The fracture began at the large inclusion particle being however mighty traps for hydrogen because their great intersurface ensures the accumulation of sufficient hydrogen quantities for the initiation of cracking^{11,12}. By quenching and tempering at 720°C the tube resistance to hydrogen embrittlement was increased which was expressed by a smaller embrittlement index, particularly specimens quenched in water where the embrittlement index is only 11,1%. The fracture are ductile, with fine dimple appearance (figure 2c). The increase of embrittlement index was induced mostly by presence of high tempered martensite microstructure (figure 3b) in which by means of X-ray diffraction the distribution of fine sphero carbides FeC, Fe₃C, Cr₇C₃ and $\alpha\text{Mo}_2\text{C}$ was determined. Fine carbides microstructured is a main microstructural parameter for improving of hydrogen embrittlement because in this case a longer time is needed for the accumulation of critical amount

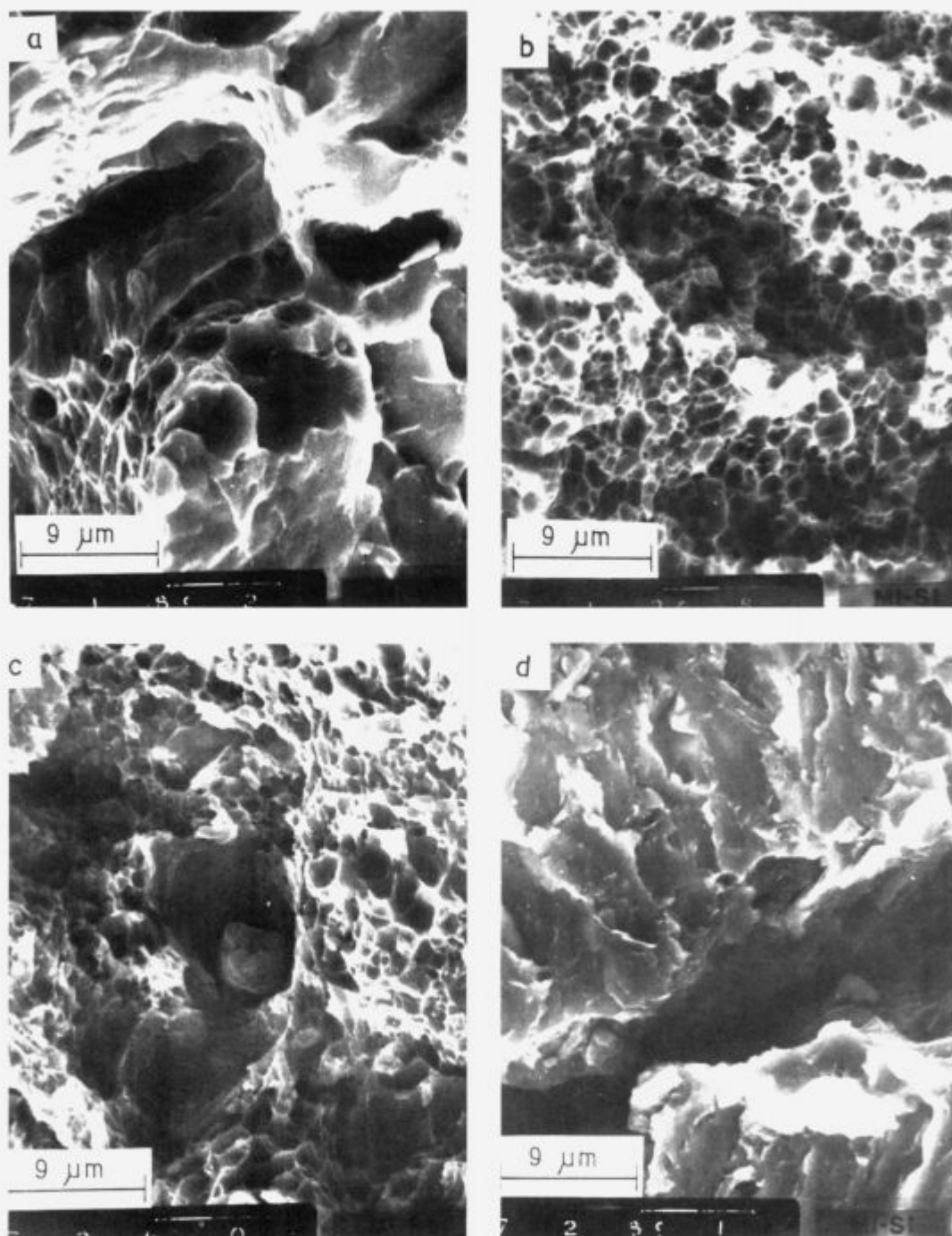


Figure 2: The microfractography of fractured surfaces of low alloy Cr-Mo steel after cathodic polarization
a) as-rolled, current density 1,6 mA/cm²
b) quenched and tempered, current density 4,0 mA/cm²
c) normalized and tempered, current density 4,0 mA/cm²
d) quenched and tempered, current density 12,0 mA/cm²

Slika 2: Mikrofraktografije prelomnih površin malolegirane Cr-Mo jekla po katodni polarizaciji
a) valjano, gostota toka 1,6 mA/cm²
b) kaljeno in popuščeno, gostota toka 4,0 mA/cm²
c) normalizirani in popuščeno, gostota toka 4,0 mA/cm²
d) kaljeno in popuščeno, gostota toka 12,0 mA/cm²

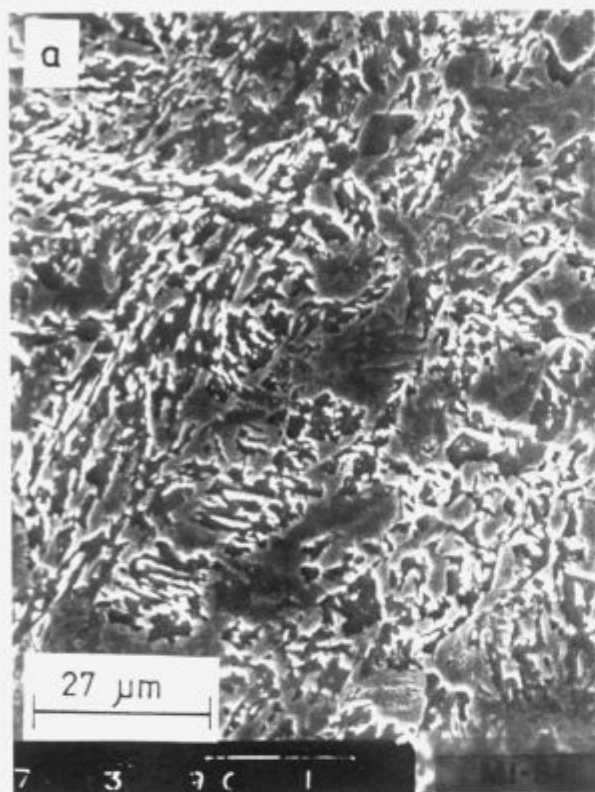


Figure 3: The microstructures tubings from low alloy Cr-Mo steel in as-rolled (a) and quenched and tempered state (b)

Slika 3: Mikrostruktura cevi iz malolegirane Cr-Mo jekla v valjanem (a) ter kaljenem in popuščanem stanju (b)

of hydrogen inducing the brittle material decay. Since the microstructure influence is manifested mainly through the absorption and trapping of hydrogen on the interfaces carbide/matrix, the defined fine chrome carbides Cr_7C_3 and $\alpha-Mo_3C$ increase resistance to hydrogen embrittlement.

5. Conclusion

The tubing of investigated Cr-Mo steel in as-rolled state (without heat treatment) in regard to mechanical properties correspond to API grade P-110 with bainite microstructure appeared in usual way by air cooling of pipes at finished rolling temperature. Their resistance to hydrogen embrittlement is small with high values of embrittlement index of 87.6%. It proves also the presence of mixed fracture with mainly brittle cleavage fractures. By normalizing of tubing at $900^\circ C$ and tempering at $700^\circ C$ is obtained API grade L-80 with a great resistance to hydrogen embrittlement ($F = 27,8\%$) and ductile fracture with a small fracture energy. However, by quenching and tempering at $720^\circ C$ API grade was obtained C-95 with significant resistance to hydrogen with ductile mainly fine dimple fractures. The reason of there are carbides Cr_7C_3 and $\alpha-Mo_3C$ in tempered martensite microstructure. However, by increasing of current density from $4,0 \text{ mA/cm}^2$ to $12,0 \text{ mA/cm}^2$ at cathodic polarization some quantity of hydrogen (5-7 ppm) was absorbed which remarkably decreased resistance to hydrogen embrittlement ($F = 86-89\%$) in the presence of the brittle cleavage transgranular fracture. The results of the test show that for the obtaining of API grade C-95 with high resistance to hydrogen embrittlement the heat treatment of tubing from investigated Cr-Mo steel needs to be carried out by quenching in water after having reached the temperature at $870^\circ C$ and air tempering from $720^\circ C$.

Literature

- ¹ E.A. Uljanin: *Struktura i korozija metallov i splavov*, Metalurgija, Moskva, 1989, s 139
- ² G.M. Pressouyre: Current solutions to hydrogen problems in steel, Proceeding of the first International Conference on Current Solutions to Hydrogen Problems in Steels, Washington, 1.-5. 11. 1982, s 18
- ³ API Specification 5CT, American Petroleum Institute, Washington, 1990, s 18
- ⁴ F. Mansfeld: *Corrosion mechanisms*, Marcel Dekker Inc, New York, 1987, s 344
- ⁵ P. McIntyre: Hydrogen effects in high strength steels, Edited by R.A. Oriani, J.P. Hirth: Hydrogen degradation of ferrous alloys, Noyes Publication, New Jersey, 1985, s 763
- ⁶ L. Vehovar: International Conference on Materials Development in Rail, Tire, Wing, Hull Transportation, Euromat 92, Genoa, s 1367
- ⁷ M. Gojić et al.: Evaluation of Mn-V steel tendency to hydrogen embrittlement, *Kovine Zlitine Tehnologije*, 26, 1992, s 349
- ⁸ S.T. Rolfe, S.R. Novak: Slow-bend K_{IC} testing of medium-strength high-toughness steels - STP 463, Philadelphia, American Society for Testing and Materials, 1970, s 124
- ⁹ E. Snape: Rolles of composition and microstructure in sulfide cracking of steels, *Corrosion*, 24, 1968, s 261
- ¹⁰ J.B. Greer: Fractors affecting of sulfide stress cracking performance of high strength steels, *Materials Performance*, 3, 11, 1975
- ¹¹ G.M. Pressouyre, I.M. Bernstein: A Quantitative Analysis of Hydrogen Trapping, *Metallurgical Transactions A*, 9A, 1978, s 1571
- ¹² J.P. Hirth: Effects of Hydrogen on the Properties of Iron and Steel, *Metallurgical Transactions A*, 11A, 1980, s 861.



UNIVERZA V MARIBORU
TEHNIŠKA FAKULTETA
KEMIJSKA TEHNOLOGIJA
62000 Maribor, Smetanova ul. 17

OBVESTILO O IZIDU PRIROČNIKA ZA ZMANJŠEVANJE NASTAJANJA ODPADKOV IN EMISIJ

Dovolite, da vas obvestimo, da je oddelek kemijske tehnologije
Tehniške fakultete Maribor izdal

PRIROČNIK ZA ZMANJŠEVANJE NASTAJANJA ODPADKOV IN EMISIJ.

Priročnik smo prevedli iz ameriške publikacije Waste Minimization Opportunity Assessment Manual (United States Environmental Protection Agency), pomagali smo si z nemško publikacijo Handbuch der Abfall- und Emissionsvermeidung (Tehniška univerza Graz). Priročnik opisuje metode in tehnike minimiranja proizvodnje vseh vrst odpadkov na viru, tehnike izbire ter tehničnega in ekonomskega vrednotenja alternativ za zmanjšanje nastajanja odpadkov in emisij. Podana metodologija je uporabna za vse vrste industrij in storitvenih dejavnosti, kjer nastajajo odpadki, koristno jo lahko uporabimo tudi za študi možnosti manjše porabe energije v proizvodnji in povečanje njene izrabe.

Minimiranje odpadkov in emisij je obsežen postopek sestavljen iz štirih faz: planiranja in organiziranja, poizvedovanja, analize možnosti izvedbe in končne izvedbe. Priročnik opisuje in podaja vse aktivnosti v podjetju, ki so potrebne za uspešno izvedbo ukrepov za zmanjšanje proizvodnje odpadkov in porabe energije. Končni rezultat je vedno profit (povečani prihranki), zmanjšanje onesnaževanja okolja, boljši položaj na trgu in ugled podjetja. V prilogi so podani delovni listi za izvedbo predraziskav in raziskave z navodili za tehnično in ekonomsko analizo izbranih ukrepov.

Priročnik je namenjen vsem podjetjem, kjer nastajajo odpadki; vodjem obratov, razvojnim oddelkom, zadolženim za varstvo okolja, izobraževalnim ustanovam in ostalim, ki se ukvarjajo z varovanjem okolja.

NAROČILA:

**Janez Petek, Tehniška fakulteta Maribor,
Oddelek kemijske tehnologije, Smetanova 17, Maribor oz.
po telefonu (062) 25-461 int. 643 ali po faksu (062) 227-774.**

Cena priročnika je 1.300 SIT.

Predicting Oxide Activities in CaO-Al₂O₃-SiO₂ System by Computer Model

Napovedovanje aktivnosti oksidov v sistemu CaO-Al₂O₃-SiO₂ z računalniškim modelom

B. Koroušič, Institut for Metals and Technology, Ljubljana

The most important metallurgical effects of ladle treatment of aluminium - killed steels with calcium, are associated with the modification of alumina inclusions. For the development of the deoxidation - control model for inclusions, the thermodynamic slag model, based on the Gibbs energy minimization and modelling approaches postulated from Hastie et al., was used to calculate component oxide activities in the system CaO-Al₂O₃ and part of the system 3CaO.Al₂O₃-SiO₂, 12CaO.7Al₂O₃-SiO₂ and CaO.Al₂O₃-SiO₂ at 1500°C and 1600°C.

Key words: Slag activities, model computations, Gibbs energy minimization

Najpomembnejši metalurški učinki pri uporabi kalcija za obdelavo jekel pomirjenih z aluminijem so povezani z modifikacijo aluminatnih vključkov. Pri razvoju modela za kontrolo vključkov smo uporabili termodinamični model, ki sloni na Gibbsovem modelu minimizacije energije in postulatu, ki ga je postavil Hastie et al. Izračunavanja aktivnosti oksidnih komponent smo izvršili za sistem 3CaO.Al₂O₃-SiO₂, 12CaO.7Al₂O₃-SiO₂ in CaO.Al₂O₃-SiO₂ pri temperaturi 1500°C in 1600°C.

Ključne besede: aktivnosti žlinder, modelna izračunavanja, Gibbsova energija minimizacije.

1. Introduction

In last two decades calcium-based additions are made to molten steel not only for deoxidation and/or desulfurisation purposes, but also for the control of inclusion composition and morphology. The ladle metallurgy offers today excellent possibilities to control of the cleanliness and quality of steels. The most important metallurgical effects of ladle treatment of aluminium-killed steels with calcium, are associated with the modification of alumina inclusions preventing his precipitation during the continuously casting known as *nozzle clogging process*. Also the role of the syntetic slags CaO-Al₂O₃-SiO₂ for the secondary refining of steel is growing dramatically because of it's excellent refining capabilities. In order to put inclusion engineering into practice, it is essential that the equilibrium relationship between the liquid steel and the corresponding inclusion should be determined. With suitable selection of the deoxidation practice (changing ratio Ca/Al) is possible to avoid nozzle clogging, ensuring inclusions with melting points lower than the steel melt temperature.

In this paper are presented equilibrium thermodynamic activity of the Al₂O₃, CaO, and SiO₂ in system CaO-Al₂O₃-SiO₂, determined with new **Gibbs Energy Minimization Model - GEMM** (The equilibrium calculation in the GEMM program is a minimization of the integral Gibbs free energy using a Lagrangian multiplier method for the constraints) and discussed in relation to their use in deoxidation and calcium treatment control.

2. Thermodynamic model of oxide phase equilibria - GEMM

Many thermodynamical models are developed in last two decades for the investigation of multiphase equilibria and for

thermodynamic predictions of multicomponent high-temperature oxide systems¹⁻³. Calculations involving thermodynamic equilibria in multi-phase oxide systems are extremely time consuming, even in the systems with relatively few components. In recent years, there has been rapid progress in the use of thermodynamic models achieving better understanding of many metallurgical, ceramical and chemical systems of commercial significance.

This progress has been made possible largely by developments in computer software technology as well as the increasing availability of reliable and comprehensive thermodynamic values compared with "hand" calculations which have traditionally been assigned to specialists.

A new modelling approach for thermodynamic predictions of multiphase high-temperature oxide systems developed by J.W. Hastie and D.W. Bonnell⁴ has been extended and applied for the investigation of the binary and ternary systems CaO-Al₂O₃ and CaO-Al₂O₃-SiO₂. Well-known examples of solution models in current use include, ideal, regular, and the molecular-level associated liquid or cluster models^{4,7}. The basic approach used in the GEMM prediction model is a description of non-ideal mixture and the formation of complex liquids and solids as mixing components. This model has a thermodynamic basis and does not rely on assumed molecular or ionic entities in the liquid phase. The liquid components are not independent molecular species, but are essentially subphases that serve as models for the local associative order-an idea that Schenk himself greatly expanded some 50 years ago⁸.

Although the components are included individually, it is assumed that in most cases, the components form short range order, and do not necessarily represent discrete molecular, ionic or other structural entities. The component and complex-component oxides formed are assumed to mix ideally, in accordance

with Raoult's law. Hence, thermodynamic activities and apparent mole fractions (X^*) are equivalent quantities for this model.

In the GEMM-prediction model, the thermodynamic activity of oxides CaO, Al₂O₃, and SiO₂ can be calculated from the corresponding thermodynamic functions. The modelling approach has been validated by comparison with experimental activity data, obtained from Taylor⁸, Kay⁹, and recently published data from Fujisawa¹⁰, and Nagata¹¹. While the thermodynamic data are incomplete they are still sufficiently extensive to allow their use in the performance of common thermodynamical calculations for many high-temperature slags and other systems. Good agreement between the model predictions and experimental activity data is obtained. The utility of even sparse experimental data can, in principle, be greatly enhanced by GEMM optimization techniques.

3. Thermodynamic data bases

Before actual calculations can begin, the necessary thermodynamic data must be collected. For most oxide systems relevant to industrial steelmaking practice, the experimental thermodynamic data base are often a variety of somewhat obscure sources or are incomplete.

The CaO-Al₂O₃ and CaO-Al₂O₃-SiO₂ systems are an exception, in that there is an adequate thermodynamic data base which can be applied to test the model computations. Such a thermodynamical optimization technique offers the important benefit that it can drastically reduce the need to conduct costly experiments. The Gibbs free energy data for the corresponding oxide phase at 1600°C are given in table 1.

Table 1: Compounds Gibbs energy of formation, negative (kJ/mol) (s)=solid, (l)=liquid

Table 1: Prosta tvorben energija nekaterih oksidov, minus (kJ/mol)

Components	1873 K(s)	1873 K(l)
Al ₂ O ₃	1089.81	1065.70
CaO	-431.08	427.47
SiO ₂	578.50	-
3CaOAl ₂ O ₃	2454.77	-
12CaO7Al ₂ O ₃	13222.86	13280.00
CaOAl ₂ O ₃	1564.62	1564.33
CaO2Al ₂ O ₃	2693.83	2688.12
CaO6Al ₂ O ₃	7063.18	7051.92

The GEMM-computer program used for calculation of the equilibrium composition, and hence activities, utilizes a data base made up of Gibbs energies of formation $\Delta(G_f)$ as a function of temperature (T). The free energies of formation $\Delta(G_f)$ are either known or can be estimated for these complex component liquids and solids.

The data for most oxides were obtained mainly from data base made by J. Hastie and Bonnell¹². In a few instances, the coefficients to the $\Delta(G_f)$ equation have been re-evaluated using new thermodynamic data obtained in the literature.

4. Results

CaO-Al₂O₃ System

The CaO-Al₂O₃ system is one of the fundamental systems of the calcium-based slags and non-metallic inclusions, and there have been many reports on the thermodynamics of this system.

Much of the published information on the thermodynamic properties for some binary aluminates has been based on work

conducted and published in 1960's. Extrapolation of these data to steelmaking temperatures may introduce large errors, especially for a particular composition range.

The CaO and Al₂O₃ activity data shown in figure 1 are consistent with the bulk of literature experimental data at T=1600°C. Electromotive force (emf) and cell-activity data have recently been obtained by Fujisawa et al¹⁰ covering a wide range of compositions. Our model activity data at T = 1500°C have been compared with recently published data by Nagata et al¹¹ and as is shown in figure 2. Good agreement between the model prediction and experimental activity data for a wide range of composition is demonstrated.

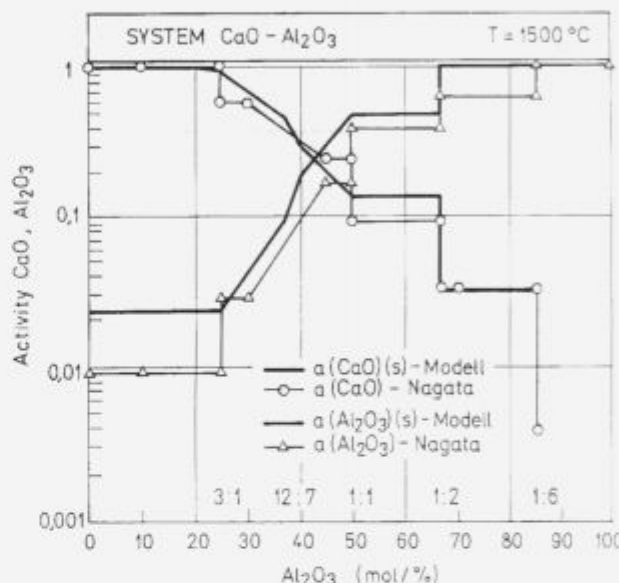


Figure 1: Model dependence of computed activity data in CaO-Al₂O₃ at T=1500°C.

Slika 1: Modelna izračunavanja aktivnosti oksidov v sistemu CaO-Al₂O₃ pri T=1500°C.

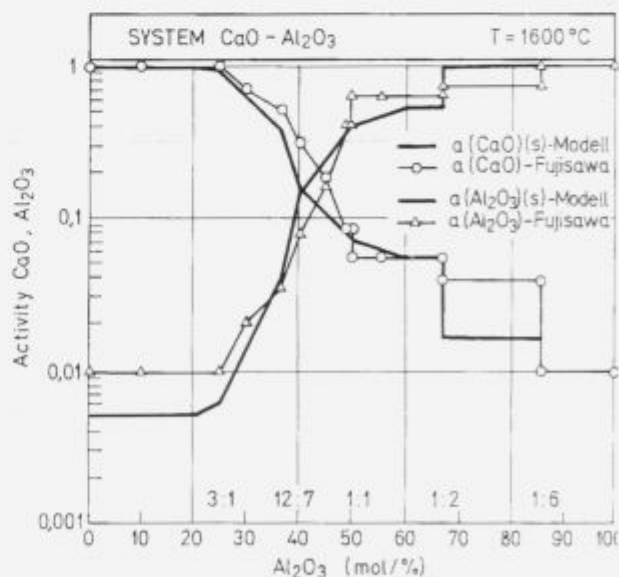


Figure 2: Model dependence of computed activity data in CaO-Al₂O₃ at T=1600°C.

Slika 2: Modelna izračunavanja aktivnosti oksidov v sistemu CaO-Al₂O₃ pri T=1600°C.

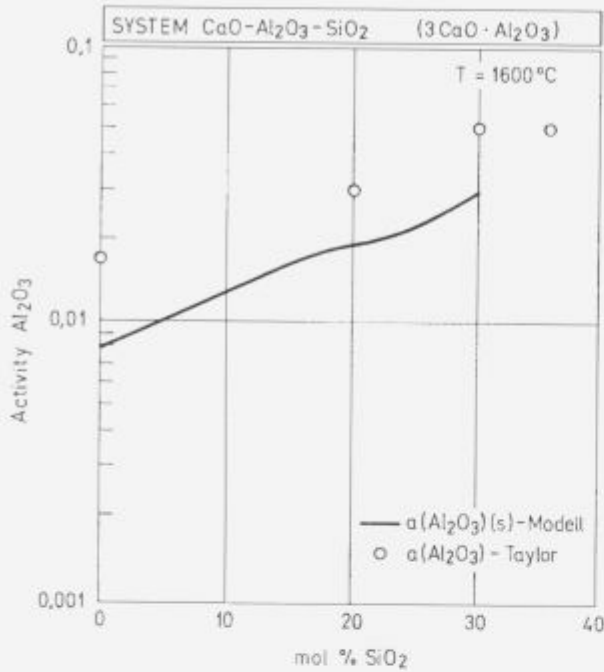


Fig. 3a

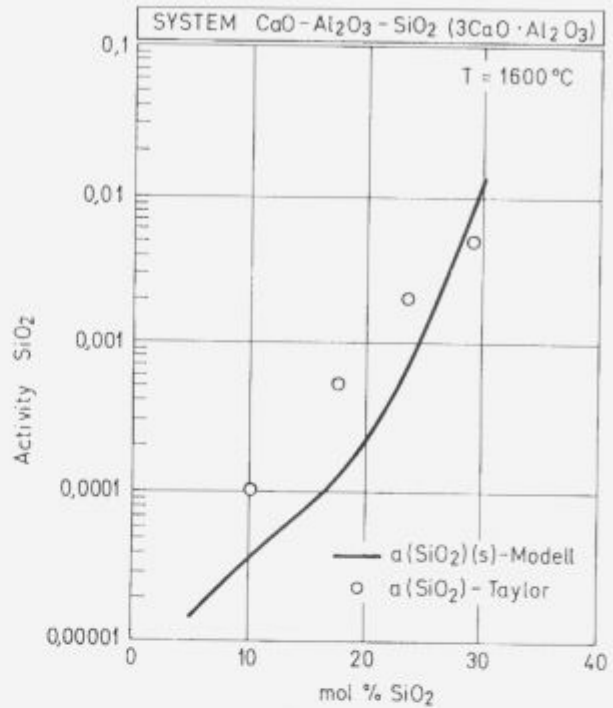


Fig. 3c

Figure 3: Model computed data of CaO, Al₂O₃ and SiO₂ in CaO-Al₂O₃-SiO₂ system for 3CaO·Al₂O₃ composition and T=1600°C

Slika 3: Modelna izračunavanja CaO, Al₂O₃ in SiO₂ v sistemu CaO-Al₂O₃-SiO₂ za sestavo 3CaO·Al₂O₃ pri T=1600°C

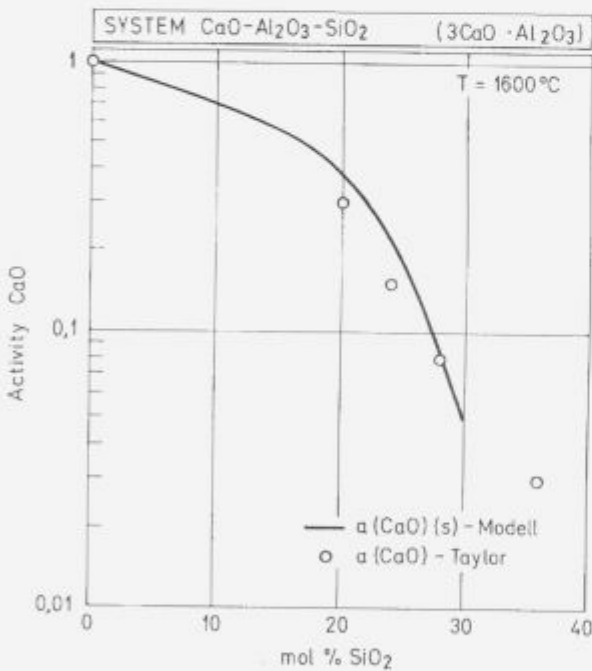


Fig. 3b

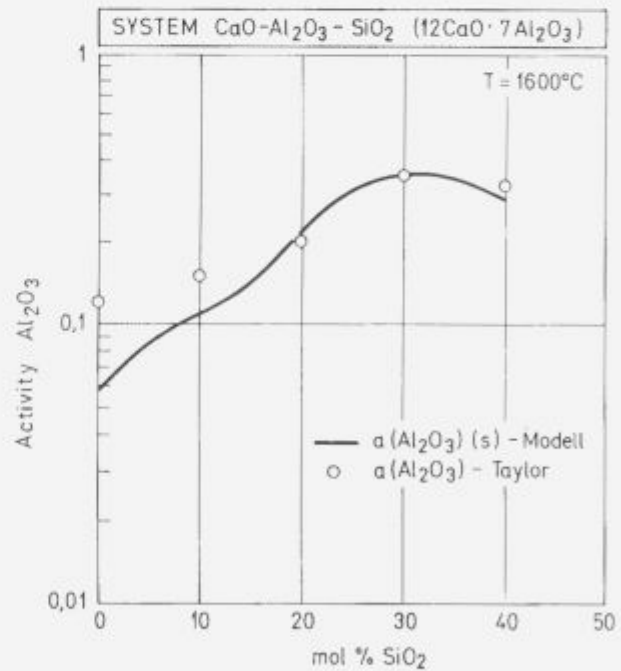


Fig. 4a

CaO-Al₂O₃-SiO₂ System

The control and prevention of multiphase in CaO-Al₂O₃-SiO₂ and a suitable deoxidation practice should be applied to avoid undesirable alumina inclusions, they are not deformable and, besides, provoke tundish nozzle blockage problems. In order to determine oxygen and sulphur contents in molten steel and the conditions for aluminate and solid sulphide coprecipitation during casting, the knowledge of the activity of CaO, Al₂O₃ and SiO₂ in molten slag and inclusions is important. One of the main advantages in the used model is the treatment as a high order sys-

tem at high temperatures where extrapolation of thermodynamic data may introduce large errors. For CaO-Al₂O₃-SiO₂ system, several experimental studies of activity measurement and phase - diagram determination are reported in the literature⁸. But, because of experimental difficulties, large discrepancies are observed between different experimental works. The activity of

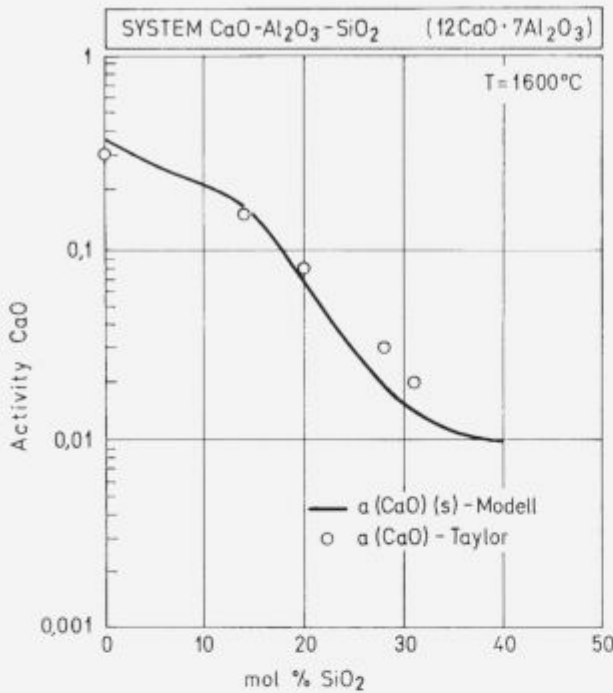


Fig. 4b

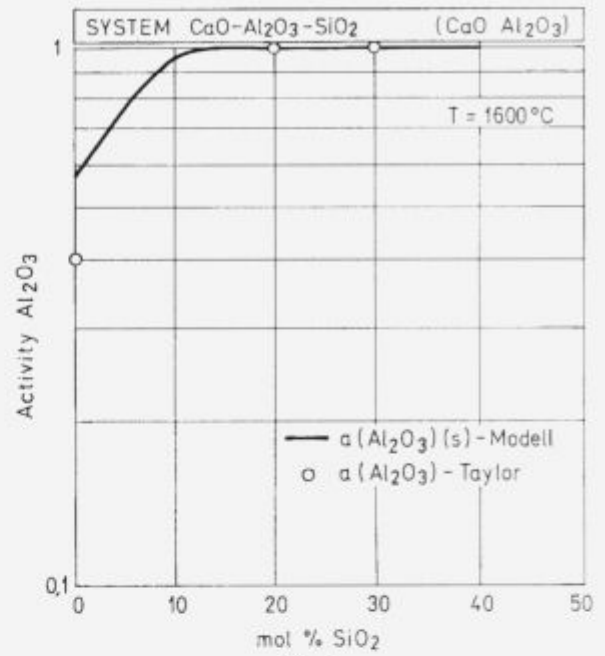


Fig. 5a

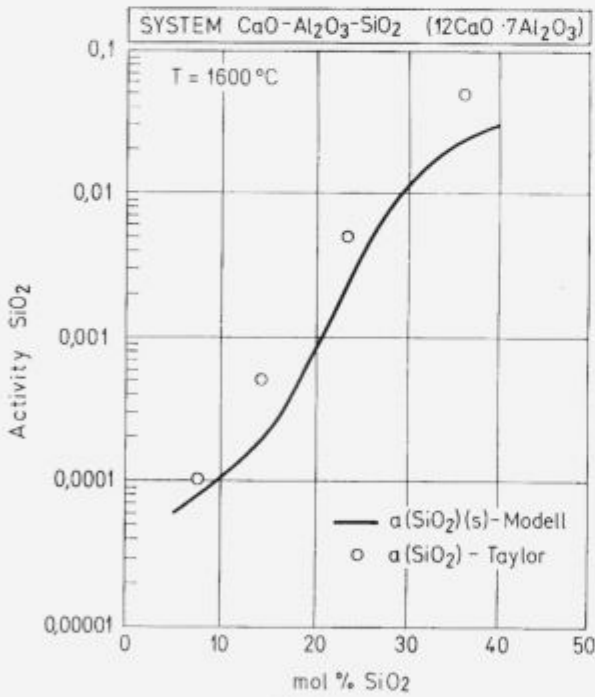


Fig. 4c

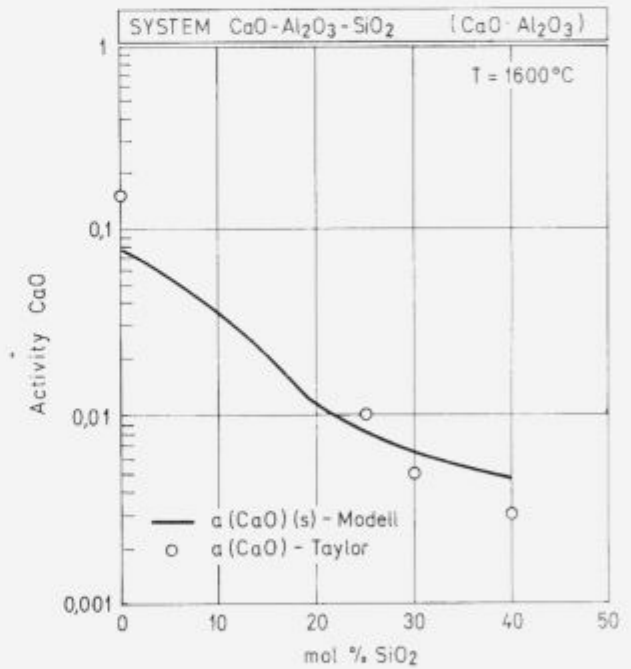


Fig. 5b

Figure 4: Model computed data of CaO, Al₂O₃ and SiO₂ in CaO-Al₂O₃-SiO₂ system for 12CaO·7Al₂O₃ composition and T=1600°C

Slika 4: Modelna izračunavanja CaO, Al₂O₃ in SiO₂ v sistemu CaO-Al₂O₃-SiO₂ za sestavo 12CaO·7Al₂O₃ pri T=1600°C

CaO, Al₂O₃, and SiO₂ in CaO-Al₂O₃-SiO₂ molten slag at 1500°C was measured by Rein and Chipman in 1963 and 1965¹³. The activity data determined the activity of silica by equilibrium with a metallic phase, of carbon - saturated iron with silicon in solution. By integration of the Gibbs - Duhem law, the activities of lime

and alumina were calculated in all of liquidus domains. The compositions are expressed in mole fractions of CaO, Al₂O₃ and SiO₂. The reason for choosing Al₂O₃ rather than Al₂O is because in the basic melts, Al₂O₃ give rise to two foreign ions AlO₂⁻, whereas SiO₂ gives rise only to one SiO⁴⁺. Thermodynamic activities calculated using Gemm - computer program are shown in figures 3 - 5. Experimental activity data for the CaO-Al₂O₃-SiO₂ system is particularly sparse and disparate^{8,13,14}. Very good agreement between the model and experiment data for the silica-

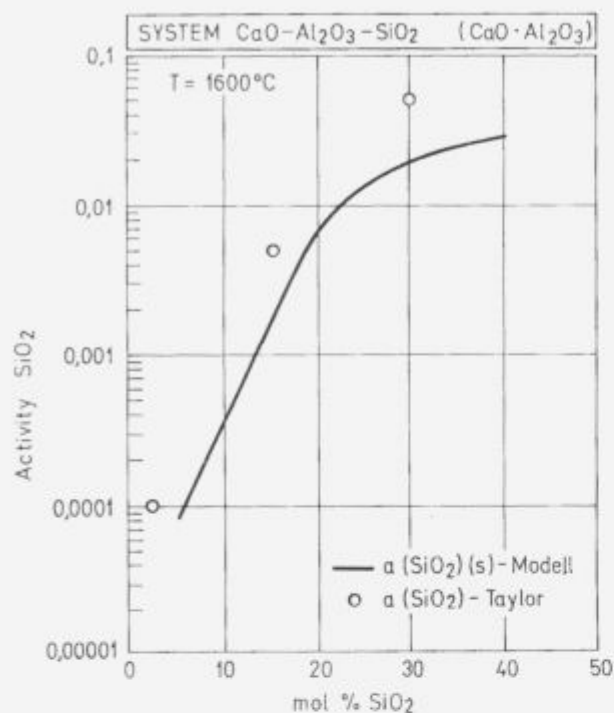


Fig. 5c

Figure 5: Model computed data of CaO, Al₂O₃ and SiO₂ in CaO-Al₂O₃-SiO₂ system for CaO:Al₂O₃ composition and T=1600°C

Slika 5: Modelna izračunavanja CaO, Al₂O₃ in SiO₂ v sistemu CaO-Al₂O₃-SiO₂ za sestavo CaO:Al₂O₃ pri T=1600°C

activities and computed thermodynamic activity data for Al₂O₃ and CaO at 1600°C is demonstrated.

5. Conclusion

The Gibbs energy minimization model (GEMM) is used with the corresponding thermodynamical data base to calculate the predicted composition of solids, liquids (non-ideal solutions), and the vapour phase.

The calculated composition of the CaO, Al₂O₃, and SiO₂ are taken as the activity. Numerous comparisons between model and the experimental activities in the systems CaO-Al₂O₃ and CaO-Al₂O₃-SiO₂ at different temperatures have confirmed the reliability of this approximation.

Considering the large number of the data base components, and the cumulative errors in the thermodynamic functions, the possibility exists that the present data base is not unique.

However, as has been pointed out by J. Hastie and D. Bonnell¹¹, the author expects that some future modifications of the data base will be relatively minor.

6. References

- Eriksson, G.: Chem. Scripta 8, 100, (1975)
- Gaye, H., D. Coulombet: Irsid PCM-RE, 1064, March, 1984
- Hastie, J.W., Horton, W. S., Plante, E.R., and Bonnell, D.W.: Thermodynamic Models of Alkali Vapor Transport in Silicate Systems, IUPAC Conf., Chemistry of Materials at High Temperature, Harwel, U.K., August 1981; High Temp.-High Pres. 14, 669, (1982)
- Ansara, I.: The modern computer applications in thermodynamics, Mattech '90, June 14-15 (1990), Helsinki
- Lin, P.L., Pelton, A.D. Bale, C.W., and Thompson, W.T.: CALPHAD 4, 47 (1980)
- Sundman, B.: Thermo-calc course, Mattech '90, June 14-15 (1990), Helsinki
- Barin, I., G. Eriksson, F. Sauert, M. Zeitler, B. Witting, W. Schmidt: Equitherm, Databank and computer program for thermodynamic calculation, Privat communication (1990)
- Verein Deutscher Eisenhüttenleute (Hrsg.) Schlackenatlas; Düsseldorf Verlag Stahleisen (1981)
- Kay, D.A.R., S.V. Subramanian and R. V. Kumar: Inclusions in Calcium Treated Steels, Proceedings of the Second International Symposium on the Effects and Control of Inclusions and Residuals in Steels, 25th Conference of Metallurgist, Toronto, (1986) CIM
- Fujisawa, T., Ch.Yamauchi, H.Sakao: Activity of CaO and Al₂O₃ in CaO-CaS slags saturated with CaS and the equilibrium between the slags and molten iron alloys at 1873 K, The Sixth Internat. Iron and Steel Congress, Vol.1, 201-208 (1990)
- Nagata, K., J. Tanabe, and K.S. Goto: Activities of Calcium oxide in CaO-based Inclusions, measured by galvanic cells, The Sixth Intern. Iron and Steel Congress, Vol. 1, 217-224 (1990)
- Hastie, J., D.W.Bonnell: A predictive phase equilibrium model for multicomponent oxide mixtures Part II. Oxide of Na-K-Ca-Mg-Al-Si, High Temperature Science, Vol. 19, (1985) 275-306
- Rein, R.H., J. Chipman: J. Trans. Metall. Soc. AIME 233, 415 (1965).



INŠTITUT ZA KOVINSKE MATERIALE
IN TEHNOLOGIJE p.o.

INSTITUTE OF METALS
AND TECHNOLOGIES p.o.

61000 LJUBLJANA, LEPI POT 11, POB 431,
SLOVENIJA

Telefon: 061/1251-161, Telefax: 061 213-780

**SLOVENSKO DRUŠTVO ZA MATERIALE
SLOVENIAN SOCIETY OF MATERIALS**

61000 Ljubljana, Lepi pot 11
tel.: 061 1251 161, Fax.: 061 213 780

SLOVENSKO DRUŠTVO ZA MATERIALE

PROGRAMSKA IZHODIŠČA

Slovensko društvo za materiale je bilo ustanovljeno z namenom, da se v njem povežejo vsi strokovnjaki, ki se ukvarjajo z materiali (anorganski nekovinski, polimeri in kovinski materiali), da bi v javnosti delovalo kot asociacija, ki mora biti konsultirana pri pomembnih odločitvah. Programska izhodišča Slovenskega društva za materiale so naslednja:

- povezava strokovnjakov, ki se ukvarjajo z materiali (anorganski nekovinski, polimerni, kovinski) v strokovno združenje;
- pričetek konstruktivnega sodelovanja na področju raziskovanja in izobraževanja;
- organizacija strokovnih predavanj, ki naj služijo boljšemu medsebojnemu poznavanju in afirmaciji mladih strokovnjakov;
- organizacija izobraževalnih seminarjev;
- razširitev vsakoletnega jesenskega srečanja v Portorožu;
- priprava spiska neodvisnih ekspertov za ocenjevanje projektov na področju materialov;
- vključitev v Evropsko federacijo za materiale, kar bi omogočilo tudi organizacijo mednarodnih manifestacij;

Sedež Slovenskega društva za materiale je na Inštitutu za kovinske materiale in tehnologije, Ljubljana, Lepi pot 11.

V društvo se lahko včlanijo vsi strokovnjaki z visoko izobrazbo in študentje.

Composite Mechanism of Scale Adhesiveness

Kompozitni mehanizem oprijemljivosti škaje

B. Kosec, L. Kosec, FNT, Odsek za metalurgijo in materiale, Ljubljana

In the scale which is formed on the surface of alloys during the annealing process, metallic and oxidic phases are interwoven in various ways, which are characterized by the shape, portions, and size of both phases. Ductile scale component enables certain deformation of the scale, and it hinders propagation of cracks in the brittle oxidic phase. Key words: scale, composite material, crack, propagation, separation, adhesiveness.

V škaji, ki nastane med žarjenjem na površini zlitin, se kovinska in oksidna faza prepletata na različne načine, ki jih karakterizira oblika, delež in velikost obeh faz. Duktilna sestavina škaje omogoča določeno deformacijo škaje in preprečuje širjenje razpok, nastalih v krhki oksidni fazi.

Ključne besede: škaja, kompozit, razpoka, napredovanje, ločitev, oprijemljivost.

Scale is product of the high temperature oxidation of metals and alloys. Structure of scale depends on the chemical composition of alloy, temperature atmosphere and on the time of annealing. The scale which adheres to metal during working and service reduces in most cases the quality of the surface of product. Therefore it should be removed in single stages of technological process. The most simple ways of scale removal are mechanical forces which appear due to temperature changes or in working.

Scale and metal differ in their physical properties, among others, also in all mechanical properties and in thermal expansion. Great differences in thermal expansion during the temperature changes cause stresses which practically separate both constituents, or they fractured only oxide. Scale adhesiveness depends on the microstructure, geometry of constituents, and the boundary with the metallic matrix.

Due to properties and the way how scale constituents are interwoven, and depending on its properties, the scale can be treated as a composite material.

Composite materials have different properties in comparison to the properties of constituents. One of essential characteristics

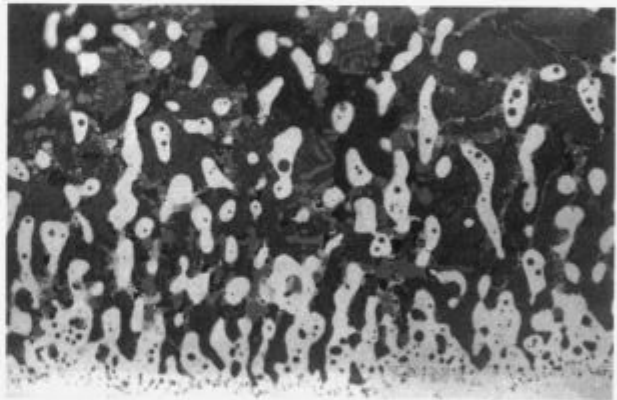


Fig. 2: Scale region with pronounced composite structure, with long, wide and overlapping metallic lamellae which successfully stop the propagation of cracks (200 x)

Slika 2: Del škaje z izrazito kompozitno zgradbo, dolgimi, širokimi in prekrivanimi lamelami kovine, ki dobro zaustavljajo razpoke (200 x)

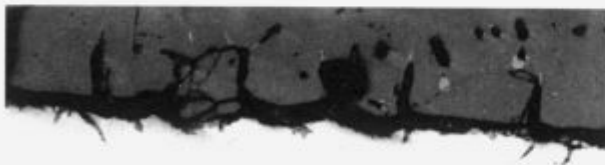


Fig. 1: Well defined simple boundary between scale and parent metal in carbon steel (200 x)

Slika 1: Dobro definirana enostavna meja med škajo in kovino v ogljikovem jeklu (200 x)

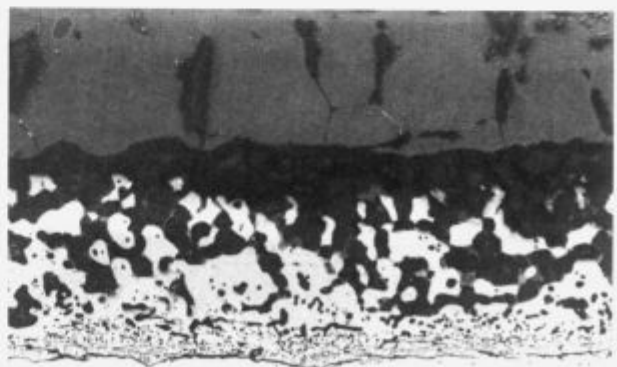


Fig. 3: Weak regions in the scale on the boundary between composite and oxide part

Slika 3: Šibka mesta v škaji na meji, ki loči oksidni del od kompozitnega

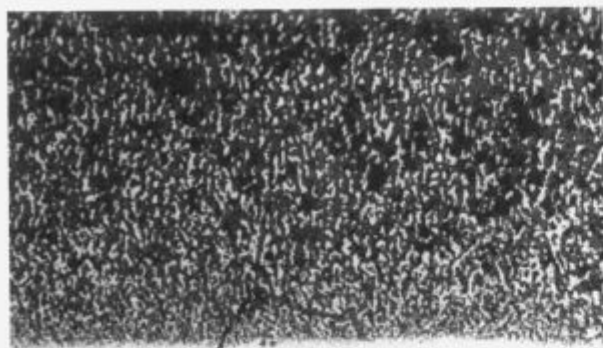


Fig. 4: Composite scale with a great amount of metal phase, which is not able to stop the crack propagation (100x)

Slika 4: Kompozitna škaja z veliko kovinske komponente, ki nisposobna ustavljati razpoke (100x)

of composite materials is crack arrest. In composite materials with ductile matrix (e.g. metallic or of polymers) cracks appear usually in rigid constituents of the armature (most frequently in fibres), while in composite materials with ceramic matrix and ductile fibres the situation is reversed.

In the scale the nonmetallic constituents are always more brittle than the metallic ones, and they have also more defects which appear already during the growth. Portion, way of being interwoven, and geometry of both constituents determine the ability for stopping crack propagation and thus the obstinacy with which the scale resists to separation from the metal. In the cases, illustrated in Figs 2, 5 and 6, the microstructure has such portions of metallic constituent, and such combination of both phases, that separation on the boundary with pure metal cannot be expected, and scale can be removed only by additional machining of the surface. On pure metals the scale has usually a well defined boundary with the metal. The oxide metal boundary is the weak point for ideal fracture and thus good separation of scale from metal (Fig. 1). In alloys the metallic and oxidic con-

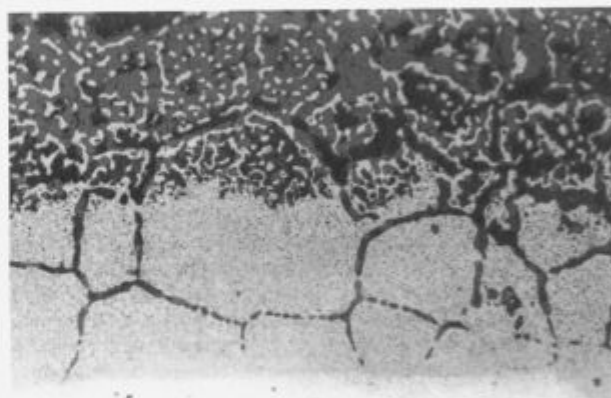
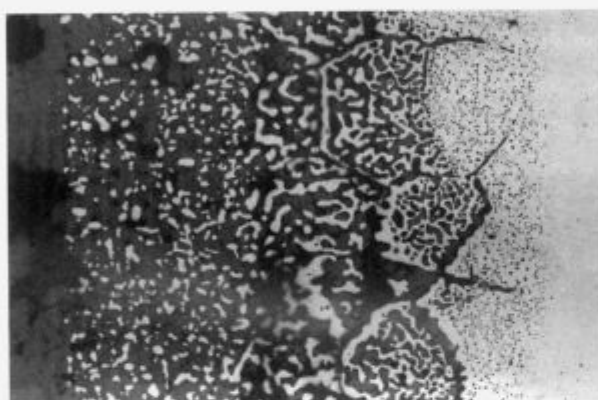


Fig.5,6: Weak directions for crack propagation in the compositescale with variously big metal "fibers", and along boundaries rich with oxide of alloying element (Cr) (200x)

Sl. 5,6: Šibki mesti na meji dveh kompozitnih con z različno velikimi "vlakni" kovine in vzdolž mej, bogatih z oksidom legirnega elementa (Cr) (200x)

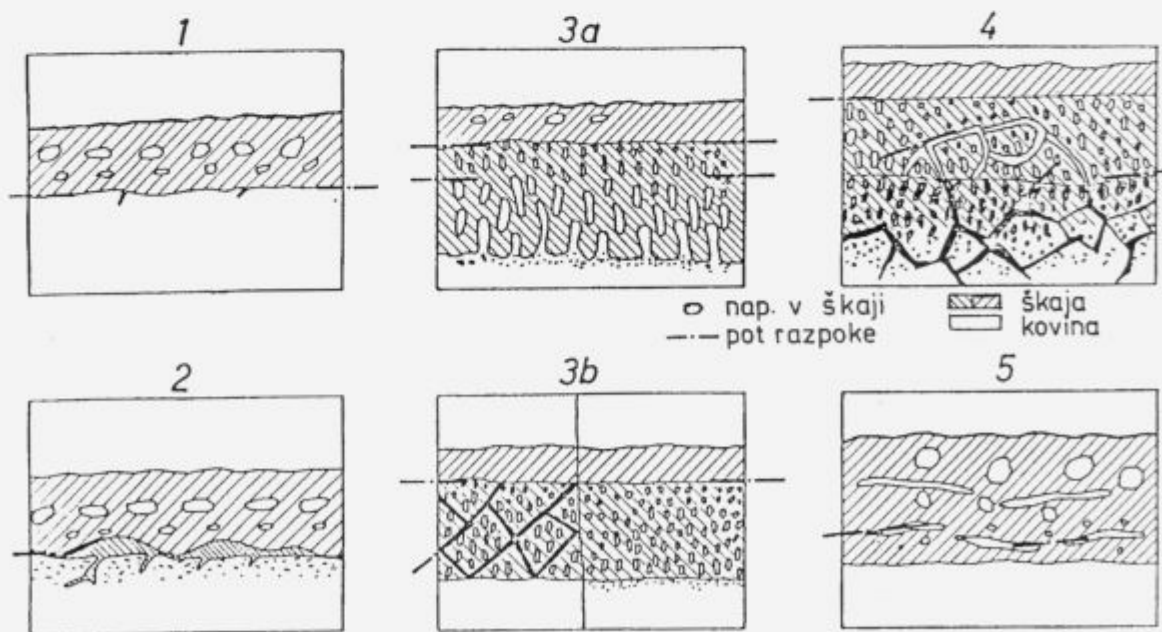


Fig. 7: Scheme of microstructural composition of some scales with composite structure

Slika 7: Shema mikrostrukturne zgradbe nekaterih škaj s kompozitno zgradbo (3a,b,4)

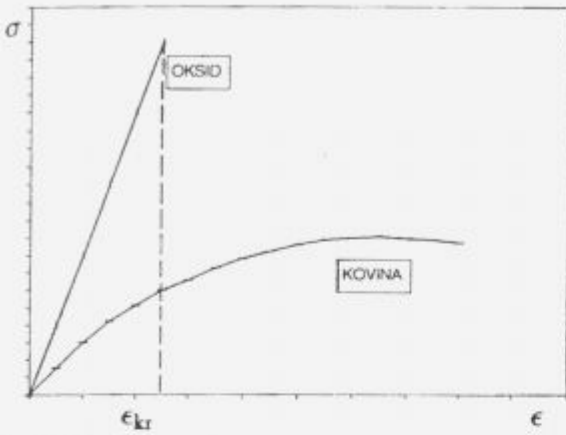


Fig. 8: Variations in mechanical characteristics of oxide and metal in the scale

Slika 8: Razlike v mehanskih lastnostih oksida in kovine

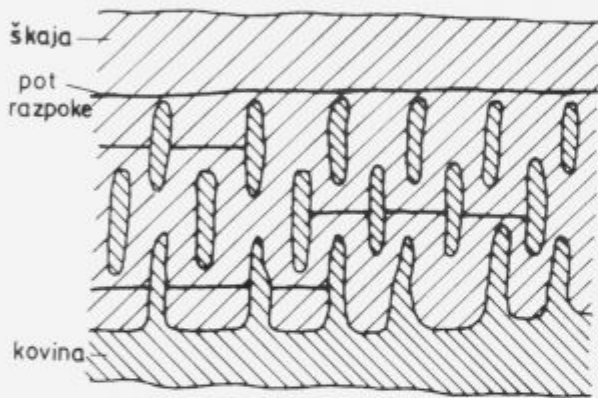


Fig. 9: Arrest of crack propagation in oxide on the metallic fibres
Slika 9: Ustavljanje širjenja razpok v oksidu na vlaknih kovine

stituents are most frequently interwoven, the boundary between scale and metal is not even which highly renders the separation of both phases more difficult (Fig. 2).

In steels composed of elements with thermodynamic properties different from those of iron, the scale of heterogeneous composition is formed. In the lower part of scale, metal and oxide particles are interwoven. This part behaves under mechanical loading identically to composite materials. The stresses which appear due to temperature variations or other loads can cause cracks in the oxide. Their propagation can be stopped by suitably distributed metal in the scale, and thus the fracture of scale is pre-

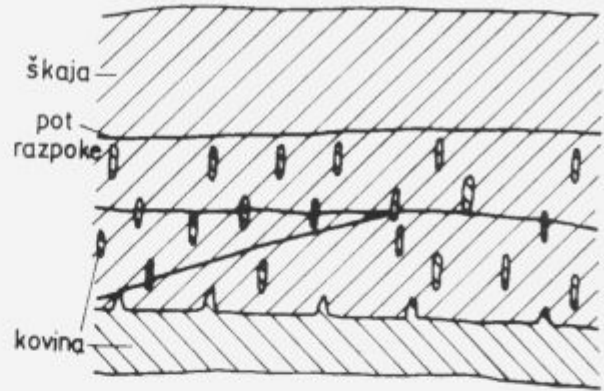


Fig. 10: Crack propagation in composite scale with unfavourable geometry of metallic phase

Sl. 10: Širjenje razpok v kompozitni škaji z neugodno geometrijo kovinske faze.

vented. The weak point in such scales is the surface between the composite zone and the upper scale layer being without metal (Fig. 3).

Some heterogeneous lower scale parts have unfavourable shape of metallic phase to stop the crack propagation in oxide. In such a scale crack propagates between metallic grains, and it can even cut some thin grains (Fig. 4).

In the oxide grains of parent metal there are also oxides of alloying elements, being either dispersed or predominantly precipitated in certain directions or in form of a net which corresponds to metal grain boundaries before the oxidation. These directions are mechanically weak points in the scale and cracks can propagate along them to parent metal matrix (Figs. 5, 6).

Some patterns how the boundary scale metal region is formed, are presented in Fig. 7.

Interwoven mineral and metal constituents give to scale all the characteristics of composite materials with the usually predominant oxidic phase also in the respect of microstructure while in the boundary with metal often metallic phase in the scale is prevailing (Figs. 7, 9 and 10).

Rigid mineral components render rigidness and compression strength to oxide, but they are very sensitive to various flaws which appear during the growth of such oxide. Metallic matrix of suitable geometry is able to stop cracks, and it increases the adhesiveness of scale (Fig. 9).

If a scale which will easily separate from metal is to be obtained, it must be composed mainly of mineral constituents.

Metallic particles being interwoven in the scale, especially if they are also connect with parent metal, can only increase the scale adherence.



INŠTITUT ZA KOVINSKE MATERIALE
IN TEHNOLOGIJE p.o.

INSTITUTE OF METALS
AND TECHNOLOGIES p.o.

61000 LJUBLJANA, LEPI POT 11, POB 431,
SLOVENIJA

Telefon: 061/1251-161, Telefax: 061 213-780

VACUUM HEAT TREATMENT LABORATORY

Vacuum Brazing

Universally accepted as the most versatile method of joining metals. Vacuum Brazing is a precision metal joining technique suitable for many component configurations in a wide range of materials.

ADVANTAGES

- Flux free process yields clean, high integrity joints
- Reproducible quality
- Components of dissimilar geometry or material type may be joined
- Uniform heating & cooling rates minimise distortion
- Fluxless brazing alloys ensure strong defect free joints
- Bright surface that dispense with expensive post cleaning operations
- Cost effective

Over five years of Vacuum Brazing expertise at **IMT** has created an unrivalled reputation for excellence and quality.

Our experience in value engineering will often lead to the use of Vacuum Brazing as a cost effective solution to modern technical problems in joining.

INDUSTRIES

- Aerospace
- Mechanical
- Electronics
- Hydraulics
- Pneumatics
- Marine
- Nuclear
- Automotive

QUALITY ASSURANCE

Quality is fundamental to the **IMT** philosophy. The choice of process, all processing operations and process control are continuously monitored by **IMT Quality Control Department**.

The high level of quality resulting from this tightly organised activity is recognised by government authorities, industry and International companies.

Embrittlement of Copper Wire Due to Oxygen

Krhkost bakra zaradi kisika

L. Kosec, V. Gontarev, B. Kosec, FNT, Odsek za metalurgijo in materiale, Ljubljana
N. Mlakar, Kolektor, Idrija

An example of the reversible oxygen embrittlement of copper is described in the paper. This phenomenon is combined with the drastic reduction of ductility and workability. It appeared at the low temperature annealing (500°C) of copper in the nitrogen atmosphere with a low oxygen concentration (5 ... 6 ppm), when diffusion of oxygen in copper took place preferentially on grain boundaries. During the cooling to the surroundings temperature oxygen precipitated from the saturated solution in the form of copper oxide (Cu_2O) on the grain boundaries, thus the conditions for the intergranular dimple fracture have been created.

Key words: oxygen, grain boundary diffusion, supersaturation, precipitation, intergranular dimple rupture, reversible embrittlement due to oxygen.

V prispevku je opisan primer reverzibilne krhkosti bakra zaradi kisika. Pojav je povezan z drastičnim zmanjšanjem duktilnosti in preoblikovalne sposobnosti bakra. Nastal je pri nizkotemperaturnem (500°C) žarenju bakra v dušiku z majhno koncentracijo kisika (5 ... 6 ppm), med katerimi je prišlo do prednostne difuzije kisika po kristalnih mejah bakra. Med ohlajanjem na temperaturo okolice je kisik iz nasičene raztopine precipitiral v obliki bakrovega oksida (Cu_2O) na kristalnih mejah in ustvaril pogoje za interkristalni prelom z jamicami.

Ključne besede: kisik, difuzija po kristalnih mejah, prenasičenje, izločanje, intergranularni jamičasti lom, krhkost zaradi kisika.

1. Introduction

Copper and some its alloys represent of high ductile and well cold workable materials. These properties can be usually obtained by annealing in the protective atmosphere. But there exist frequent exceptions. They are numerous since many products are made by advanced technology of the bulk shaping instead of machining. Limited ductility in the bulk shaping allowed only a certain amount of plastic deformation. Further plastic deformation initiated cracking till final fracture of material (Fig. 1).

These problems are often caused by oxygen which concentration could be detected by the metallographic analyse of oxide inclusions or chemical^(1,2). The copper oxide inclusions well follow the deformation of metal if extreme degrees are not exceeded.

Oxygen in the solid solution which simultaneously hardens copper and reduces its ductility is harmful. In some cases the chemically measured differences in the oxygen concentration between ductile and brittle copper are very small, even within the measuring error. In such cases oxygen is expected to be concentrated on certain sites in the microstructure, for instance on the grain boundaries, but it could be detected only by an analytical in situ method.

Before rolling, the copper wire of 12.8 mm in diameter have been annealed for 1 hour at 500°C in the nitrogen atmosphere with 5 ... 6 ppm of oxygen. During the annealing proces the average concentration of oxygen in the copper increased from approximately 0.001% to approximately 0.002%.

Already after first or second pass through the grooved roll (round - square) the surface cracked. It was an obviously sign that further rolling was not possible any more. The cracks were approximately in the radial direction with characteristic changes of directions on the short sections. In single areas the surface damages were so intensive that even some small metallic particles split off. The wire with the limited ductility had the same strength and the yield stress as that which was be shaped into the demanding sections. The reduced ductility was explained by fracture surfaces and by the careful analysis of the microstructure. The contraction of the copper wire before annealing was approximately 90%, and it was reduced to less than 30% after the annealing process. Essential difference between the two wires was in the form of fracture. Not annealed copper wire exhibited ductile transgranular dimpled fracture with characteristic deep unidirected dimples (Fig. 6). On the fracture surface of the test bar broken in the air, the adsorbed carbon and oxygen have been measured (Fig. 9). After annealing the ductility was rapidly reduced while the fracture was completely intercrystalline. Intergranular fracture surface consisted of many fine and shallow dimples with inclusions of copper oxyde (Fig. 2-5).

High oxygen concentration on that fracture surface was proved by the AES analysis. Oxygen was distributed obviously deeper under the fracture surface when compared with the not-annealed copper (Fig. 10).

The oxygen concentration on the surface corresponded to the composition Cu_2O and was rapidly reduced away from the grain boundaries. The initiation of cracks in the annealed copper is



Figure 1: Cracks on copper wire surface after cold rolling (first step of reduction); 100x

Slika 1: Površina bakrene žice z razpokami po prvi redukciji pri hladnem valjanju; 100x

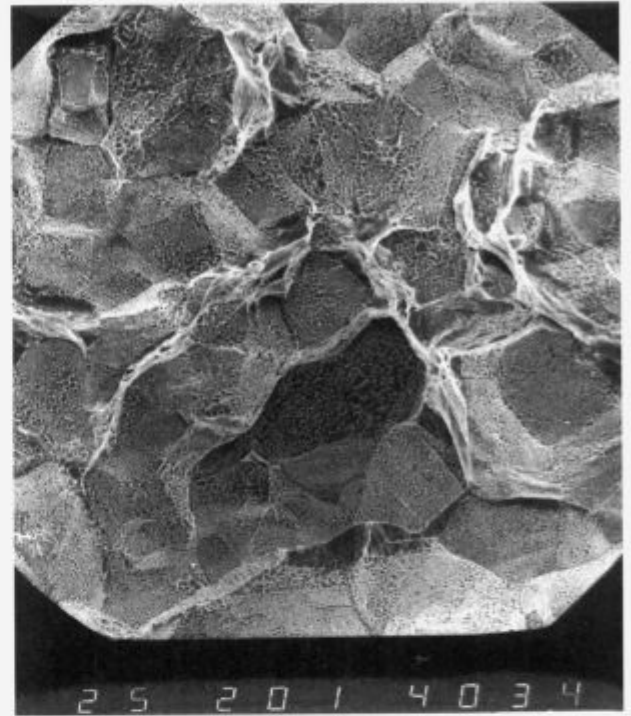


Figure 3: Intergranular dimple rupture in copper wire resulting from microvoids coalescence at grain boundaries ($Z = 25\%$); 200x

Slika 3: Intergranularna jamničasta površina preloma bakrene žice ($Z = 25\%$); 200x

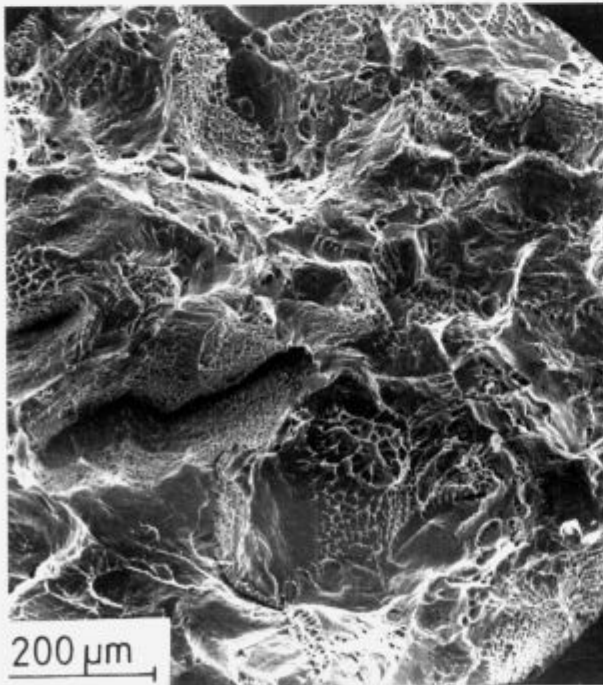


Figure 2: Intergranular dimple rupture in copper wire resulting from microvoids coalescence at grain boundaries; 100x

Slika 2: Intergranularna jamničasta površina preloma valjane bakrene žice; 100x

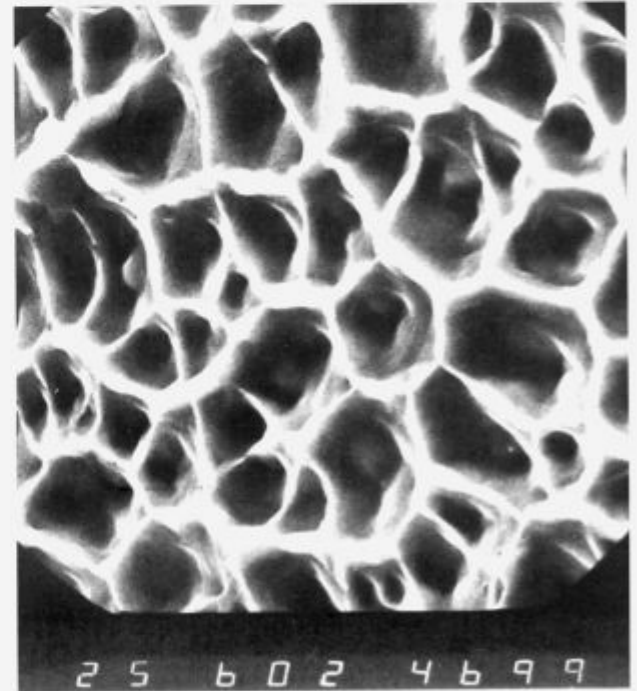


Figure 4: Detail of intergranular rupture surface with copper oxide inclusions in dimples (**fig.3**); 6000x

Slika 4: Detalj intergranularne prelomne površine z vključki Cu_2O v jamicah (**sl.3**); 6000x

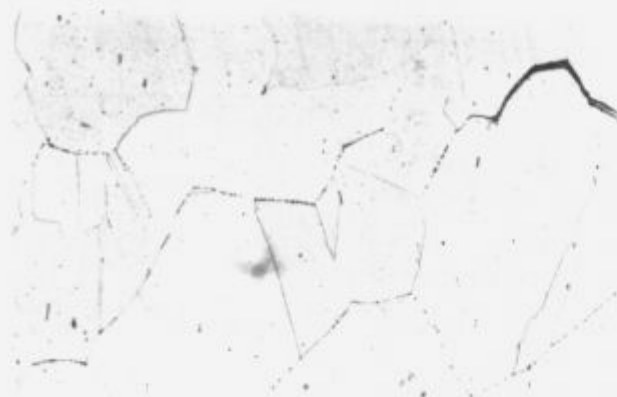


Figure 5: Small cracks on grain boundaries and copper oxide precipitates; 200x

Slika 5: Kratke razpoke na kristalnih mejah s precipitati bakrovega oksida; 200x

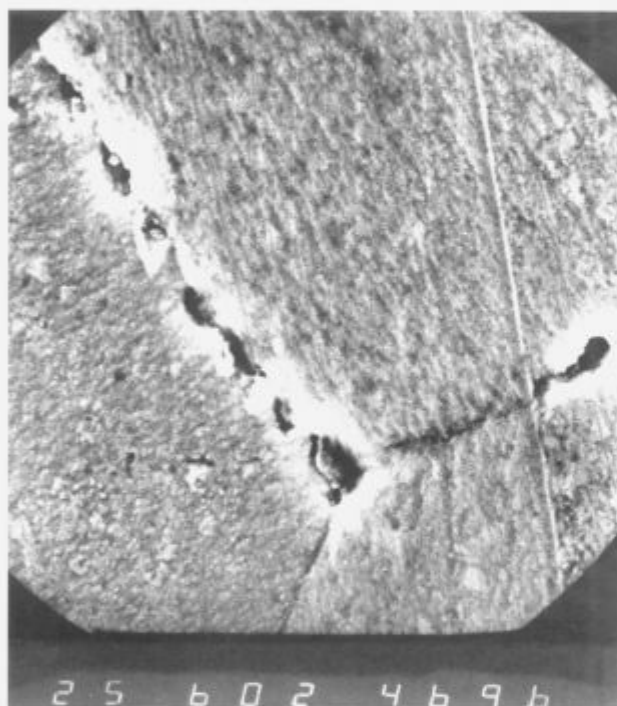


Figure 6: Copper oxide precipitates on grain boundary; 6000x

Slika 6: Precipitati bakrovega oksida na kristalni meji; 6000x

connected with the inclusions of copper oxide on the grain boundaries (Fig. 3,5). As reference, also the surface of copper wire which has been covered with thin layer of corrosive products during storing has been analysed. The composition was not the same on the whole surface. On one section of the surface the chemical composition of the corrosive products corresponded to the CuO copper oxide (Fig. 13). The layer is thin and it adheres to the unchanged metal at a high oxygen concentration gradient. In the other surface area, there was found a layer with high carbon concentration and it was thicker than that rich in oxygen (Fig. 14). The oxygen embrittlement of copper exhibited reversibility. Annealing in the vacuum (5.10^{-6} mbar, 850°C, 10 hours) essentially increased ($Z = 75\%$) the copper ductility. The fracture surface of that annealed copper was predominantly transgranular dimpled ductile fractured with a very small amount of residual intergranular dimpled fracture (Fig. 8). The chosen annealing conditions in the vacuum were obviously not so

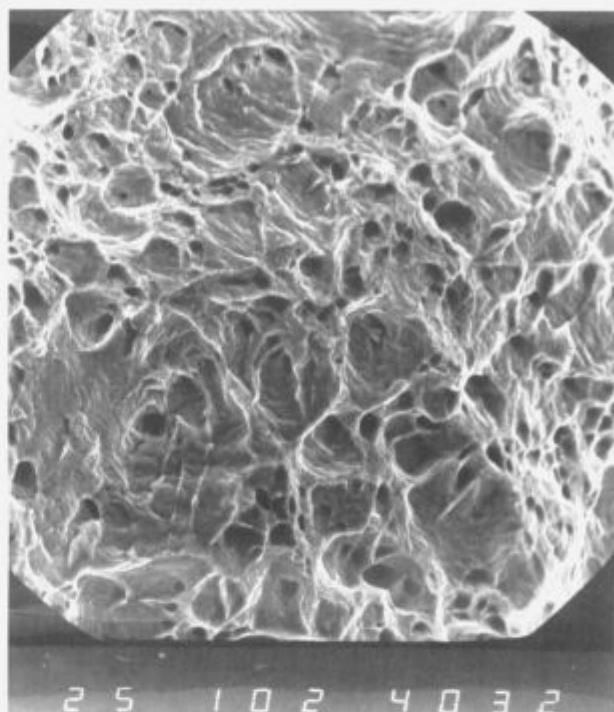


Figure 7: Ductile fracture of copper wire ($Z = 90\%$); 1000x

Slika 7: Duktilni prelom bakrene žice ($Z = 90\%$); 1000x

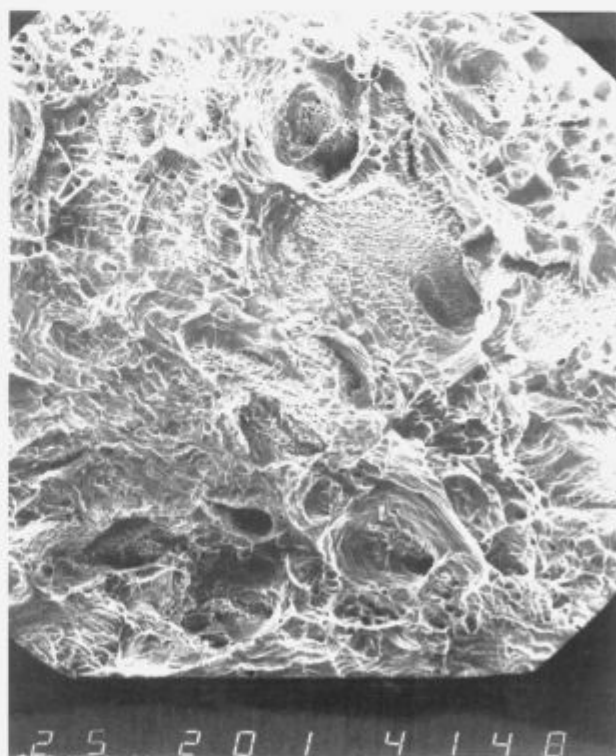


Figure 8: Fracture surface of copper wire after vacuum annealing ($Z = 90\%$); 200x

Slika 8: Prelomna površina žice po žarenju v vakuumu ($Z = 75\%$); 200x

favourable enough to remove all the oxygen accumulated in the copper during the annealing in the nitrogen atmosphere. The not uniform removal of oxygen was proved also by the AES analy-

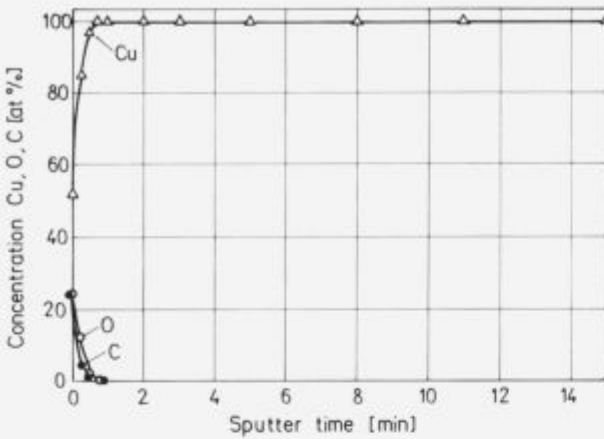


Figure 9: Copper, oxygen and carbon concentration distribution on fracture surfaces of high ductility copper (Z = 90%)

Slika 9: Profil koncentracij bakra, kisika in ogljika na prelomu bakra z veliko duktilnostjo (Z = 90%)

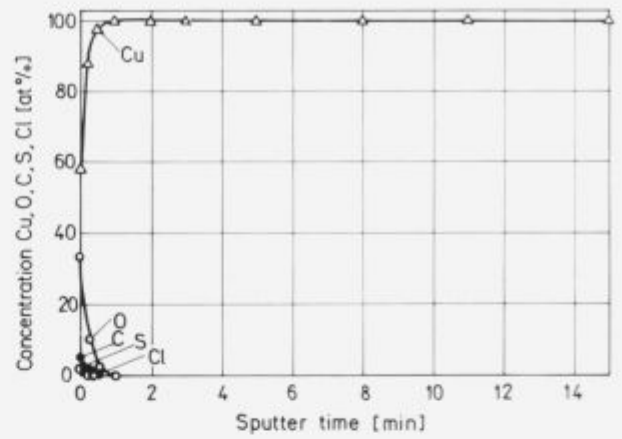


Figure 11: Copper, oxygen and other elements concentration distribution on fracture surface of copper after vacuum annealing (fracture after annealing)

Slika 11: Profil koncentracij bakra, kisika in drugih elementov na prelomu bakra z majhno duktilnostjo po žarjenju v vakuumu (prelomljeno po žarjenju v vakuumu)

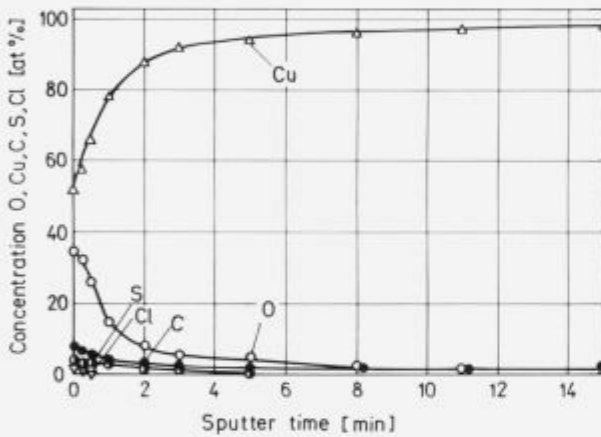


Figure 10: Copper and oxygen concentration distribution on fracture surface of copper after annealing in nitrogen (5 ... 6 ppm O₂)

Slika 10: Profil koncentracij kisika in bakra na prelomu bakra z majhno duktilnostjo po žarjenju v vakuumu (5 ... 6 ppm O₂) na temperaturi 500°C

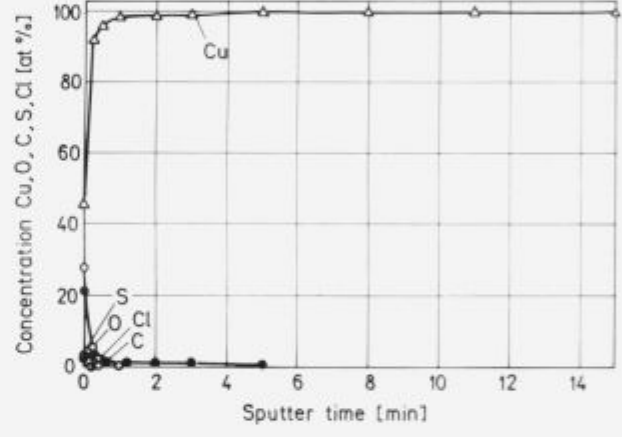


Figure 12: Copper, oxygen and other elements distribution on fracture surface after vacuum annealing (fracture before annealing)

Slika 12: Profil koncentracij bakra, kisika in drugih elementov na prelomu bakra z majhno duktilnostjo po žarjenju v vakuumu; (prelomljeno pred žarjenjem v vakuumu)

sis of oxygen and of other elements on the fracture surface. The effect of the oxygen removal by the annealing in vacuum has been estimated by the comparison of the oxygen concentration on the fracture of the vacuum annealed copper wire and those when the fracture surface of the brittle copper was annealed in vacuum (Fig. 12,13). During the vacuum annealing much more oxygen has been removed from the fracture surface than from the bulk wire sample.

2. The Mechanism of the Copper Embrittlement

At 500°C, the grain boundary diffusion in the copper is preferential to the diffusion inside grains⁽³⁾.

The solubility of oxygen in copper is about 10 ppm⁽³⁾ at 500°C. At the annealing temperature of 500°C the grain boundary diffusion rate of oxygen is higher for few orders of magnitude to the bulk diffusion rate inside grains. Thus mainly grain boundaries become enriched with oxygen. After completed annealing the temperature of copper dropped to the surroundings temperature. Major amount of oxygen was precipitated in form of the copper oxide Cu₂O on the grain boundaries. The precipi-

tation from solid solution is characterized by the formation of many fine particles distributed on the grain boundaries. At suitable stresses or deformation, pores appear on the boundary between the precipitates of the copper oxide and the metal matrix along the grain boundaries. Since precipitates are numerous the dimples are small and shallow. The oxygen embrittlement is a reversible phenomenon if oxygen enriched copper is annealed under the conditions which enables the oxygen removal below the solubility limit at the surroundings temperature.

3. Conclusions

In annealing copper in the atmosphere with a very low partial pressure of oxygen at a temperature favourable for the grain boundary diffusion, higher oxygen concentrations has been detected only on grain boundaries. During the cooling to the surroundings temperature oxygen precipitated from the metal in the form of the copper oxide (Cu₂O). Such a formation of the copper oxide favours the formation of a great number of fine precipitates. On the boundary between the precipitates and the metal matrix pores appear at a suitable high deformation, and they

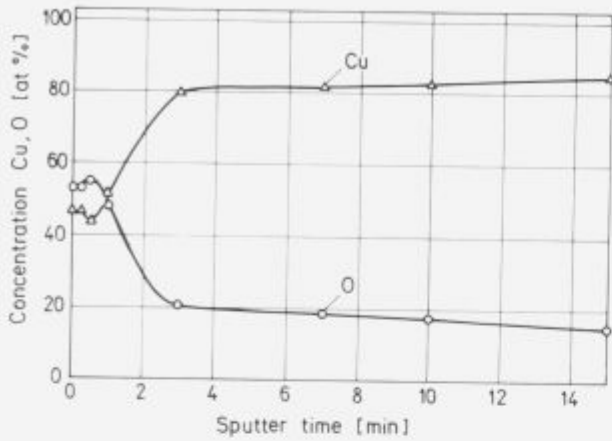


Figure 13: Copper and oxygen distribution on wire surface before annealing in nitrogen

Slika 13: Profil koncentracij kisika in bakra na površini bakrene žice pred žarjenjem v dušiku

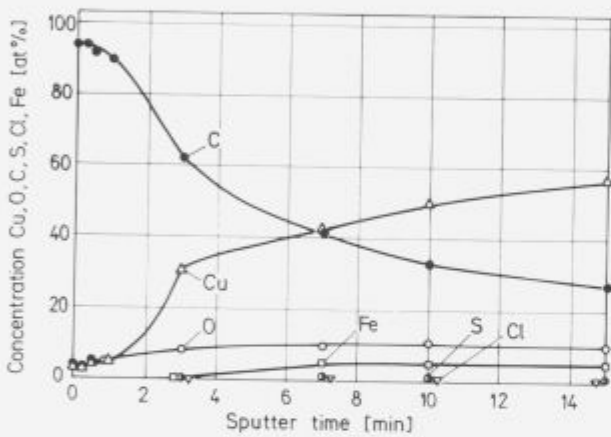


Figure 14: Oxygen, copper and other elements concentration distribution on wire surface before annealing in nitrogen

Slika 14: Profil koncentracij kisika, bakra in drugih elementov na površini bakrene žice pred žarjenjem v dušiku

propagate into a intergranular fracture with the small microscopic and macroscopic degree of deformation. The phenomenon of the oxygen embrittlement of copper is reversible. If the oxygen is removed from the metal below the solubility limit at

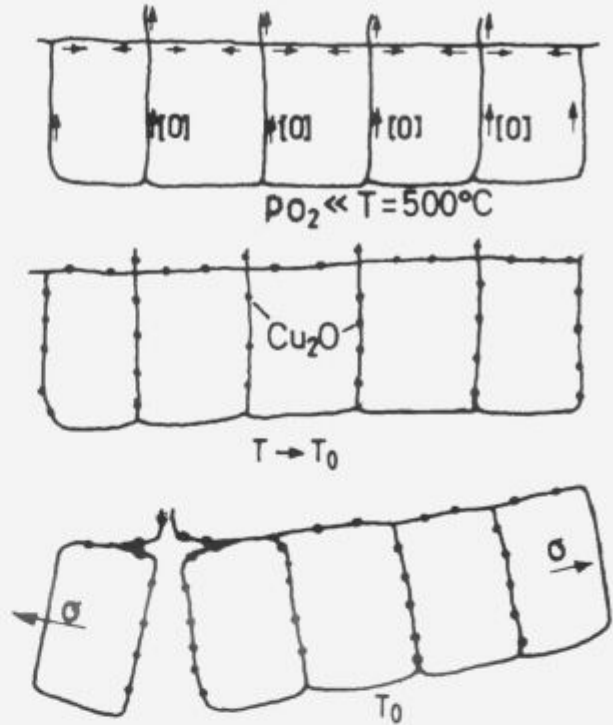


Figure 15: Mechanism sequences of copper wire embrittlement

Slika 15: Mehanizem krhkosti bakrene žice

the surroundings temperature, there exist conditions for the formation of the intergranular dimpled fracture. In the analyzed case the oxygen was found to be distributed unevenly in the metal and predominantly on the grain boundaries. Thus it is essential the reduced oxygen concentration on the grain boundaries and not the average oxygen concentration in the bulk metal.

4. Literature

1. T.G.Nieh, W.D.Nix: Embrittlement of Copper Due to Segregation of Oxygen to Grain Boundaries, Metal. Transact., vol. 12A, May, 1981, (893 - 901)
2. L.E.Pope, F.A.Olson: Degassing of Copper Wires in an Ultrahigh Vacuum P.1. Diffusion, Metal. Transact., vol. 2, Sept., 1971, (2711 - 2716)
3. I.Kaur, W.Gust: Fundamentals of Grain and Interphase Boundary Diffusion, Ziegler Press, Stuttgart, 1989.



INŠTITUT ZA KOVINSKE MATERIALE
IN TEHNOLOGIJE p.o.

INSTITUTE OF METALS
AND TECHNOLOGIES p.o.

61000 LJUBLJANA, LEPI POT 11, POB 431,
SLOVENIJA

Telefon: 061/1251-161, Telefax: 061 213-780

VACUUM HEAT TREATMENT LABORATORY

Vacuum Heat Treatment

Vacuum Heat Treatment is recognised as a high quality cost effective and ultra clean method for processing a wide range of components and materials currently in use in today's industry. The range of our equipment enables us to heat treat most sizes of load, from small batches to work up to 350 mm diameter, 910 mm high, and weight up to 380 kg.

ADVANTAGES

- Clean, bright surface finish
- Minimal distortion
- Minimal post treatment operations, e.g., grinding or polishing

Five years of continual investment has ensured that **VHTL** maintains its position as market leader in the field of high quality sub-contract metal processing.

We operate the latest generation of IPSEN VTTC furnace capable of processing components up to 350 mm in diameter, which in addition to our high pressure, rapid quenching facilities increases the range of materials suitable for Vacuum Heat Treatment.

TYPICAL APPLICATIONS

- Bright Annealing
- Bright Stress Relieving
- Hardening/Tempering
- Brazing/Hardening/Tempering
- Solution Treatment
- Demagnetisation
- Degassing
- Diffusion Treatments
- Sintering

QUALITY ASSURANCE

Quality is fundamental to the **IMT** philosophy. The choice of process, all processing operations and process control are continuously monitored by IMT Quality Control Department.

The high level of quality resulting from this tightly organised activity has been acknowledged by government authorities, industry and International companies.

KOVINE ZLITINE TEHNOLOGIJE, 27, 1993, 1-4

I. Kronološko kazalo

Grabke H.J.: Surface and Grain Boundary Segregation on and in Iron and Steels - Effects on Steel Properties	KZT 27 (1993) 1-2, 009-020
Grešovnik Ferdo: Paramagnetna jekla	KZT 27 (1993) 1-2, 021-024
Ažman Slavko, J. Vojvodič-Gvardjančič, B. Ule: Ocena nizkotemperaturne uporabnosti drobnozrnatih mikrolegiranih jekel kot izhodišče pri konstruiranju objektov	KZT 27 (1993) 1-2, 025-027
Koroušič Blaženko: Dušik v tekočem jeklu	KZT 27 (1993) 1-2, 029-031
Ivančan A., J. Krajcar: Simulacija djelovanja lijevno praša pomoću krivulja taljenja	KZT 27 (1993) 1-2, 033-038
Rodič Jože, K. Habijan, A. Rodič: Razvoj nove tehnologije "HKL" za litje drobnih palic nekonvencionalnih presekov	KZT 27 (1993) 1-2, 039-042
Legat Franc, A. Lagoja: Osvajanje izdelave verig iz nerjavnih jekel	KZT 27 (1993) 1-2, 043-049
Krivec Stane, A. Rodič: Nov postopek ogljičenja z dodajanjem amoniaka	KZT 27 (1993) 1-2, 051-056
Tasevski M.: Tankoplastne prevleke za zaščito orodij za tlačno litje plastike	KZT 27 (1993) 1-2, 057-060
Zupanič F., A. Križman: Raziskave difuzijskega žarjenja pocinkanega jekla Č.5432	KZT 27 (1993) 1-2, 061-063
Arzenšek Boris, B. Šuštaršič, I. Kos, K. Zalesnik: Tehnologija vlečenja orodnih jekel pri povišanih temperaturah	KZT 27 (1993) 1-2, 065-067
Kmetič D., V. Leskovšek, J. Žvokelj, J. Gnamuš: Trdnostne lastnosti visokotemperaturno spajkanih spojev v vakuumu	KZT 27 (1993) 1-2, 069-073
Šegel Jože, B. Kaker, B. Urnaut: Celovito obvladovanje kakovosti v metalurgiji	KZT 27 (1993) 1-2, 075-081
Sirk, S., F. Vodopivec: Duktilnost zlitine RAVNAL 2 z nazivno sestavo 22% Cr, 5% Al in do 0,1% C	KZT 27 (1993) 1-2, 083-087
Saje B., I.R. Harris, A.J. Villiams, S. Beseničar: Magnetne lastnosti izotropnih Nd-Fe-B trajnih magnetov pripravljenih z rotacijskim stiskanjem	KZT 27 (1993) 1-2, 089-092
Anžel I., A. Križman, L. Kosec, S. Spaič: Vpliv parametrov pri kontinuirnem litju na mikrostrukturo zlitine Cu-Cr-Zr	KZT 27 (1993) 1-2, 093-095
Godec M., P. Panjan, B. Navinšek, J. Gašperič, M. Remškar, V. Kraševac: TEM analiza prerezov (XTEM) tankih plasti	KZT 27 (1993) 1-2, 097-101
Bricelj Erika: Analiza vključkov z napravo za avtomatsko obdelavo slike	KZT 27 (1993) 1-2, 103-105
Spruk S., M. Jenko, L. Koller, D. Railič: Vakuumsko tesni laserski zvari za hermetično inkapsulacijo elektronskih sestavnih delov	KZT 27 (1993) 1-2, 107-109
Hertl B., B. Breskvar, A. Osojnik: Uporaba in izdelava primarnih referentnih materialov vrste AlSi12 in AlSi2Cu	KZT 27 (1993) 1-2, 111-114
Bizjak M., L. Kosec, A. Smolej: Izdelava zlitine aluminija z veliko koncentracijo železa po postopku hitrega strjevanja	KZT 27 (1993) 1-2, 115-118

Kolenko T., F. Pavlin, B. Sicherl, B. Glogovac: Razvoj programske opreme za procesno vodenje potisne peči z vidika energetskega optimiranja	KZT 27 (1993) 1-2, 119-121
Šuštaršič B., M. Torkar, M. Jenko, B. Breskvar, V. Leskovšek, F. Vodopivec, A. Rodič: Procesi atomizacije kovinskih gradiv in konsolidacija kovinskih prahov - III. del	KZT 27 (1993) 1-2, 123-127
Godec B., L. Vehovar: Določevanje korozijske odpornosti jekla NIOMOL 490K v medijih petrokemije	KZT 27 (1993) 1-2, 129-131
Uršič V., M. Tonkovič-Prijanovič, R. Jud: Potrebno napajanje ulitkov iz nodularne litine	KZT 27 (1993) 1-2, 133-136
Vojvodič-Gvardjančič Jelena, B. Ule, S. Ažman: Vpliv staranja mikrolegiranih jekel na njihovo uporabnost pri nizkih temperaturah	KZT 27 (1993) 1-2, 137-140
Kurbos Mojca: Izbira livnih praškov pri kontinuirnem vlivanju jekel za debelo pločevino	KZT 27 (1993) 1-2, 141-144
Kanalec Slavko: Vpliv sistema VVS na procese v EOP	KZT 27 (1993) 1-2, 145-147
Beseničar S., J. Holc, G. Dražič, B. Saje: Vpliv dodatka ZrO ₂ na korozijsko obstojnost Nd-Dy-Fe-B magnetov	KZT 27 (1993) 1-2, 149-152
Koller L., M. Jenko, S. Spruk, D. Railič: Vpliv vlage in nečistoč na kontaktne materiale, vgrajene v hermetično inkapsulirane sestavne dele	KZT 27 (1993) 1-2, 153-155
Mozetič M., M. Kveder, F. Breclj, M. Drobnič: Plazemsko čiščenje kovinskih površin	KZT 27 (1993) 1-2, 157-159
Obal M., S. Rozman, M. Kolenc, A. Osojnik: Določevanje izoterme izmenjave v sistemu naravni zeolit - raztopine kovin	KZT 27 (1993) 1-2, 161-165
Petač H., M. Veber, S. Gomišček: Nastanek in stabilnost kompleksa med bakrovimi in kadmijevimi ioni ter huminsko kislino v vodni raztopini	KZT 27 (1993) 1-2, 167-170
Šalamun I., A. Stritar, B. Šarler: Spremljanje parametrov kontinuiranega ulivanja na osebem računalniku	KZT 27 (1993) 1-2, 171-174
Štok B., N. Mole: Matematično modeliranje rotacijskega litja - analiza termomehanskega stanja v orodju	KZT 27 (1993) 1-2, 175-180
Runovc F., L. Kosec: Computer modeling of Ion Implantation in Modification of Material Surface Properties	KZT 27 (1993) 1-2, 181-184
Vižintin J., F. Vodopivec: Obraba jekla 100 Cr6 pri majhnih oscilacijah	KZT 27 (1993) 1-2, 185-190
Špan T., K. Kuzman: Ugotavljanje preoblikovalnih lastnosti tanke pločevine za potrebe proizvodnje in simulacij	KZT 27 (1993) 1-2, 191-193
Leskovšek V., B. Ule, A. Rodič: Razvoj modificirane metode za določevanje lomne žilavosti hitroreznega jekla, s cilindričnimi preizkušanci z zarezo po obodu	KZT 27 (1993) 1-2, 195-204
Doberšek M., I. Kosovine: Električne lastnosti zlitin v ternem sistemu Pd-Cu-Zn	KZT 27 (1993) 1-2, 205-206
Holc J., S. Beseničar: Optimizacija sintranja NdFeB magnetov	KZT 27 (1993) 1-2, 207-208
Smolej A., V. Dragojevič, A. Gorčenko, M. Jelen, T. Smolar, J. Kopač, M. Sokovič, S. Tršar: Vpliv toplotne obdelave na lastnosti avtomatne zlitine AlMgSiPbBi	KZT 27 (1993) 1-2, 209-212

Kejžar Rajko: Prednosti uporabe novih sintetičnih repromaterialov pri izdelavi dodatnih materialov za varjenje	KZT 27 (1993) 1-2, 213-216
Rodič Jože, K. Habijan, M. Strohmaier, A. Rodič, A. Osojnik, J. Žvokelj: Domače superzlitine za stomatološko protetiko	KZT 27 (1993) 3, 221-226
Cundrič Ivo, M. Lah, S. Mihelčič, M. Hladnik: Izračun stroškovnih nosilcev oz. kalkulacije s pomočjo analize in sinteze poteka dela po metodi REFA	KZT 27 (1993) 3, 227-235
Drofenik Bernarda: Mehanske lastnosti in korozivna odpornost superzlitine Ravnic2	KZT 27 (1993) 3, 237-239
Godec Boštjan, J. Vojvodič-Gvardjančič, L. Vehovar: Korozivna odpornost tračno navarjenih posod izdelanih iz drobnozrnatega mikrolegiranega jekla NIOMOL 490	KZT 27 (1993) 3, 241-248
Gnamuš Janko: Napetostno žarjenje orodij podaljšuje njihovo življensko dobo	KZT 27 (1993) 3, 249-251
Legat Franc: Vpliv nitriranja na premene jekla X38CrMoV51	KZT 27 (1993) 3, 253-259
Arzenšek Boris, D. Kmetič, A. Lagoja: Maziva in hladno preoblikovanje jekel	KZT 27 (1993) 3, 261-266
Ule B., M. Lovrečič-Saražin, J. Vojvodič-Gvardjančič, S. Ažman, A. Lagoja: Relationship Between Fracture Toughness and Mechanical Properties of Some Structural Steels at Low Temperatures	KZT 27 (1993) 4, 283-287
Torkar M., B. Šuštaršič, F. Vodopivec: Recrystallization of Ni-based Superalloy after Cold Deformation	KZT 27 (1993) 4, 289-299
Shlomchack G.G., I. Mamuzić: The Rheological Model of Deformation Nidus in the Proces of Rolling	KZT 27 (1993) 4, 295-299
Osojnik Andreja, T. Drglin: Comparison of Graphite Furnace - and Hydride Generation AAS for Trace Analysis of Tin in Steels and Nickel Alloys	KZT 27 (1993) 4, 301-306
Gojić Mirko, M. Balenović, L. Kosec, L. Vehovar: The Susceptibility to Hydrogen Embrittlement of Low Alloy Cr-Mo Steel Tubing	KZT 27 (1993) 4, 307-311
Koroušič Blaženko: Predicting Oxide Activites in CaO-Al ₂ O ₃ -SiO ₂ System by Computer Model ..	KZT 27 (1993) 4, 313-317
Kosec B., L. Kosec: Composite Mechanism of Scale Adhesiveness	KZT 27 (1993) 4, 319-321
Kosec L., V. Gontarev, B. Kosec, M. Mlakar: Embrittlement of Copper Wire Due to Oxygen	KZT 27 (1993) 4, 323-327

2. Avtorsko kazalo

Anžel L., A. Križman, L. Kosec, S. Spaič: Vpliv parametrov pri kontinuirnem litju na mikrostrukturo zlitine Cu-Cr-Zr	KZT 27 (1993) 1-2, 093-095
Arzenšek Boris, B. Šuštaršič, I. Kos, K. Zalesnik: Tehnologija vlečenja orodnih jekel pri povišanih temperaturah	KZT 27 (1993) 1-2, 065-067
Arzenšek Boris, D. Kmetič, A. Lagoja: Maziva in hladno preoblikovanje jekel	KZT 27 (1993) 3, 261-266
Ažman Slavko, J. Vojvodič-Gvardjančič, B. Ule: Ocena nizkotemperaturne uporabnosti drobnozrnatih mikrolegiranih jekel kot izhodišče pri konstruiranju objektov	KZT 27 (1993) 1-2, 025-027
Beseničar S., J. Holc, G. Dražič, B. Saje: Vpliv dodatka ZrO ₂ na korozivno obstojnost Nd-Dy-Fe-B magnetov	KZT 27 (1993) 1-2, 149-152
Bizjak M., L. Kosec, A. Smolej: Izdelava zlitine aluminija z veliko koncentracijo železa po postopku hitrega strjevanja	KZT 27 (1993) 1-2, 115-118
Bricelj Erika: Analiza vključkov z napravo za avtomatsko obdelavo slike	KZT 27 (1993) 1-2, 103-105
Cundrič Ivo, M. Lah, S. Mihelčič, M. Hladnik: Izračun stroškovnih nosilcev oz. kalkulacije s pomočjo analize in sinteze poteka dela po metodi REFA	KZT 27 (1993) 3, 227-235
Doberšek M., I. Kosovinc: Električne lastnosti zlitin v ternernem sistemu Pd-Cu-Zn	KZT 27 (1993) 1-2, 205-206
Drofenik Bernarda: Mehanske lastnosti in korozivna odpornost superzlitine Ravnic2	KZT 27 (1993) 3, 237-239
Godec B., L. Vehovar: Določevanje korozivne odpornosti jekla NIOMOL 490K v medijih petrokemije	KZT 27 (1993) 1-2, 129-131
Godec Boštjan, J. Vojvodič-Gvardjančič, L. Vehovar: Korozivna odpornost tračno navarjenih posod izdelanih iz drobnozrnatega mikrolegiranega jekla NIOMOL 490	KZT 27 (1993) 3, 241-248
Godec M., P. Panjan, B. Navinšek, J. Gašperič, M. Remskar, V. Kraševac: TEM analiza prerezov (XTEM) tankih plasti	KZT 27 (1993) 1-2, 097-101
Gojić Mirko, M. Balenović, L. Kosec, L. Vehovar: The Susceptibility to Hydrogen Embrittlement of Low Alloy Cr-Mo Steel Tubing	KZT 27 (1993) 4, 307-311
Gnamuš Janko: Napetostno žarjenje orodij podaljšuje njihovo življensko dobo	KZT 27 (1993) 3, 249-251
Grabke H.J.: Surface and Grain Boundary Segregation on and in Iron and Steels - Effects on Steel Properties	KZT 27 (1993) 1-2, 009-020
Grešovnik Ferdo: Paramagnetna jekla	KZT 27 (1993) 1-2, 021-024
Hertl B., B. Breskvar, A. Osojnik: Uporaba in izdelava primarnih referentnih materialov vrste AlSi12 in AlSi2Cu	KZT 27 (1993) 1-2, 111-114
Holc J., S. Beseničar: Optimizacija sintranja NdFeB magnetov	KZT 27 (1993) 1-2, 207-208
Ivančan A., J. Krajcar: Simulacija djelovanja lijevno praha pomoću krivulja taljenja	KZT 27 (1993) 1-2, 033-038
Kanalec Slavko: Vpliv sistema VVS na procese v EOP	KZT 27 (1993) 1-2, 145-147
Kejžar Rajko: Prednosti uporabe novih sintetičnih repromaterialov pri izdelavi dodatnih materialov za varjenje	KZT 27 (1993) 1-2, 213-216

- Kmetič D., V. Leskovšek, J. Žvokelj, J. Gnamuš:** Trdnostne lastnosti visokotemperaturno spajkanih spojev v vakuumu KZT 27 (1993) 1-2, 069-073
- Kolenko T., F. Pavlin, B. Sicherl, B. Glogovac:** Razvoj programske opreme za procesno vodenje potisne peči z vidika energetskega optimiranja KZT 27 (1993) 1-2, 119-121
- Koller L., M. Jenko, S. Spruk, D. Railič:** Vpliv vlage in nečistoč na kontaktne materiale, vgrajene v hermetično inkapsulirane sestavne dele KZT 27 (1993) 1-2, 153-155
- Koroušič Blaženko:** Dušik v tekočem jeklu KZT 27 (1993) 1-2, 029-031
- Koroušič Blaženko:** Predicting Oxide Activities in CaO-Al₂O₃-SiO₂ System by Computer Model ... KZT 27 (1993) 4, 313-317
- Kosec B., L. Kosec:** Composite Mechanism of Scale Adhesiveness KZT 27 (1993) 4, 319-321
- Kosec L., V. Gontarev, B. Kosec, M. Mlakar:** Embrittlement of Copper Wire Due to Oxygen KZT 27 (1993) 4, 323-327
- Krivec Stane, A. Rodič:** Nov postopek ogljičenja z dodajanjem amoniaka KZT 27 (1993) 1-2, 051-056
- Kurbos Mojca:** Izbira livnih praškov pri kontinuiranem vlivanju jekel za debelo pločevino KZT 27 (1993) 1-2, 141-144
- Legat Franc, A. Lagoja:** Osvajanje izdelave verig iz nerjavnih jekel KZT 27 (1993) 1-2, 043-049
- Legat Franc:** Vpliv nitriranja na premene jekla X38CrMoV51 KZT 27 (1993) 3, 253-259
- Leskovšek V., B. Ule, A. Rodič:** Razvoj modificirane metode za določevanje lomne žilavosti hitroreznega jekla, s cilindričnimi preizkušanci z zarezo po obodu ... KZT 27 (1993) 1-2, 195-204
- Mozetič M., M. Kveder, F. Brecelj, M. Drobnič:** Plazemsko čiščenje kovinskih površin KZT 27 (1993) 1-2, 157-159
- Obal M., S. Rozman, M. Kolenc, A. Osojnik:** Določevanje izoterme izmenjave v sistemu naravni zeolit - raztopine kovin ... KZT 27 (1993) 1-2, 161-165
- Osojnik Andreja, T. Drglin:** Comparison of Graphite Furnace - and Hydride Generation AAS for Trace Analysis of Tin in Steels and Nickel Alloys KZT 27 (1993) 4, 301-306
- Petač H., M. Veber, S. Gomišček:** Nastanek in stabilnost kompleksa med bakrovimi in kadmijevimi ioni ter huminsko kislino v vodni raztopini KZT 27 (1993) 1-2, 167-170
- Rodič Jože, K. Habijan, A. Rodič:** Razvoj nove tehnologije "HKL" za litje drobnih palic nekonvencionalnih presekov KZT 27 (1993) 1-2, 039-042
- Rodič Jože, K. Habijan, M. Strohmaier, A. Rodič, A. Osojnik, J. Žvokelj:** Domače superzlitine za stomatološko protetiko KZT 27 (1993) 3, 221-226
- Runovc F., L. Kosec:** Computer modeling of Ion Implantation in Modification of Material Surface Properties KZT 27 (1993) 1-2, 181-184
- Saje B., I.R. Harris, A.J. Williams, S. Beseničar:** Magnetne lastnosti izotropnih Nd-Fe-B trajnih magnetov pripravljenih z rotacijskim stiskanjem KZT 27 (1993) 1-2, 089-092
- Shlomchack G.G., I. Mamuzić:** The Rheological Model of Deformation Nidus in the Proces of Rolling KZT 27 (1993) 4, 295-299
- Sirk, S., F. Vodopivec:** Duktilnost zlitine RAVNAL 2 z nazivno sestavo 22% Cr, 5% Al in do 0,1% C KZT 27 (1993) 1-2, 083-087
- Smolej A., V. Dragojevič, A. Gorčenko, M. Jelen, T. Smolar, J. Kopač, M. Sokovič, S. Tršar:** Vpliv toplotne obdelave na lastnosti avtomatne zlitine AlMgSiPbBi KZT 27 (1993) 1-2, 209-212
- Spruk S., M. Jenko, L. Koller, D. Railič:** Vakuumsko tesni laserski zvari za hermetično inkapsulacijo elektronskih sestavnih delov KZT 27 (1993) 1-2, 107-109
- Šalamun L., A. Stritar, B. Šarler:** Spremljanje parametrov kontinuiranega ulivanja na osebem računalniku KZT 27 (1993) 1-2, 171-174
- Šegel Jože, B. Kaker, B. Urnaut:** Celovito obvladovanje kakovosti v metalurgiji KZT 27 (1993) 1-2, 075-081
- Špan T., K. Kuzman:** Ugotavljanje preoblikovalnih lastnosti tanke pločevine za potrebe proizvodnje in simulacij KZT 27 (1993) 1-2, 191-193
- Štok B., N. Mole:** Matematično modeliranje rotacijskega litja - analiza termomehanskega stanja v orodju KZT 27 (1993) 1-2, 175-180
- Šuštaršič B., M. Torkar, M. Jenko, B. Breskvar, V. Leskovšek, F. Vodopivec, A. Rodič:** Procesi atomizacije kovinskih gradiv in konsolidacija kovinskih prahov - III. del KZT 27 (1993) 1-2, 123-127
- Tasevski M.:** Tankoplastne prevleke za zaščito orodij za tlačno litje plastike KZT 27 (1993) 1-2, 057-060
- Torkar M., B. Šuštaršič, F. Vodopivec:** Recrystallization of Ni-based Superalloy after Cold Deformation KZT 27 (1993) 4, 289-294
- Ule B., M. Lovrečič-Saražin, J. Vojvodič-Gvardjančič, S. Ažman, A. Lagoja:** Relationship Between Fracture Toughness and Mechanical Properties of Some Structural Steels at Low Temperatures KZT 27 (1993) 4, 283-287
- Uršič V., M. Tonkovič-Prijanovič, R. Jud:** Potrebno napajanje ulitkov iz nodularne litine KZT 27 (1993) 1-2, 133-136
- Vižintin J., F. Vodopivec:** Obraba jekla 100 Cr6 pri majhnih oscilacijah KZT 27 (1993) 1-2, 185-190
- Vojvodič-Gvardjančič Jelena, B. Ule, S. Ažman:** Vpliv staranja mikrolegiranih jekel na njihovo uporabnost pri nizkih temperaturah KZT 27 (1993) 1-2, 137-140
- Zupanič F., A. Križman:** Raziskave difuzijskega žarjenja pocinkanega jekla Č.5432 KZT 27 (1993) 1-2, 061-063



INŠTITUT ZA KOVINSKE MATERIALE
IN TEHNOLOGIJE p.o.

INSTITUTE OF METALS
AND TECHNOLOGIES p.o.

61000 LJUBLJANA, LEPI POT 11, POB 431,
SLOVENIJA

Telefon: 061/1251-161, Telefax: 061 213-780

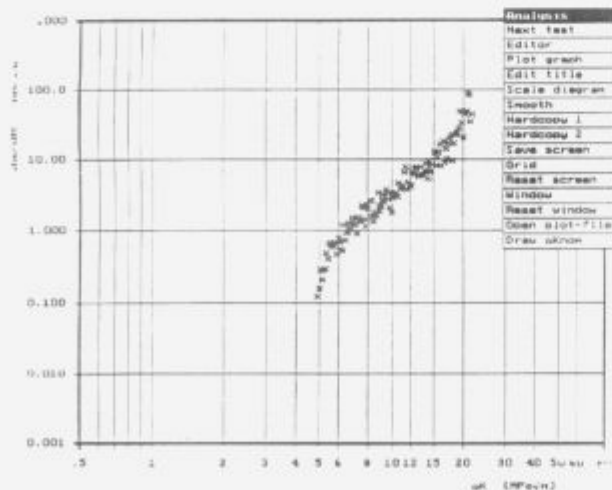
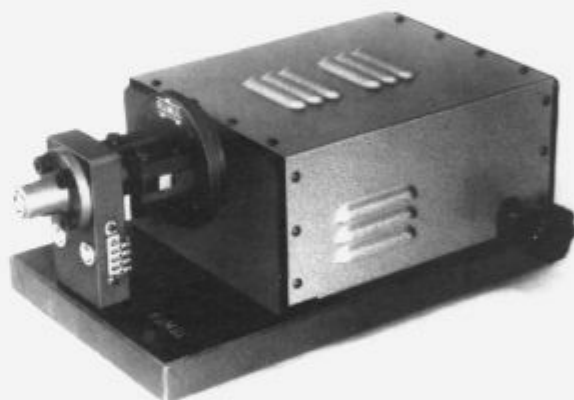


NOVO NA IMT!

Rezonantni pulzator CRACKTRONIC,
naprava za raziskave v mehaniki loma ter
merjenja kinetike propagacije utrujenostnih
razpok.

Naprava je računalniško vodena, omogoča
pa merjenja na preiskušancih, ki niso večji
od charpyjevih preiskušancev za merjenje
udarne žilavosti.

S to napravo prihranite čas in denar.



Računalniška obdelava rezultatov dosledno
upoštevata zahteve ASTM standardov.
Na osnovi meritev z resonantnim
pulzatorjem CRACKTRONIC lahko uspešno
napovedujemo preostalo življenjsko dobo
dinamično obremenjenih konstrukcij.

slovenske železarne 

ACRONI

SŽ ACRONI d.o.o. Cesta železarjev 8, 64270 Jesenice

tel. centrala: +386 64 861-441

tel. direktor: +386 64 861-443

tel. komerciala: +386 64 861-474

Fax: +386 64 861-379

Telex: 37219 ZELJSN SI

Slovenija



**ELECTRICAL SHEETS
AND STRIPS**

**STAINLESS
STEELS**

**MICROALLOYED
STEELS**

**HIGH CARBON
STEELS for hardening
and tempering**

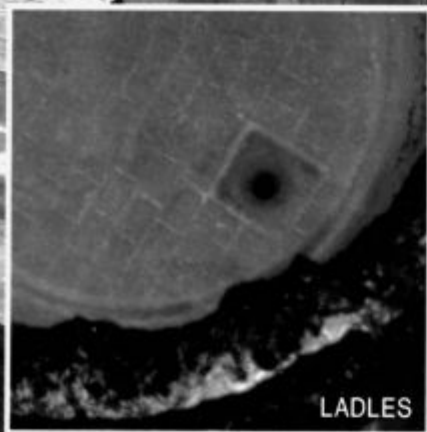
OUR PRODUCTION PROGRAM INCLUDES:

- * general structural steels
- * finegrained and HSLA structural steels
- * carbon and alloyed steels
 - for quenching and tempering
 - case hardening
- * silicon steels for electrical sheets
- * stainless steels

- * hot rolled plates, wide and slit strips and bars
- * cold rolled sheets, wide and slit strips
- * cold rolled sections
- * metal door posts
- * blanks

WE ALSO OFFER:

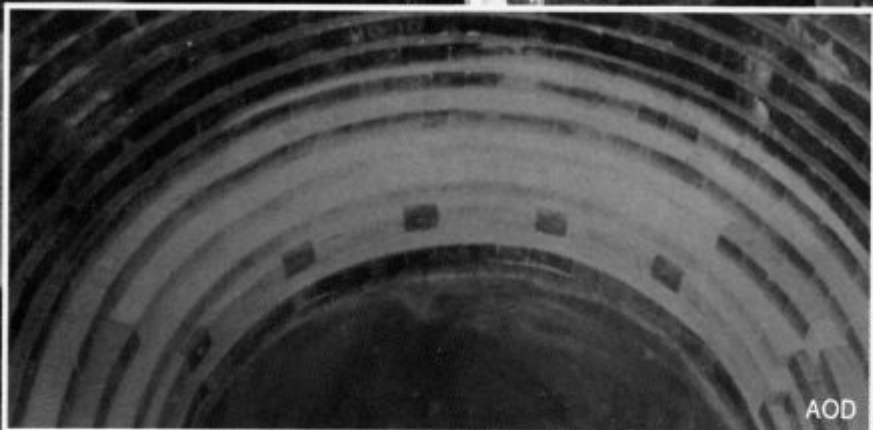
- * hot and cold rolling
- * blanking
- * torch cutting by drawing
- * straightening
- * heat treating of plates, strips and sheets



LADLES



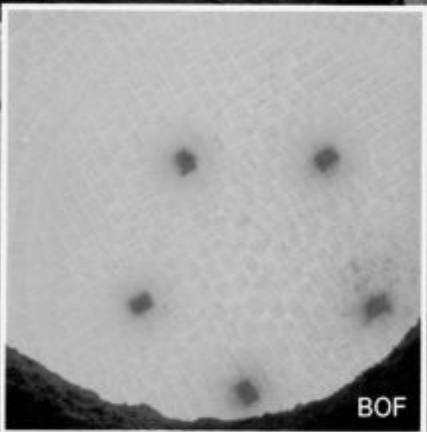
MIXES



AOD



DEGASSER



BOF



EAF



EAF

The refractory specialist

RADEX Austria
Aktiengesellschaft
für feuerfeste Erzeugnisse
A-9545 Radenthein / Austria
Phone 0 42 46/21 00-0
Telex 45655 rad a
Telefax 04246/2100/555 oder 556

RADEX Deutschland
Aktiengesellschaft
für feuerfeste Erzeugnisse
D-5401 Urmitz / Germany
Phone 0 26 30/89-0
Telex 867715-0 ur d
Telefax 02630/89360

RADEX